1964

Nature of the energy levels in hydrated thulium ethylsulphate

Lewis Clark Bartel
Iowa State University

NATURE OF THE ENERGY LEVELS IN HYDRATED THULIUM ETHYLSULPHATE

by

Lewis Clark Bartel

A Dissertation Submitted to the
Graduate Faculty in Partial Fulfillment of
The Requirements for the Degree of
DOCTOR OF PHILOSOPHY

Major Subject: Physics

Approved:

Signature was redacted for privacy.

In Charge of Major Work

Signature was redacted for privacy.

Head of Major Department

Signature was redacted for privacy.

Dean of Graduate College

Iowa State University
Of Science and Technology
Ames, Iowa

1964

TABLE OF CONTENTS

INTRODUCTION

One of the big successes of quantum mechanics was the qualitative and quantitative description of the spectra of field free atoms and ions. There were, as in almost all subjects of physics and chemistry, very many who contributed to the experimental and theoretical knowledge of the subject. The theory of atomic spectra has probably best been given by Condon and Shortley (1) and Slater (2), and descriptive accounts are given in Herzberg (3) and White (4).

In order to explain the spectra of atoms and ions in crystalline materials Bethe (5, 6) proposed the crystal field model. In this model the paramagnetic ions in a crystal are thought of as being in an electric field produced by all the other charges and electric dipoles in the crystal. This model neglects the overlap of the atomic electron wave functions with those of the ligands (the other charges and electric dipoles in the crystal). In the following years many workers in the field contributed greatly to establishing that this model had some validity. Work on spectra and paramagnetic susceptibilities in the 1930's was carried out by many scientists (7-21). Some of the conclusions that were arrived at during this time for rare earth salts were (a) Russell

Saunders coupling was inadequate to describe the free ions and an intermediate coupling scheme had to be used, (b) the crystal field could be thought of as a perturbation on the free ion, and (c) the observed spectra came from transitions within the 4f shell.

After World War II in the late 1940's and the 1950's there was a revival of interest in crystal field theory as it applied to salts of the rare earth metal atoms. Hellwege (22, 23) extended the work of Bethe and established a system of notation which other have used to discuss experimental results. Bleaney and Stevens (24) applied the crystal field theory to paramagnetic resonance. Extensions to the crystal field theory for the rare earth ethylsulphates in C_{3h} symmetry were made by Stevens (25), Elliott (26), Elliott and Stevens (27-29), and Scovil and Stevens (30a). Dieke with various co-workers has done quite a considerable amount of work with the spectra of rare earth salts. Just to mention some of the work, Dieke and Heroux (30b) measured the absorption spectra with the Zeeman effect of some neodymium salts, Dieke and Hall (30c) worked on fluorescent lifetimes of some rare earth salts, and Dieke and Sarup (30d) worked on the fluorescent spectra of praseodymium chloride. Crystal structure deter-

minations of the rare earth ethylsulphates were made by Ketelaar (31) in 1937 and by Fitzwater and Rundle (32) in 1959; it was found that the rare earth ion is at a site which possesses C_{3h} symmetry.

Over the years there have been speculations as to the mechanism by which electric dipole transitions can take place between electronic states of a 4f shell. Since the electric dipole operator has odd parity and if states of a $4f^n$ configuration are made up of strictly 4f electron wave functions, electric dipole transitions between two 4f electronic states are forbidden. Bethe and Spedding (16) had speculated on the nature of the transitions. Van Vleck (11) and Broer et al. (33) calculated transition rates for various types of transitions, and recently Judd (34) had repeated some of the same calculations. Calculations were made for electric dipole transitions where the perturbation of the non-inversion-symmetric terms in the crystal field bring in the needed opposite parity terms. The non-inversion-symmetrical crystal fields can occur naturally or can arise because of the lattice vibrations. Calculations were also made for magnetic dipole and electric quadrupole transitions. The conclusions of Boer et al. and Judd were that the electric dipole transi-

tion rates were sufficiently large to account for the observed intensities of the absorption lines in the spectra and that magnetic dipole and electric quadrupole transitions were less important.

In 1958 Johnsen (35) determined the energy levels for some of the multiplets of thulium ethylsulphate (hereafter known as Tm ES). He measured the zero magnetic field values as well as the Zeeman splitting of the levels. Johnsen (35) reported only the splitting factors of the levels for the magnetic field parallel to the c-axis of the crystal and did not report splitting factors for the field perpendicular to the c-axis. Gruber and Conway (36, 37) did some work on Tm ES and determined crystal field constants, constants for the electrostatic interaction (F integrals), and the constant for the spin-orbit interaction (ζ). Margolis (38) from work on Pr^{3+} and Tm^{3+} obtained values for the F integrals and ζ. Wong and Richman (39) measured the spectra of Tm ES diluted in lanthanum ethylsulphate, and using the F's and ζ of Margolis determined a set of crystal field constants. In addition Wong and Richman (39) calculated theoretical splitting factors for levels with the magnetic field parallel to the c-axis of the crystal and compared these to the values

given by Johnsen. Gerstein et al. (40) found that the crystal field constants of Wong and Richman as applied to the ground multiplet fit their heat capacity data better than those of Gruber and Conway. Recently the crystal field constants have been interpreted by Jørgensen et al. (41) as a measure of covalent bonding between the metal ions and the ligands. Watson and Freeman (42) have examined the contributions to the energy of the closed atomic shells to the crystal field electrostatic interaction. They found that this interaction could be divided into two parts. The first part was interpreted as shielding of the 4f electrons from the crystal field. The second part had the effect that the ordering and relative spacing of the levels were not necessarily those implied by the 4f electron crystal field matrix elements alone. In some cases severe deviations from the 4f crystal field level scheme resulted, making questionable the standard crystal field parameterization.

It is the purpose of this investigation to obtain the splitting factors for the magnetic field parallel to the c-axis of some of the levels that Johnsen (35) did not measure and to measure and interpret the spectra for the magnetic field perpendicular to the c-axis in light of the recent theory of Murao, Spedding and Good (43). The data taken in

this investigation are believed to be more accurate than that of the previous workers because of using a higher dispersion instrument. In addition to the experimental work, a basis for discussing the interaction of lattice vibrations with the 4f electrons of the thulium ion will be made. This theoretical work is similar in nature to that of some previous workers (44-49). The so-called extra lines appearing in the spectra have long been thought to arise from transitions to electron-vibrational coupled states of the crystals. An example of which has been shown by several authors (11, 15, 19, 50). Recently experimental determinations of some of the normal mode energies for rare earth ethylsulphates have been made (50, 51). With the aid of the theoretical discussion of the electron-phonon interaction in this thesis it is hoped to improve the understanding of the interaction of the electrons and the vibrations so that at some later date some concrete calculations can be made.

THEORY

Field Free Ion States

The spectra of field free atoms containing more than one electron have been discussed at length by Condon and Shortley (1) and Slater (2). When the central field approximation is applied to electrons in an unfilled shell in an atom, Condon and Shortley (1) have shown that the Hamiltonian of all the electrons can be simplified to be,

$$H_{ion} = \sum_{j=1}^{n} [\, P_j^2/2m + U'(r_j) + \xi(r_j)\, \underline{l}_j \cdot \underline{s}_j] + \sum_{j<k}^{n} e^2/r_{jk}, \qquad (1)$$

where n is the number of electrons in the unfilled shell, $U'(r_j)$ is the effective potential that the j-th electron feels due to the closed shells interior as well as exterior to the unfilled shell, $\underline{l}_j$ is the orbital angular momentum, $\underline{s}_j$ is the spin angular momentum of the j-th electron, and $\underline{p}_j$ the momentum operator. The term $\sum_j \xi(r_j)\, \underline{l}_j \cdot \underline{s}_j$ is known as the spin-orbit interaction and $\sum_{j<k} e^2/r_{jk}$ is known as the electrostatic interaction.

In order to solve the eigenvalue problem for H_{ion}, various types of coupling schemes are usually considered to

simplify the problem. Russell Saunders coupling assumes that the spin-orbit term can be treated as a perturbation on the rest of the Hamiltonian, while the j-j coupling scheme assumes that the electrostatic interaction term can be treated as the perturbation. It has been demonstrated (16, 19) and (36-39) that in order to get the best results for the rare earth spectra the intermediate coupling scheme must be used. The electrostatic and spin-orbit interactions are introduced as perturbations of comparable strength in the intermediate coupling scheme. In this scheme the total angular momentum $\underline{J}$ and its z projection M are good quantum numbers. An exact method of solution would be to work in the product 4f electron wave function representation and diagonalize the grand matrix to determine the eigenvalues and eigenvectors.

The notation demonstrated in the following equations will be used:

$$H_{ion}\,\phi_{\gamma JM} = W_{\gamma JM}\,\phi_{\gamma JM}$$

where

$$J^2\,\phi_{\gamma JM} = \hbar^2 J(J+1)\,\phi_{\gamma JM} \qquad (2)$$

and

$$J_z\,\phi_{\gamma JM} = \hbar M\,\phi_{\gamma JM}.$$

Here γ represents additional quantum numbers needed to describe the configuration and distinguish multiplets for the same J, J is the total angular momentum, and M is the projection of J on the axis of quantization which will be taken as the z-axis. It should be noted here that the $\phi_{\gamma JM}$'s can be expressed as linear combinations of products of individual electron wave functions of the type,

$$\phi(\underline{r})_{n\ell m_\ell m_s} = R_{n\ell}(r)\, Y(\hat{r})_{\ell m_\ell}\, \chi_{\frac{1}{2} m_s}. \qquad (3)$$

Condon and Shortley (1, p. 284) have shown that the problem of n electrons in an unfilled shell which when filled has N electrons is equivalent to the problem of N-n positive holes. Therefore for a triply ionized thulium atom which has a $4f^{12}$ configuration of electrons, it is an equivalent problem to consider the problem of a configuration of $4f^2$ positive holes (52).

The free ion solutions for Tm^{3+} have been worked out by several authors (19, 36, 38) where even for the intermediate coupling scheme the Russell Saunders notation is used. The multiplets of a f^2 configuration are (1, 36, 52)

$$^1(S\ D\ G\ I) \quad ^3(P\ F\ H)$$

and the relative order (36) of the multiplets is shown in Figure 1.

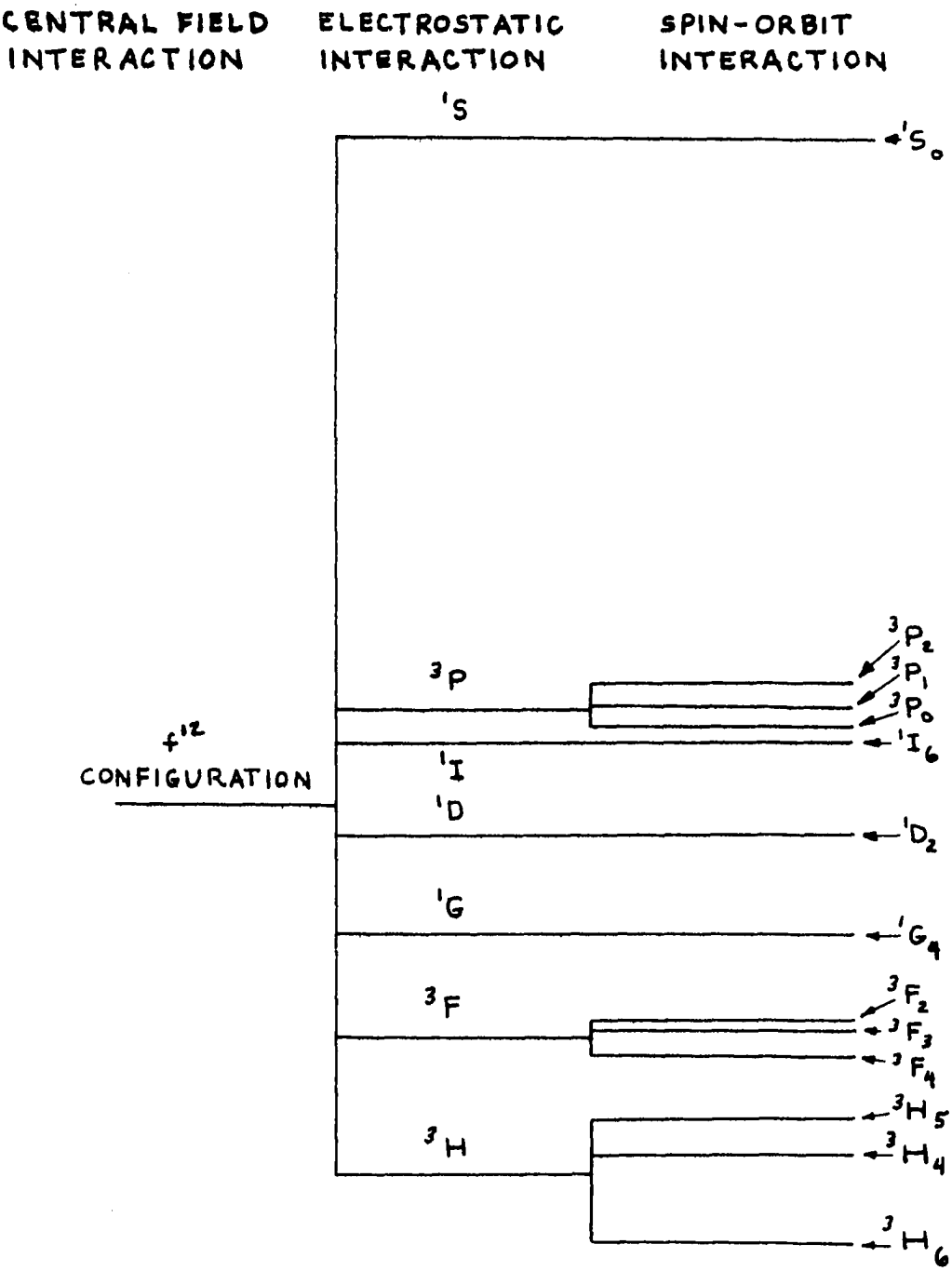

Figure 1. The multiplet structure of the $4f^{12}$ configuration of the Tm^{3+} ion as given by Gruber and Conway (36)

Crystal Field

In the crystal field theory the ions are placed in the field of all the other atoms in the crystal. The rare earth ions (in particular Tm^{3+}) will be thought of as being held in an equilibrium position by the interactions of the outer electrons of the ions with the surrounding atoms. To a first approximation the 4f electrons will only be thought of as being perturbed by the crystal field and not contributing to any covalent bonding (41). The interaction that will be considered here is the action of the crystal field on the 4f shell of the rare earth ion. The Hamiltonian is of the form,

$$H_o = H_{ion} + \sum_{j=1}^{n} e\,\phi(\underline{r}_j), \qquad (4)$$

where H_{ion} is given by Equation 1 and $\phi(\underline{r}_j)$ is the electrostatic potential due to the external charges and electric dipoles as seen by the j-th electron. Here the vector potential arising from the motions of the charges is neglected because experimentally the spectra are taken at low temperatures.

The electrostatic crystal field potential is given by,

$$\phi(\underline{r}_j) = \sum_k q_k / |\underline{R}_k - \underline{r}_j|, \qquad (5)$$

where the sum of k runs over all the charges in the crystal other than the atom under consideration. Because of the shielding of the 4f shell electrons by the other electrons in the rare earth ion (42), q_k is the effective charge on the k-th atom. In the static crystal field approximation the atoms are all taken at their equilibrium positions. For the case where they are not at their equilibrium positions, the reader is referred to section on electron-phonon interactions. $\underline{R}_k$ is the equilibrium position of the k-th charge and $\underline{r}_j$ the position vector of the j-th electron referred to the rare earth nucleus as the origin. The potential energy of the n 4f electrons is,

$$V = \sum_{j=1}^{n} \sum_k e q_k / |\underline{R}_k - \underline{r}_j| . \qquad (6)$$

Expanded in terms of spherical harmonics V becomes,

$$V = \sum_{j=1}^{n} \sum_k e q_k \sum_{L,M} (4\pi/2L+1)(r_<^L / r_>^{L+1}) \cdot Y(\hat{r})_{LM} \, Y^*(\hat{R}_k)_{LM}, \qquad (7a)$$

where $r_<$ is the lesser of r_j or R_k and $r_>$ is the greater. Here it will be assumed that the wave functions of the electrons do not overlap those of the external charges so that r_j is always less than R_k such that,

$$V = \sum_{j=1}^{n} \sum_{L,M} A_{LM} \, r_j^L \, Y(\hat{r}_j)_{LM} \, . \qquad (7b)$$

The crystal field potential V will have the point group symmetry at the rare earth ion of C_{3h} (43, 53). In order for V to have this C_{3h} symmetry, it has been shown (43) that the L, M terms to consider are given in Table 1.

Table 1. Terms of V for C_{3h} symmetry

L	M
2	0
4	0
3	± 3
5	± 3
6	0, ± 6

The crystal field potential V is then treated as a perturbation on H_{ion}. Solutions to,

$$H_o = H_{ion} + V \qquad (8)$$

will be taken as,

$$H_{\cdot}\,\phi_{\lambda\mu i} = \epsilon_{\lambda\mu i}\,\phi_{\lambda\mu i}, \tag{9}$$

where $\phi_{\lambda\mu i}$ can be expanded in terms of the free ion solutions to give,

$$\phi_{\lambda\mu i} = \sum_{\gamma J M} C^{\lambda\mu i}_{\gamma J M}\,\phi_{\gamma J M}\,. \tag{10}$$

λ designates the multiplet, μ designates the crystal field quantum number (discussed below), and i labels the different μ's for the same λ (43).

In addition to being expressed as a linear combination of the $\phi_{\gamma JM}$'s, the $\phi_{\lambda\mu i}$'s can be expressed as linear combinations of single electron product wave functions of the type given in Equation 3. For the case of Tm^{3+} ion in an external crystal field the wave functions are,

$$\phi(\underline{r}_1, \underline{r}_2)_{\lambda\mu i} = \sum_{n_1 n_2} C^{\lambda\mu i}_{n_1 n_2}\,\phi(\underline{r}_1)_{n_1}\,\phi(\underline{r}_2)_{n_2}\,. \tag{11}$$

n stands for all the quantum numbers n 1 m_l m_s. (Here the 12 electron problem has been replaced by the two positive hole problem).

The eigenvalues $\epsilon_{\lambda\mu i}$ and the expansion coefficients $C^{\lambda\,\mu i}_{\gamma JM}$ or $C^{\lambda\,\mu i}_{n_1 n_2}$ may be found from solving the secular equations. An alternative method would be to use the ordinary first and second order perturbation techniques (54) to solve for the

eigenvalues and eigenfunctions. The method of operator equivalents has been applied to the solution of the Tm^{3+} ion in thulium ethylsulphate (36, 37, 39).

Matrix elements for V (or for any operator) will be denoted by,

$$\int \phi^{+}_{\lambda'\mu'i'} V \phi_{\lambda\mu i}$$

or by

$$\langle \lambda'\mu' i' | V | \lambda\mu i \rangle$$

where these two integration symbols have an identical meaning.

The crystal field quantum numbers μ are given by Hellwege (22) and Murao et al. (43). The reader is referred to (43) for a clear, concise derivation of the μ quantum numbers. The crystal field μ quantum numbers are $\mu = 0, \pm 1, \pm 2, 3$ (43). These differ slightly from those of Hellwege (22) and the difference is pointed out by Murao et al. (43). For the even numbered electron case the following μ quantum states are used (43),

$$(0), (1,-1) (2,-2), (3),$$

where the states (1,-1) and the states (2,-2) are time reversally degenerate. The relationship between the μ quantum

number and the M quantum number is given for a Tm^{3+} ion in Table 2 (43).

Table 2. Relation between μ and M quantum numbers for Tm^{3+}

μ values	M values totally even parity
0	0, ± 6
1	1, -5
-1	-1, 5
2	2, -4
-2	-2, 4
3	3, -3

The relationship between the C_{3h} point group character table (53) and the μ quantum numbers[1] is given in Table 3. For example, the r sinθ $e^{i\phi}$ and the μ = -2 representations are shown equivalent in the following discussion. Murao, Spedding, and Good (43) have defined an operator 0 operating on a function $f(r,\theta,\phi)$ to give,

$$O f(r,\theta,\phi) = f(r,\pi-\theta,\phi+\tfrac{4\pi}{3}), \qquad (12a)$$

and the eigenvalues a_o of the operator 0 are found from,

[1]Good, Roland H., Jr., Ames, Iowa. Notes on group theory. Private communication. 1962.

$$O f = a_o f, \tag{12b}$$

where the eigenvalues a_o and the μ quantum numbers are related by,

$$a_o = e^{i\frac{\pi}{3}\mu}. \tag{12c}$$

Therefore,

$$\begin{aligned} O f(r, \theta, \phi) &= f(r, \pi-\theta, \phi + 4\pi/3) \\ &= e^{i\frac{\pi}{3}\mu} f(r, \theta, \phi) . \end{aligned} \tag{12d}$$

When $f(r,\theta,\phi)$ is replaced by $r \sin\theta\, e^{i\phi}$ one obtains the following result,

$$\begin{aligned} O\, r \sin\theta\, e^{i\phi} &= r \sin(\pi-\theta)\, e^{i\phi + i\frac{4\pi}{3}} \\ &= e^{i\frac{\pi}{3}\mu} r \sin\theta\, e^{i\phi}, \end{aligned} \tag{12e}$$

$$r \sin\theta\, e^{i\phi} e^{i\frac{4\pi}{3}} = e^{i\frac{\pi}{3}\mu} r \sin\theta\, e^{i\phi}.$$

Hence, $\mu = -2$ since $e^{i\frac{4\pi}{3}} = e^{-i\frac{2\pi}{3}}$.

Table 3. Relation between C_{3h} character table and the μ quantum number for particles with integer total angular momentum where $\epsilon = \exp(i2\pi/3)$

C_{3h}	E	C_3	C_3^2	σ_h	$\sigma_h C_3$	$\sigma_h C_3^2$	μ Rep.
r sinθ	1	1	1	1	1	1	0
r sin θ $e^{i\phi}$	1	ϵ	ϵ^2	1	ϵ	ϵ^2	-2
r sinθ $e^{-i\phi}$	1	ϵ^2	ϵ	1	ϵ^2	ϵ	2
r cosθ	1	1	1	-1	-1	-1	3
r cosθ $e^{i\phi}$	1	ϵ	ϵ^2	-1	$-\epsilon$	$-\epsilon^2$	1
r cosθ $e^{-i\phi}$	1	ϵ^2	ϵ	-1	$-\epsilon^2$	$-\epsilon$	-1

One can easily determine, as will be shown, how the levels of a free atom will split due to an external crystalline electric field.[1] The system to consider is the levels of a given J as forming the basis of a representation of the symmetry operations of the crystal field. The irreducible representations contained in this reducible representation will correspond to the levels into which the original state will split. For a general group theory treatment, the reader is referred to Landau and Lifshitz (53). The characters of the C_{3h} symmetry group are found from Appendix I, A1, where J

[1]Good, Roland H., Jr., Ames, Iowa. Notes on group theory. Private communication. 1962.

is the free ion angular momentum and ϕ is the angle through which the symmetry operation rotates. The character table is given by Table 4, where the last column shows the irreducible μ representations, as given by Table 3, contained in the reducible J representations. The number of times a μ representation, a $^{(\mu)}$, is contained in the reducible J representation can be found from,

$$a^{(\mu)} = \frac{1}{g} \sum_{G} \chi^{(J)}(G)\, \chi^{(\mu)}(G)^{*}, \qquad (13)$$

where g is the dimensionality of the representation and G stands for the elements of the symmetry group (53).

Table 4. C_{3h} symmetry character table for integral J

J	E	C_3	C_3^2	σ_h	$\sigma_h C_3$	$\sigma_h C_3^2$	Reps. μ
0	1	1	1	1	1	1	0
1	3	0	0	-1	2	2	0, +1, -1
2	5	-1	-1	1	1	1	0, +1, -1, +2, -2
3	7	1	1	-1	-1	-1	0, +1, -1, +2, -2, 3, 3
4	9	0	0	1	-2	-2	0, +1, -1, +2, +2, -2, -2, 3, 3
5	11	-1	-1	-1	-1	-1	0, +1, +1, -1, -1, +2, +2, -2, -2, 3,3
6	13	1	1	1	1	1	0, 0, 0, +1, +1, -1, -1, +2, +2, -2, -2, 3, 3

For an example of how to calculate the number of irreducible μ representations contained in a reducible J representation, the reader is referred to Appendix II where the J = 4 case is examined. Hellwege (22, 23) has worked out for a general J the number of irreducible representations contained in the reducible J representations for several crystal symmetries including C_{3h}.

In the absence of an external magnetic field, the representations which are complex conjugates of each other are still degenerate. These representations are the $\mu = \pm 2$ and $\mu = \pm 1$. The $\mu = 0$ and $\mu = 3$ representations are single; therefore the corresponding levels with these quantum numbers are non degenerate. Aside from accidental degeneracies, the only levels which are degenerate are the $\mu = \pm 2$ and $\mu = \pm 1$ levels.

The crystal field potential expanded by Murao et al. (43) is,

$$V = \sum_j \sum_{L,M} \alpha_{LM}\left[y(j)_{LM} + y(j)_{L-M} \right] + i\beta_{LM}\left[y(j)_{LM} - y(j)_{L-M} \right], \tag{14}$$

where,

$$y_{LM} = i^L Y_{LM},$$

and the α's and β's include the r_j^L's. The Y_{LM}'s are the ordinary spherical harmonics (1). The α's and the β's are real quantities. The L and M terms to consider for C_{3h} symmetry are given in Table 2. When one only considers matrix elements of V between states of a $4f^n$ configuration, the odd L terms do not contribute because of the oddness of the parity of the integrand. However, these odd parity crystal field terms do connect $4f^n$ configuration states with different parity electronic states. These odd parity crystal field terms are important in theories of transitions within a $4f^n$ configuration (11, 33, 34, 43). The significance of the α's and β's will become clear later in the discussion of the theory for transitions when the magnetic field is perpendicular to the c-axis.

In determining the matrix elements of the secular determinant one has matrix elements of the type,

$$\int \phi^{+}_{\gamma' J' M'} V \phi_{\gamma J M},$$

where one must evaluate,

$$\int \phi^{+}(\underline{r})_{4f\, m_l' m_s'} \{ A_{20}\, r^2\, Y(\hat{r})_{20} + \cdots \} \phi(\underline{r})_{4f\, m_l\, m_s}\, d\underline{r} \tag{15}$$

$$= A_{20} \langle r^2 \rangle \delta_{m_s' m_s} \int Y^{*}(\hat{r})_{3 m_l'}\, Y(\hat{r})_{20}\, Y(\hat{r})_{3 m_l}\, d\Omega ,$$

where

$$\langle r^2 \rangle = \int R^{*}(r)_{4f}\, r^2\, R(r)_{4f}\, r^2\, dr .$$

The terms like α_{20} or $A_{20} \langle r^2 \rangle$ are treated as arbitrary parameters to be determined from the data.

Gruber and Conway (37), and Wong and Richman (39) have made determinations of these constants for thulium ethylsulphate from spectral data. It is felt (40, 55) that Wong and Richman's constants represent some of the experimental facts better than Gruber and Conway's. The above authors (37, 39) used the operator equivalent method (25) to solve the crystal field problem.

An alternative method of solution is to use the product 4f electron wave function approach to diagonalize the Hamilton H_o. The resulting matrix to diagonalize is 91 by 91 (52) for a $4f^2$ configuration of positive "holes". Some work in determining crystal field constants in this represen-

tation has been done[1] and has yielded substantially the same results as the crystal field constants of Wong and Richman (39) and the F integrals and ξ of Margolis (38). The determined constants are very much dependent upon the eigenvalues put into the least squares determination. The calculation of the constants from knowing the eigenvalues depends upon correctly identifying the transitions. Sometimes this is not easy because of the large number of lines in the spectra thought to come about by a coupling of the electrons with the lattice vibrations (11, 15, 19, 50). The so-called "pure" electronic levels are shifted away from the value they would have from considering only the 4f shell crystal field matrix elements. The shift comes from several sources one of which is the interaction of the 4f shell with the closed shells (42). Another source is the interaction with the lattice vibrations as will be discussed below.

Electron-Phonon Interaction

Many of the lines appearing in the absorption spectra are thought (11, 15, 19, 50) to arise from transitions to electronic states which are coupled to the vibrational states

---

[1]Spedding, F. H. and Haas, W. J., Ames, Iowa. Constants for thulium ethylsulphate. Private communication. 1962.

of the crystal. It will be the purpose of this section, as well as Appendix III, to present the general theory and a few conclusions that must follow from the theory.

The potential energy of an electron, produced by the charges external to its host atom in a distorted lattice, can be found by performing the following sum,

$$V(\underline{r}_i) = \sum_{j\bar{n}}{}' e q_{j\bar{n}} / |\underline{a}_{\bar{n}} + \underline{d}_j + \underline{u}_{j\bar{n}} - \underline{r}_i - \underline{u}_{oo}|, \qquad (16)$$

where the vectors are shown in Figure 2, and the prime on the sum means omit the term $j = o$, $\bar{n} = o$ from the sum. $\underline{a}_{\bar{n}}$ is a lattice vector to the $\bar{n}$-th unit cell and $\underline{d}_j$ is a vector within the $\bar{n}$-th unit cell to the j-th atom in the unit cell. $\underline{u}_{j\bar{n}}$, as defined by Equation A30 of Appendix III, is the displacement from equilibrium of the j-th particle in the $\bar{n}$-th unit cell and $q_{j\bar{n}}$ is the effective charge on that atom or ion. $\underline{u}_{oo}$ is the displacement from equilibrium of the host rare earth ion. The equilibrium position of this host atom will be taken as the origin.

Here it is assumed that the i-th electron follows the motion of the rare earth nucleus exactly. This is much the same sort of treatment that has been given by other workers (44-48). It is assumed also that the 4f electrons do not, at

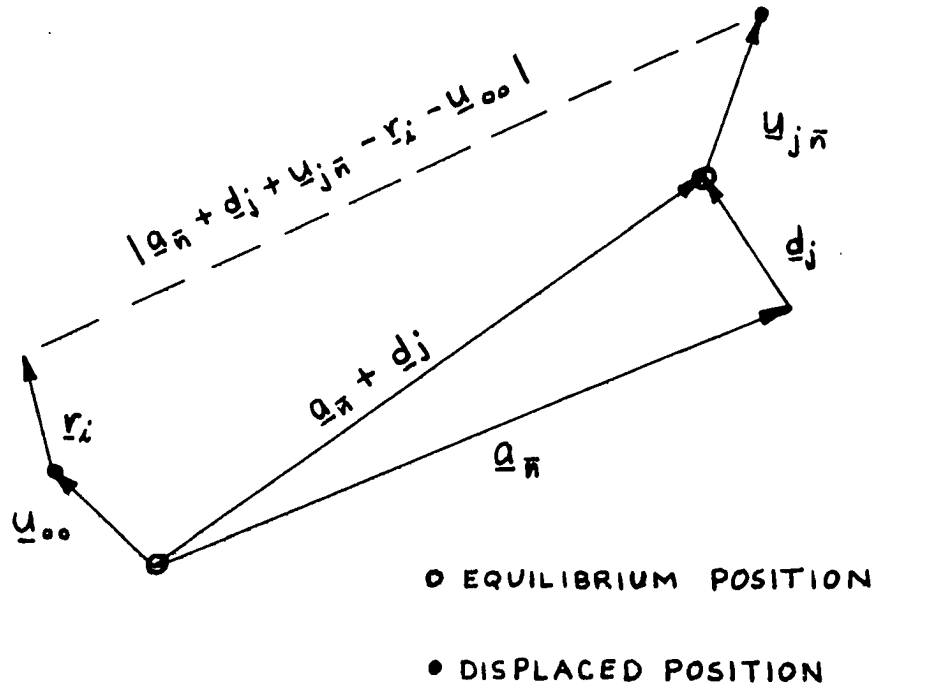

Figure 2. Vectors needed to describe the electron-phonon interaction

least to any large degree, participate in the bonding between the atoms. The outer electrons which may participate in the bonding, will be assumed to remain in the same electronic configuration throughout any future discussions.

The potential energy of the n 4f electrons due to the external charges in the crystal is obtained by summing $V(\underline{r}_i)$ up over the n 4f electrons. When the displacements $\underline{u}$ can be considered small, V can be expanded in a Taylor's series to give,

$$\begin{aligned} V = &\sum_i \sum_{j\bar{n}}{}' e q_{j\bar{n}} / |\underline{a}_{\bar{n}} + \underline{d}_j - \underline{r}_i| \\ &+ \sum_i \sum_{j\bar{n}}{}' e q_{j\bar{n}} \{ \underline{u}_{j\bar{n}} \cdot \underline{\nabla}_{j\bar{n}} (1/|\underline{a}_{\bar{n}} + \underline{d}_j - \underline{r}_i|) \\ &\qquad + \underline{u}_{oo} \cdot \underline{\nabla}_i (1/|\underline{a}_{\bar{n}} + d_j - \underline{r}_i|) \}. \end{aligned} \tag{17a}$$

The zeroth order Taylor's series term is just the ordinary static crystal field potential term as discussed earlier, while the second term is the electron-phonon interaction term denoted by H_{ep}. H_{ep} can then be readily written in the form,

$$H_{ep} = \sum_i \sum_{j\bar{n}} \sum_{j'\bar{n}'}{}' e q_{j'\bar{n}'} \underline{u}_{j\bar{n}} \cdot \underline{\nabla}_{j\bar{n}} \frac{1}{|\underline{a}_{\bar{n}'} + d_{j'} - \underline{r}_i|}, \tag{17b}$$

where when $j = 0$ and $\bar{n} = 0$ means differentiate with respect to the electrons coordinates and the prime on the sum means omit the $j' = 0$ $\bar{n}' = 0$ term. The displacement from equilibrium $\underline{u}_{j\bar{n}}$ is given by Equation A30. H_{ep} then becomes,

$$H_{ep} = \sum_i \sum_{j\bar{n}} \sum_{j'\bar{n}'}{}' e\, q_{j'\bar{n}'} \sum_{\underline{q}s} \sqrt{\frac{\hbar}{2M\omega_{\underline{q}s}}} \tag{17c}$$

$$\underline{e}_{\underline{q}sj} \cdot \underline{\nabla}_{j\bar{n}} \frac{1}{|\underline{a}_{\bar{n}'} + \underline{d}_{j'} - \underline{r}_i|} \left[b_{\underline{q}s} e^{i\underline{q}\cdot\underline{a}_{\bar{n}}} + b^+_{\underline{q}s} e^{-i\underline{q}\cdot\underline{a}_{\bar{n}}} \right].$$

b^+ and b are the boson creation and annihilation operators. A new quantity ζ can be defined by the following,

$$\zeta_{\underline{q}s}(\underline{r}_i - \underline{a}_{\bar{n}}) = \sum_j \sum_{j'\bar{n}'}{}' \frac{e\, q_{j'\bar{n}'}\, \underline{e}_{\underline{q}sj} \cdot \underline{\nabla}_{j\bar{n}}}{\sqrt{M}} \frac{1}{|\underline{a}_{\bar{n}'} + \underline{d}_{j'} - \underline{r}_i|}, \tag{17d}$$

and H_{ep} becomes,

$$H_{ep} = \sum_i \sum_{\bar{n}} \sum_{\underline{q}s} \sqrt{\hbar/2\omega_{\underline{q}s}}\, \zeta_{\underline{q}s}(\underline{r}_i - \underline{a}_{\bar{n}}) \tag{18}$$

$$\left[b_{\underline{q}s} e^{i\underline{q}\cdot\underline{a}_{\bar{n}}} + b^+_{\underline{q}s} e^{-i\underline{q}\cdot\underline{a}_{\bar{n}}} \right],$$

where ζ has the periodicity of the lattice.

The Hamiltonian for the 4f electrons of a rare earth

atom in an external crystal field including lattice vibrations is,

$$H = H_L + H_{ion} + V_o + H_{ep}, \tag{19}$$

where H_L is defined by Equation A27, H_{ion} by Equation 1, V_o by Equation 7 or 14, and H_{ep} by Equation 18.

Since the potential that the 4f electrons see is a periodic potential, wave functions that satisfy Bloch's theorem must be used (56, 57). The so-called tight binding wave functions (56, 57, 58) satisfy this condition, and these wave functions are,

$$\psi(\underline{r})_{\underline{k};\lambda\mu i} = \sum_{\pi} \frac{e^{i\underline{k}\cdot\underline{a}_\pi}\,\phi(\underline{r}-\underline{a}_\pi)_{\lambda\mu i}}{\sqrt{N}}, \tag{20}$$

where $\phi(\underline{r} - \underline{a}_n) = \phi(\underline{r})$, i.e. has the periodicity of the lattice. N is the number of unit cells and $\underline{r}$ stands for the coordinates of all the electrons.

If the overlap of the wave functions of neighboring rare earth atoms is neglected entirely, the electronic dispersion curve from H_o alone is flat in wave vector space (56, 58). However, with the addition of the perturbation H_{ep} (as will be shown) the resultant dispersion curve will no longer be flat, even when the overlap of the wave functions is neglected. The product of the $\psi_{\underline{k};\lambda\ \mu i}$'s and the phonon states

$|n_{\underline{q}s}\rangle$ will be taken as basis functions for a stationary state perturbation calculation.

The perturbed energy to second order is,

$$E(n_{\underline{q}s}:\underline{k};\lambda\mu i) = \epsilon_{\lambda\mu i} + \hbar\omega_{\underline{q}s} n_{\underline{q}s}$$

$$+\sum_{\underline{k}',n_{\underline{q}'s'}\lambda'\mu'i'}{}' \frac{|\int\psi^{+}_{\underline{k}';\lambda'\mu'i'}\langle n'_{\underline{q}'s'}|H_{ep}|n_{\underline{q}s}\rangle\psi_{\underline{k};\lambda\mu i}|^2}{\epsilon_{\lambda\mu i}+n_{\underline{q}s}\hbar\omega_{\underline{q}s}-\epsilon_{\lambda'\mu'i'}-n'_{\underline{q}'s'}\hbar\omega_{\underline{q}'s'}} . \tag{21}$$

Prime on the sum means that the diagonal term is omitted. However, there will be no diagonal matrix elements of H_{ep} since it can only connect states differing by one phonon. Here,

$$\epsilon_{\lambda\mu i} = \int \psi^{+}_{\underline{k};\lambda\mu i} H_0 \psi_{\underline{k};\lambda\mu i} , \tag{22}$$

where the overlap of neighboring rare earth ion wave functions is neglected. $\epsilon_{\lambda\mu i}$ is independent of $\underline{k}$. For the special case of $n_{\underline{q}s} = 0$ the energy E becomes,

$$E(0:\underline{k};\lambda\mu i) = \epsilon_{\lambda\mu i}$$

$$+\sum_{\underline{k}'\lambda'\mu'i's} \frac{(\hbar/2\omega_{\underline{k}-\underline{k}',s})|\zeta^{\lambda'\mu'i';\lambda\mu i}_{\underline{k}-\underline{k}',s}|^2}{\epsilon_{\lambda\mu i}-\epsilon_{\lambda'\mu'i'}-\hbar\omega_{\underline{k}-\underline{k}',s}} . \tag{23}$$

The electron-phonon interaction term then makes the resultant energy a function of the wave vector $\underline{k}$ and has broadened the level by an amount dependent upon ζ . Also the term H_{ep} shifts the energy away from the value where it would be if one only considered the static crystalline field. The fit of crystal field constants, the F integrals, and ξ are dependent upon how large the second term is in Equation 23. This is in addition to the closed shell type of interaction discussed by Watson and Freeman (42).

The energy of a state with one phonon excited is,

$$E(1_{\underline{q}s}:\underline{k};\lambda\mu i) = E(0:\underline{k};\lambda\mu i) + \hbar\omega_{\underline{q}s}$$

$$+ \sum_{\lambda'\mu'i'} \frac{(\hbar/\omega_{\underline{q}s})(\epsilon_{\lambda\mu i} - \epsilon_{\lambda'\mu'i'})\left|\zeta_{\underline{q}s}^{\lambda'\mu'i';\lambda\mu i}\right|^2}{(\epsilon_{\lambda\mu i} - \epsilon_{\lambda'\mu'i'})^2 - \hbar^2\omega_{\underline{q}s}^2} . \qquad (24)$$

Therefore in subtracting $E(0:\underline{k};\lambda\mu i)$ from $E(1_{\underline{q}s}:\underline{k};\lambda\mu i)$ the resultant is not just $\hbar\omega_{\underline{q}s}$, but there is an additional term which is a function of $\underline{q}$ and s. One could define a new ω and get,

$$\hbar\omega(\lambda\mu i)'_{\underline{q}s} = \hbar\omega_{\underline{q}s} + P(\lambda\mu i;\underline{q}s), \qquad (25)$$

where $P(\lambda \mu i; \underline{g}s)$ is the last term of Equation 24.

From the work of Wong and Erath (50), where they tentatively identified the normal energies, it is apparent that the measured normal mode energies are a function of the electronic level from which the normal mode energy was measured. This suggests that the normal mode energies could be of the form of Equation 25. Therefore at best, the energies given by Wong and Erath (50) are only an estimate of the unperturbed normal mode energies. The Raman spectrum has been obtained for lanthanum ethylsulphate (51). For lanthanum ethylsulphate the 4f shell is completely empty and hence the function $P = 0$; therefore the unperturbed normal mode energies $\hbar \omega_{\underline{g}s}$ are obtained from the Raman spectra. The unperturbed normal mode energies would be slightly different for different rare earths because of the different masses and ionic sizes. However, the difference is probably small for the majority of the normal modes.

If one could correctly identify which perturbed normal mode obtained from the absorption spectra (50) corresponded to the unperturbed ones for La ES obtained from Raman spectra (51), the function P could be evaluated and the approximate size of the effect of H_{ep} could be determined. (This, of course, would mean that the effect of the different masses and

ionic sizes on the normal mode energies is known.) However, a larger number of the normal modes are observed in the absorption spectra than are observed in the Raman spectra. Therefore unless the approximate size of P is known in the first place, it would be hard to identify which normal mode of Wong and Erath (50) (obtained for several rare earth ethylsulphates) corresponded to the normal mode obtained from the Raman spectra of lanthanum ethylsulphate. It is estimated, however, that the value of P is from 1 cm^{-1} to 5 cm^{-1}. In order to make a complete analysis of the effect of H_{ep}, one must know all the unperturbed normal mode energies in addition to the phonon polarization vectors. The complete problem is extremely difficult and no attempt will be made to calculate these here.

The time reversal operator (43) is,

$$T = \prod_{j=1}^{n} (i\sigma_y)_j K , \qquad (26)$$

where σ_y is the y-component of the Pauli spin matrices, K is an operator which means complex conjugate what follows, and j is the serial number of the electron. The Hamiltonian, even when the atoms in the crystal are not at their equilibrium positions, is invariant to the time reversal operator T. H_{ion} is invariant to the operator T (43). $V(\underline{r}_i)$ as given by

Equation 16 is invariant to T because it is real and spin independent.

Therefore the time reversal degeneracy cannot be removed by the electron-phonon interaction as considered above. The degeneracy can be removed, however, by considering the vector potential $\underline{A}$ and magnetic field connected with the motion of the charges in the crystal. The interaction term is,

$$H_{int.} = -\sum_{j=1}^{n} \left[(e/mc)\underline{A}\cdot\underline{p}_j + (e/mc)\underline{B}\cdot\underline{s}_j \right], \qquad (27)$$

where $\underline{A}$ is the vector potential and $\underline{B}$ is the magnetic field of the moving charges in the crystal. The motion of the charges must be such that $\underline{A}$ and $\underline{B}$ are not zero and the degeneracy is removed in accordance with the Jahn-Teller theorem (53, p. 370). The irreducible representations of the degenerate state are complex conjugates of each other and therefore the Jahn-Teller theorem is thought to apply.

To sum up, the splitting of the degenerate levels at zero external magnetic field must come about because of an interaction of the type given in Equation 27. The Jahn-Teller splitting has not been observed directly for thulium ethylsulphate. From magnetic susceptibility measurements, an upper bound of .1 cm^{-1} has been given for any Jahn-Teller splitting

of the ground state of holmium ethylsulphate (59).

Electromagnetic Radiation Interaction

The perturbation Hamiltonian of the electromagnetic radiation as given by Schiff (60) is,

$$H_{rad.} = -\sum_{j} (e/mc)\,\underline{A}\cdot\underline{p}_j\,, \qquad (28)$$

where $\underline{p}_j$ is the momentum operator of the j-th electron (or positive hole) and $\underline{A}$ is the vector potential of the radiation at the atom site (or ion) under consideration. The absorption part of $\underline{A}$ is, $\underline{A} = \underline{A}_o\, e^{i\underline{k}\cdot\underline{r}-i\omega t}$. The dipole approximation (60) is,

$$e^{i\underline{k}\cdot\underline{r}} = 1 + i\underline{k}\cdot\underline{r} + \text{---}\,, \qquad (29)$$

when the wave length of the incident radiation is large compared to the size of the atom. The electric dipole approximation is to replace the exponential by 1. Thus in the electric dipole approximation the vector potential $\underline{A}$ becomes independent of the coordinates of the electron, where $\underline{A}$ is proportional to $e^{i\underline{k}\cdot\underline{r}}$ (60).

The selection rules for the matrix elements of $\underline{P}$ between states of different μ quantum numbers have been given by Murao *et al.* (43) as,

$\langle \mu_1 | P_{\pm} | \mu_2 \rangle$ is zero unless

$$\mu_2 - \mu_1 = \pm 2, \mp 4 \tag{30}$$

and

$\langle \mu_1 | P_z | \mu_2 \rangle$ is zero unless

$$\mu_2 - \mu_1 = \pm 3$$

where,

$$\underline{P} = \sum_j \underline{p}_j, \tag{31}$$

$$P_{\pm} = -i\hbar \sum_j [\partial/\partial x_j \pm i \partial/\partial y_j],$$

$$P_z = -i\hbar \sum_j \partial/\partial z_j .$$

Transitions between various states will be of interest in this work. The transition probability w is,

$$w = (2\pi/\hbar)\rho \ \langle \text{final} | H^o_{rad} | \text{initial} \rangle \tag{32}$$

where,

$$H_{rad} = H^o_{rad} e^{\pm i\omega t} \tag{33}$$

and ρ is the density of final states (60).

$\underline{P}$ will be referred to as the dipole operator. The unit polarization vector of the incident light will be taken as $\underline{e}$ where $|\underline{e}| = 1$. The radiation Hamiltonian is proportional to $P_\perp$ for light polarized perpendicular to the c-axis, $P_\perp = \underline{e}_\perp \cdot P$; for light polarized parallel to the c-axis, $P_{||}$ is

defined as $P_{\parallel} = \underline{e}_{\parallel} \cdot \underline{P} = P_z$. The polarization vector $\underline{e}_{\perp}$ is shown in Figure 3 along with the angle ϕ that $\underline{e}_{\perp}$ makes with the crystallographic x-axis. (Figure 3 shows the case for the magnetic field perpendicular to the c-axis.) Therefore, $P_{\perp}$ when referred to coordinates of the crystal becomes,

$$P_{\perp} = \underline{e}_{\perp} \cdot \underline{P} = e_{\perp x} P_x + e_{\perp y} P_y$$

$$P_{\perp} = P_x \cos\phi + P_y \sin\phi \tag{34}$$

$$e_{\perp x} = |\underline{e}| \cos\phi, \; e_{\perp y} = |\underline{e}| \sin\phi, \; |\underline{e}| = 1.$$

Using $P_+ = P_x + iP_y$ and $P_- = P_x - iP_y$, $P_{\perp}$ can be written,

$$P_{\perp} = \tfrac{1}{2}(P_+ e^{-i\phi} + P_- e^{+i\phi}). \tag{35}$$

For light polarized parallel to the c-axis, $P_{\parallel}$ becomes,

$$P_{\parallel} = P_z. \tag{36}$$

For completeness, the magnetic dipole selection rules are for $\langle \mu_1 | M\pm | \mu_2 \rangle$ and $\langle \mu_1 | M_z | \mu_2 \rangle$ (43) ($M\pm$ contains M_x and M_y),

$$\begin{aligned} \mu_2 - \mu_1 &= \mp 1, \pm 5 \quad \text{for } M\pm \\ \mu_2 - \mu_1 &= 0 \qquad\quad \text{for } M_z \end{aligned} \tag{37}$$

or else the matrix elements are zero.

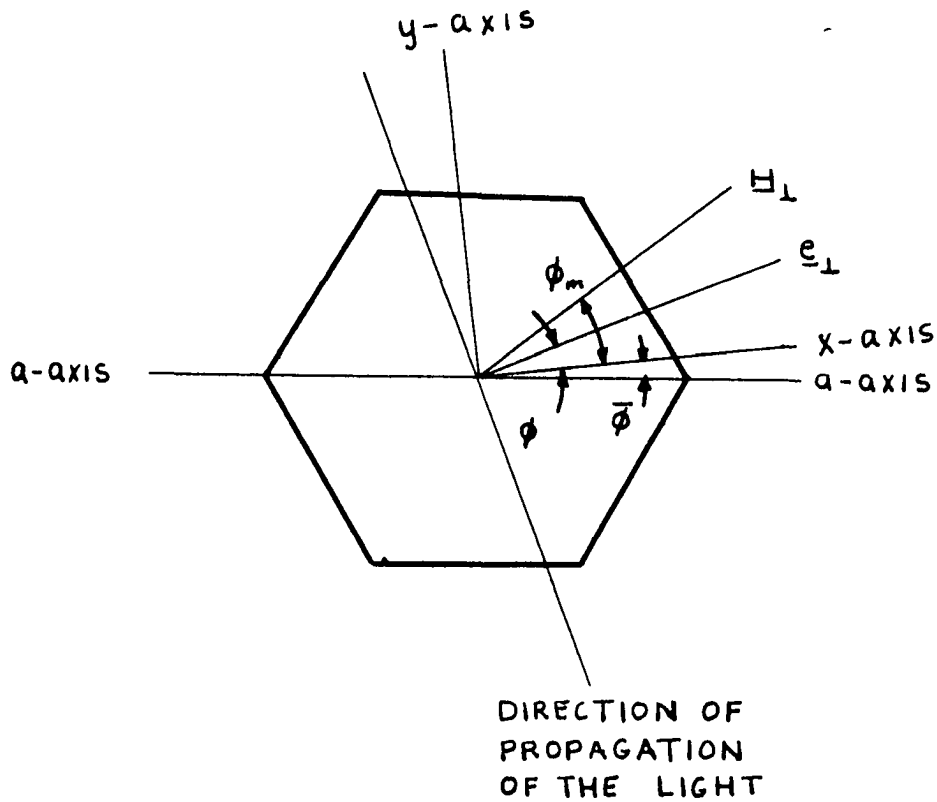

Figure 3. Schematic drawing of the angles referred to in the discussion for when the magnetic field is perpendicular to the c-axis

It should be noted here that if the wave functions representing the problem contain only products of single 4f electronic wave functions, the resulting electronic wave functions all have the same parity. The electric dipole operator has odd parity. Therefore matrix elements of $\underline{P}$ between states of the same parity are zero, and hence there would no electric dipole transitions between states of a $4f^n$ configuration. According to various authors (33, 34), the strong absorption lines of the rare earth spectra are in general too strong to be of the magnetic dipole variety and therefore must be electric dipole in nature. There are, however, some weak absorption lines in some of the spectra that are thought to be magnetic dipole in nature.

The natural odd parity crystal field terms, as mentioned previously, can bring in states of a different parity as a perturbation and thereby allow electric dipole transitions (33, 34, 43). Another mechanism that allows electric dipole transitions is the lattice vibrations bringing in states of a different parity to the wave functions representing the electronic states of the system (11, 33, 34).

In reference to the interaction with vibrations, Pollack and Satten (48) observed no transitions between "pure" elec-

tronic states for a U^{4+} ion in salts of O_h symmetry where the U^{4+} ion has a $5f^2$ configuration. Crystal fields with O_h symmetry have only even parity terms. They observed only transitions where a phonon was created or absorbed, i.e., they (48) observed transitions between energy levels $E(0:\underline{k};\lambda\ \mu i)$ and $E(1_{gs}:\underline{k}',\ \lambda'\mu'i')$ for instance. In this type of transition, the creation of the phonon destroys the center of inversion symmetry giving rise to odd parity crystal field terms. These odd parity terms have matrix elements between states of opposite parity. Therefore in a perturbation calculation, they lead to states that are a mixture of parities and so permit electric dipole transitions. The absence of "pure" electronic transitions also means that magnetic dipole transitions are extremely weak. Transitions from states where there are no phonons to states where there are phonons existing are second order transitions of the type discussed by Pollack and Satten (48) and Richman et al. (49).

In the case of the rare earth ethylsulphates, there is no center of inversion symmetry which means that transitions between energy levels of the type $E(0:\underline{k};\lambda\ \mu i)$ and $E(0:\underline{k}';\lambda'\ \mu'i')$ can take place. Wave functions representing these states for no phonons already contain the needed different

parity parts (interconfigurational mixing via the natural odd parity crystal field terms) in order to have electric dipole transitions. In addition to transitions between "pure" electronic states, there are transitions between levels of the type discussed in the previous paragraph. These transitions will be of the second order type as discussed above.

The above observations lead one to two conclusions. The first is that it is the electric dipole transitions which are the most important, while the higher multipole transitions are of less importance. The second conclusion is that the natural non-inversion-symmetrical crystal fields or the vibration distorted fields cause the mixing of states with a different parity than the $4f^n$ states and thereby allow electric dipole transitions.

In discussing transitions between various energy levels, the transition from a $\lambda\mu i$ state to a $\lambda'\mu'i'$ state will be designated as ($\lambda\mu i$ - $\lambda'\mu'i'$) or for simplicity a (μ - μ') designation will be used. Transitions between states where n_{gs} is not zero will still be designated in the above manner.

Magnetic Field Interactions

The interaction term of the Hamiltonian for a magnetic field is given by Schiff (60) and Condon and Shortley (1) as,

$$H' = -\sum_{i=1}^{n} (e/2mc)(\underline{l}_i + 2\underline{s}_i)\cdot\underline{H}, \qquad (38)$$

where $\underline{H}$ is the magnetic field and n is the number of electrons in the unfilled shell. The Hamiltonian for the Zeeman effect can also be written in the form (60, 61, 62),

$$H' = g(\gamma J)\beta\underline{J}\cdot\underline{H}, \qquad (39)$$

where the $\underline{J}$ operator has the $\hbar$ taken out of it. The $\hbar$ factor is included in β which is the Bohr magneton $e\hbar/2mc$. $g(\gamma J)$ is an effective Lande' g_L factor which is in general not the same as the g_L factor calculated from Russell Saunders coupling, since in the intermediate coupling scheme the LS states are mixed. $g(\gamma J)\beta\underline{J}$ is the magnetic moment operator $\underline{M}$.

When the wave functions which diagonalize the Hamiltonian, including the crystal field term, are expressed as a linear combination of the free ion wave functions, the wave functions are of the type given by Equation 10. The time reversal operator given by Equation 26 when applied to a degenerate state gives the following results of Murao *et al.* (43).

$$T\phi_{\lambda\mu i} = \eta_{\lambda\mu i}\,\phi_{\lambda\tilde{\mu}i} = \sum_{\gamma JM} C^{\lambda\mu i\,*}_{\gamma JM}(-1)^{J+M}\phi_{\gamma J-M}, \qquad (40)$$

where

$$\eta_{\lambda\mu i} = \pm 1.$$

Hence,

$$\phi_{\lambda\tilde{\mu}i} = \eta_{\lambda\mu i}\sum_{\gamma JM} C^{\lambda\mu i\,*}_{\gamma JM}(-1)^{J+M}\phi_{\gamma J-M}\,. \qquad (41)$$

Since H' as given by Equation 38 or 39 is not invariant to the time reversal operator T, the degeneracy of the time reversally degenerate states is removed (43).

Koster and Statz (61) and Statz and Koster (62) have studied the magnetic field interaction for various symmetries, but had confined most of their calculations to the unfilled d-shell in crystalline solids with cubic symmetry. Their method uses the same considerations of group theory and time inversion as does the method of Murao, Spedding, and Good (43). The work of Murao _et al_. (43) was confined to the rare earth ions of the C_{3h} symmetry of the ethylsulphates; therefore it is more applicable to discuss the experimental results of this work. For a discussion of the parallel field case in addition to that which will be done in the following section, the

reader is referred to Bethe (63).

The magnetic field parallel to the c-axis

The Hamiltonian for the magnetic field perturbation for the field in the direction of the c-axis (z-axis) from Equations 39 and 38 becomes,

$$H' = g(\gamma J)\beta H J_z \tag{42}$$

or

$$\begin{aligned} H' &= -\sum_{j=1}^{n} (e/2mc)(l_{z_j} + 2s_{z_j})H \\ &= M_z H, \end{aligned} \tag{43}$$

where H is the magnitude of the applied magnetic field and M_z is the magnetic moment operator.

The energy of a $\lambda \mu i$ state, using as a basis functions the type given by Equation 10, to second order is,

$$E_{\lambda\mu i} = \epsilon_{\lambda\mu i} + \langle \lambda\mu i | H' | \lambda\mu i \rangle + \sum_{\lambda' i'} \frac{|\langle \lambda'\mu i' | H' | \lambda\mu i \rangle|^2}{\epsilon_{\lambda\mu i} - \epsilon_{\lambda'\mu i'}} \tag{44}$$

where $H' = gHJ_z$ connects only those states for $\Delta\mu = 0$. This selection rule for the matrix elements is obtained from the following considerations. Since

$$J_z \, |\gamma JM\rangle = \hbar M |\gamma JM\rangle, \tag{45}$$

the selection rules on J_z for matrix elements using the $|\gamma JM\rangle$'s as basis functions is $\Delta M = 0$. Now since there is a one-to-one correspondence between μ quantum numbers and the M quantum numbers (Table 2), the selection rule on μ is then $\Delta\mu = 0$.

The energy of the $\lambda\tilde{\mu}i$ state where $\epsilon_{\lambda\mu i} = \epsilon_{\lambda\tilde{\mu}i}$ becomes,

$$E_{\lambda\tilde{\mu}i} = \epsilon_{\lambda\mu i} + \langle\lambda\tilde{\mu}i|H'|\lambda\tilde{\mu}i\rangle + \sum_{\lambda' i'} \frac{|\langle\lambda'\tilde{\mu}i'|H'|\lambda\tilde{\mu}i\rangle|^2}{\epsilon_{\lambda\mu i} - \epsilon_{\lambda'\mu i'}} . \tag{46}$$

From Murao, Spedding, and Good (43),

$$\begin{aligned}\langle\lambda'\tilde{\mu}i'|H'|\lambda\tilde{\mu}i\rangle &= -\eta_{\lambda'\mu i'}\eta_{\lambda\mu i}\langle\lambda'\mu i'|H'|\lambda\mu i\rangle^* \\ &= -\eta_{\lambda'\mu i'}\eta_{\lambda\mu i}\langle\lambda'\mu i'|H'|\lambda\mu i\rangle,\end{aligned} \tag{47}$$

where the matrix elements of H' as given by Equations 42 and 43 are real. Hence

$$E_{\lambda\tilde{\mu}i} = \epsilon_{\lambda\mu i} - \langle\lambda\mu i|H'|\lambda\mu i\rangle + \sum_{\lambda' i'} \frac{|-\eta_{\lambda'\mu i'}\eta_{\lambda\mu i}\langle\lambda'\mu i'|H'|\lambda\mu i\rangle|^2}{\epsilon_{\lambda\mu i} - \epsilon_{\lambda'\mu i'}}, \tag{48}$$

where $(\eta_{\lambda\mu i})^2 = 1$.

Therefore, the splitting defined as $\Delta_{\lambda\mu i} = E_{\lambda\mu i} - E_{\lambda\tilde{\mu}i}$ becomes,

$$\Delta_{\parallel}(\lambda\mu i) = |2\langle\lambda\mu i|H'|\lambda\mu i\rangle|, \tag{49}$$

where the second order terms cancel out. The splitting is therefore linear in the magnetic field H when the perturbation is carried out to second order. Now if $|\lambda\mu i\rangle$ is expanded as in Equation 10, the level splitting becomes,

$$\Delta_{\parallel}(\lambda\mu i) = \left|2\beta H\sum_{\gamma JM}|C^{\lambda\mu i}_{\gamma JM}|^2 g(\gamma J)\, M\right|. \tag{50}$$

A level splitting factor $g_{\parallel}(\lambda\mu i)$ is defined by the following equation,

$$\Delta_{\parallel}(\lambda\mu i) = g_{\parallel}(\lambda\mu i)\beta H. \tag{51}$$

So therefore,

$$\begin{aligned} g_{\parallel}(\lambda\mu i) &= (2/|\beta|\, H)|\langle\lambda\mu i|H'|\lambda\mu i\rangle| \\ &= 2\left|\sum_{\gamma JM}|C^{\lambda\mu i}_{\gamma JM}|^2 g(\gamma J)\, M\right|. \end{aligned} \tag{52}$$

The magnetic field even affects the non degenerate levels. The first order matrix elements of a non degenerate level $\langle\lambda\mu i|H'|\lambda\mu i\rangle$ are zero as will be shown below. However, there is a second order energy term which is not zero. Since for a non degenerate level $|\lambda\mu i\rangle = |\lambda\bar{\mu} i\rangle$, the diagonal matrix element of the $\lambda\mu i$ state is,

$$\begin{aligned}\langle \lambda\mu i | H' | \lambda\mu i \rangle &= \langle \lambda\tilde{\mu} i | H' | \lambda\tilde{\mu} i \rangle \\ &= -(\eta_{\lambda\mu i})^2 \langle \lambda\mu i | H' | \lambda\mu i \rangle^* \\ &= -\langle \lambda\mu i | H' | \lambda\mu i \rangle \\ &= 0 .\end{aligned} \tag{53}$$

Here extensive use of the theory as developed by Murao et al. (43) has been made and the fact that the matrix elements of H' are real (43) was used. The off diagonal matrix elements needed in the second order energy term are,

$$\begin{aligned}\langle \lambda'\mu i' | H' | \lambda\mu i \rangle &= \langle \lambda'\tilde{\mu} i' | H' | \lambda\tilde{\mu} i \rangle \\ &= -\eta_{\lambda'\mu i'} \eta_{\lambda\mu i} \langle \lambda'\mu i' | H' | \lambda\mu i \rangle^* \\ &= -\eta_{\lambda'\mu i'} \eta_{\lambda\mu i} \langle \lambda'\mu i' | H' | \lambda\mu i \rangle .\end{aligned} \tag{54}$$

Hence $\eta_{\lambda\mu i} = \pm 1$ and $\eta_{\lambda'\mu i'} = \mp 1$, or else the matrix element $\langle \lambda'\mu i' | H' | \lambda\mu i \rangle$ is zero.

To sum up, $H' = g\beta H J_z$ has no diagonal matrix elements for non degenerate $\lambda\mu i$ states, but has off diagonal elements between states for the same μ and for η numbers of the opposite sign. The energy of a non degenerate level to second order is then,

$$E_{\lambda\mu i} = \epsilon_{\lambda\mu i} + \sum_{\lambda' i'} \frac{\beta^2 H^2 \left| \sum_{\gamma J M} C^{\lambda'\mu i'*}_{\gamma J M} C^{\lambda\mu i}_{\gamma J M} g(\gamma J) M \right|^2}{\epsilon_{\lambda\mu i} - \epsilon_{\lambda'\mu i'}} . \qquad (55)$$

In spectra the absorption of energy between various states is observed. To analyse the spectra for the level splittings for the magnetic field parallel to the c-axis, transitions between various levels were observed and were analysed in accordance with the cases described below. In the following, when there will be no ambiguity, the λ subscript will be dropped. The second order energy terms for simplicity will be denoted by $SO(\mu)$. Whether the μ or $\hat{\mu}$ state splits toward

higher energy can only be determined from a detailed knowledge of the expansion coefficients $C_{\gamma JM}^{\lambda \mu i}$. Light polarized parallel and perpendicular to the c-axis will be labeled p and s respectively in the figures.

Case 1 In this case, transitions from the non degenerate $\mu = 0$ ground state to $\mu = \pm 2$ levels split by the magnetic field parallel to the c-axis will be considered. The transitions considered are shown in Figure 4a.

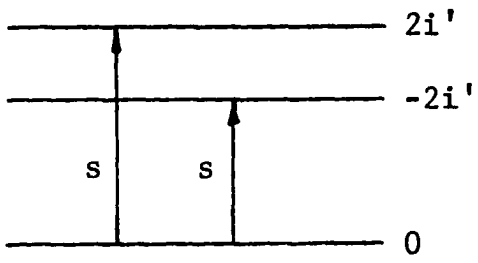

Figure 4a. Transition (0-2)

The energies to second order the $\mu = \pm 2$ level and the $\mu = 0$ level are given by Equations 44, 48 and 55 respectively.

$$E(2i') = \epsilon_{2i'} + \langle 2i'|H'|2i'\rangle + SO(2i'),$$

and

$$E(-2i') = \epsilon_{2i'} - \langle 2i'|H'|2i'\rangle + SO(2i') \quad . \qquad (56)$$

$$E(0i) = \epsilon_{0i} + SO(0i).$$

The splitting of the (0-2) line is given by,

$$\Delta_{line} = E(2i') - E(0i) - [E(-2i') - E(0i)]$$

$$= 2\,|\langle 2i'|\ H'\ |\ 2i'\rangle|$$

$$= \left|2\beta H \sum_{\gamma JM} |C^{\lambda 2i'}_{\gamma JM}|^2\ g(\gamma J)M\right| \qquad (57)$$

$$= \Delta_{||}(\pm 2i').$$

Case 2 The $\mu = \pm 1$ level at 31 cm^{-1} of the $^3H_6$ multiplet has energies of the type given by Equations 44 and 48 where here $\mu = 1$ and $\tilde{\mu} = -1$ will be used. The transitions to another $\mu = \pm 1$ level are depicted in Figure 4b

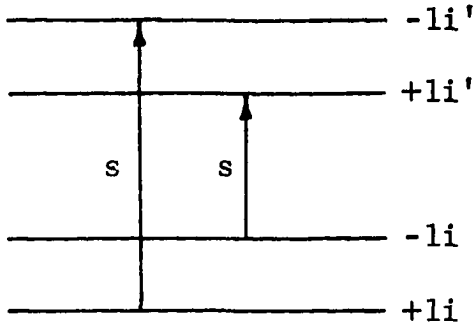

Figure 4b. Transition (1-1)

The energies of the transitions are given by,

$$E(1i') - E(-1i) = \epsilon_{1i'} - \epsilon_{1i} + \langle 1i'|\ H'\ |1i'\rangle - \langle -1i|\ H'\ |-1i\rangle + SO(1i') - SO(1i) \qquad (58a)$$

$$= \epsilon_{1i'} - \epsilon_{1i} - \langle -1i'|H'|-1i'\rangle - \langle -1i|H'|-1i\rangle + SO(1i') - SO(1i),$$

and

$$E(-1i') - E(1i) = \epsilon_{1i'} - \epsilon_{1i} + \langle -1i' | H' | -1i' \rangle - \langle 1i | H' | 1i \rangle + SO(1i') - SO(1i) \quad (58b)$$

$$= \epsilon_{1i'} - \epsilon_{1i} + \langle -1i' | H' | -1i' \rangle + \langle -1i | H' | -1i \rangle + SO(1i') - SO(1i) \; .$$

The line splitting is given by,

$$\Delta_{line} = E(-1i') - E(1i) - [E(1i') - E(-1i)]$$

$$= 2\langle -1i' | H' | -1i' \rangle + 2\langle -1i | H' | -1i \rangle$$

$$= \Delta_{||}(\pm 1i') + \Delta_{||}(\pm 1i) \; . \quad (59)$$

Therefore,

$$\Delta_{||}(\pm 1i') = \Delta_{line} - \Delta_{||}(\pm 1i) \; . \quad (60)$$

Case 3 The other possibility to consider for transitions to a $\mu = \pm 1$ level from a $\mu = \pm 1$ level is shown in Figure 4c.

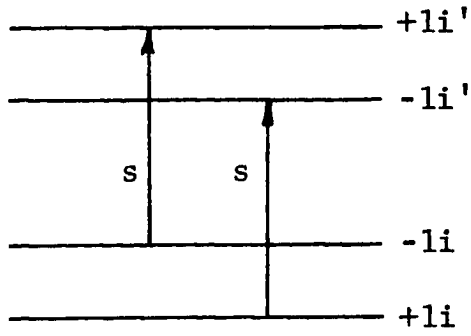

Figure 4c. Transition (1-1)

Using the results of Case 2,

$$\Delta_{line} = \left| E(-1i') - E(1i) - \left[E(1i') - E(-1i)\right] \right|$$

$$= \left| \langle -1i'|H'|-1i'\rangle - \langle 1i|H'|1i\rangle - \left[\langle 1i'|H'|1i'\rangle - \langle -1i|H'|-1i\rangle\right] \right| \qquad (61)$$

$$= \left| 2\langle -1i|H'|-1i\rangle - 2\langle 1i'|H'|1i'\rangle \right| .$$

$$\Delta_{line} = \left| \Delta_{\parallel}(\pm 1i) - \Delta_{\parallel}(\pm 1i') \right| .$$

So for $\Delta_{\parallel}(\pm 1i) > \Delta_{\parallel}(\pm 1i')$, $\Delta_{\parallel}(\pm 1i') = \Delta_{\parallel}(\pm 1i) - \Delta_{line}$; and for $\Delta_{\parallel}(\pm 1i') > \Delta_{\parallel}(\pm 1i)$, $\Delta_{\parallel}(\pm 1i') = \Delta_{line} + \Delta_{\parallel}(\pm 1i)$.

Case 4 Another case to consider is a transition from a $\mu = \pm 1$ level to a $\mu = \pm 2$ level of the type shown in Figure 4d.

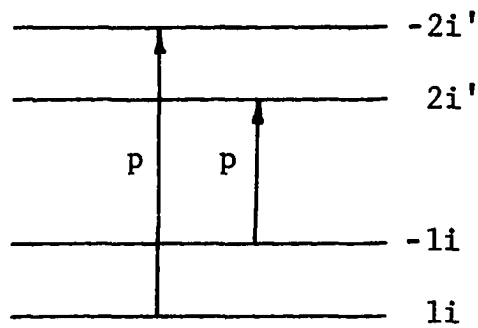

Figure 4d. Transition (1-2)

Using the results of the previous cases, the line splitting is,

$$\Delta_{line} = E(-2i') - E(1i) - \left[E(2i') - E(-1i)\right]$$

$$= \langle -2i|H'|-2i'\rangle - \langle 1i|H'|1i\rangle - \left[\langle 2i|H'|2i'\rangle - \langle -1i|H'|-1i\rangle\right] \qquad (62)$$

$$= 2\langle -1i|H'|-1i\rangle + 2\langle -2i'|H'|-2i'\rangle .$$

$\Delta_{line} = \Delta_{\parallel}(\pm 1i) + \Delta_{\parallel}(\pm 2i')$.

So,

$$\Delta_{\parallel}(\pm 2i') = \Delta_{line} - \Delta_{\parallel}(\pm 1i) \tag{63}$$

Case 5 The next case to consider is a transition from a $\mu = \pm 1$ level to a $\mu = \pm 2$ level of the type shown in Figure 4e.

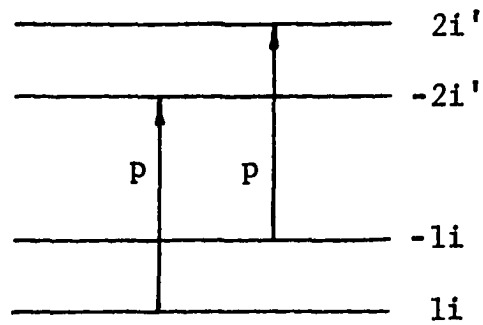

Figure 4e. Transition (1-2)

Again using the results of the previous cases considered, the line splitting is,

$$\begin{aligned}\Delta_{line} &= \left|E(-2i') - E(1i) - \left[E(2i') - E(-1i)\right]\right| \\ &= \left|\langle -2i'|H'|-2i'\rangle - \langle 1i|H'|1i\rangle - \left[\langle 2i'|H'|2i'\rangle - \langle -1i|H'|-1i\rangle\right]\right| \\ &= \left|\Delta_{\parallel}(\pm 1i) - \Delta_{\parallel}(\pm 2i')\right|\end{aligned} \tag{64}$$

So for $\Delta_{\parallel}(\pm 1i) > \Delta_{\parallel}(\pm 2i')$, $\Delta_{\parallel}(\pm 2i') = \Delta_{\parallel}(\pm 1i) - \Delta_{line}$ and $\Delta_{\parallel}(\pm 1i) = \Delta_{line} + \Delta_{\parallel}(\pm 2i')$; and for $\Delta_{\parallel}(\pm 1i) < \Delta_{\parallel}(\pm 2i')$ $\Delta_{\parallel}(\pm 2i') = \Delta_{line} + \Delta_{\parallel}(\pm 1i)$ and $\Delta_{\parallel}(\pm 1i) = \Delta_{\parallel}(2i') - \Delta_{line}$.

Case 6 The last case to consider are transitions from a $\mu = \pm 1$ level to $\mu = 3$ levels. These transitions are pictured in Figure 4f. From the figure it is obvious that the $\mu = \pm 1$ level splitting is given by $\Delta_{line} = \Delta_{\parallel}(\pm 1i)$.

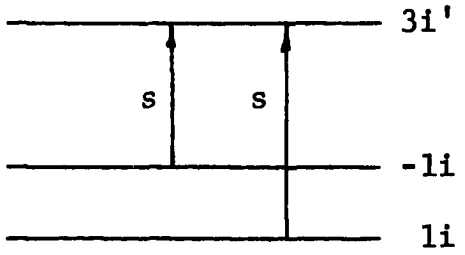

Figure 4f. Transition (1-3).

Magnetic field perpendicular to the c-axis

For the magnetic field perpendicular to the c-axis, the perturbation Hamiltonian, Equations 39 and 38 becomes,

$$H' = g(\gamma J)\beta[H_x J_x + H_y J_y]$$
$$= g(\gamma J)\beta H[J_x \cos\phi_m + J_y \sin\phi_m], \tag{65}$$

or,

$$H' = -(e/2mc)\sum_j [(l_{x_j} + 2s_{x_j})H_x + (l_{y_j} + 2s_{y_j})H_y]$$
$$= M_x H_x + M_y H_y \qquad (66)$$
$$= H[M_x \cos\phi_m + M_y \sin\phi_m],$$

$$H_x = H\cos\phi_m \text{ and } H_y = H\sin\phi_m, \qquad (67)$$

where H is the magnitude of the applied field in a plane perpendicular to the c-axis, ϕ_m is the angle the magnetic field makes with the crystallographic x-axis pictured in Figure 3, and M_x and M_y are the magnetic moment operators. For an extensive treatment of the perpendicular field case, the reader is referred to Murao, Spedding, and Good (43).

The perturbation H' as given by Equation 65 can be put into another form using the step up and step down operators defined by, $J_+ = J_x + iJ_y$ and $J_- = J_x - iJ_y$.

$$H' = g(\gamma J)\beta H[J_+ e^{-i\phi_m} + J_- e^{i\phi_m}]. \qquad (68)$$

Since J_+ and J_- connect states for $\Delta M = \pm 1$, it follows that H' connects states for $\Delta\mu = \pm 1$ (43). Therefore H' as given by Equation 65 or 66 has no diagonal matrix elements. To remove the degeneracy, one has to go to second order. The method employed is that given by Schiff (60).

The resultant levels, or states, no longer have μ as a good quantum number since all μ states are connected in some order of the perturbation H' of Equations 65 or 66. The degree to which the μ quantum number fails to be a good quantum number depends on the magnitude of the magnetic field H.

The energy of the $\mu = \pm 1$ levels for the magnetic field perpendicular to the c-axis is given by Murao et al. (43) as,

$$E(\pm 1,i) = \epsilon_{1,i} + \sum_j \left\{ \frac{|a_{ji}|^2}{\epsilon_{1,i} - \epsilon_{0j}} + \frac{|b_{ij}|^2}{\epsilon_{1,i} - \epsilon_{2j}} \right\} H^2 \pm \left| \sum_j \frac{n_{1,i}\, n_{0j}\, (a_{ji})^2}{\epsilon_{1,i} - \epsilon_{0j}} \right| H^2, \tag{69}$$

and the energy of a $\mu = \pm 2$ level is,

$$E(\pm 2,i) = \epsilon_{2,i} + \sum_j \left\{ \frac{|b_{ji}|^2}{\epsilon_{2i} - \epsilon_{1j}} + \frac{|c_{ij}|^2}{\epsilon_{2i} - \epsilon_{3j}} \right\} H^2 \pm \left| \sum_j \frac{n_{2i}\, n_{3j}\, (c_{ij})^2}{\epsilon_{2i} - \epsilon_{3j}} \right| H^2, \tag{70}$$

where the a_{ij}'s, b_{ij}'s and c_{ij}'s are defined by the following matrix elements,

$$\begin{aligned} \langle 0i|H'|1j\rangle &= a_{ij}\, e^{i\phi_m} H \\ \langle 1i|H'|2j\rangle &= b_{ij}\, e^{i\phi_m} H \\ \langle 2i|H'|3j\rangle &= c_{ij}\, e^{i\phi_m} H. \end{aligned} \tag{71}$$

The angle ϕ_m is defined in Figure 3.

A splitting factor $g_\perp(\lambda\mu i)$ will be defined by,

$$\Delta_\perp(\lambda\mu i) = g_\perp(\lambda\mu i)\,\beta^2 H_\perp^2 \tag{72}$$

using the energy splittings implied by Equations 69 and 70. Thus for the $\mu = \pm 1$ level,

$$g_\perp(\lambda 1 i) = 2(1/\beta^2)\left|\sum_j \frac{n_{1i}\, n_{0j}\,(a_{ji})^2}{\epsilon_{1i} - \epsilon_{0j}}\right| \tag{73}$$

and for the $\mu = \pm 2$ level,

$$g_\perp(\lambda 2 i) = 2(1/\beta^2)\left|\sum_j \frac{n_{2i}\, n_{3j}\,(c_{ij})^2}{\epsilon_{2i} - \epsilon_{3j}}\right| \tag{74}$$

The wave functions for the levels are (43),

$$|(\pm 1) i s\rangle = \frac{1}{\sqrt{2}}\left[\,|1i\rangle + s A_i\, e^{i2\phi_m}\,|-1i\rangle\right], \tag{75}$$

and

$$|(\pm 2) i s\rangle = \frac{1}{\sqrt{2}}\left[\,|2i\rangle + s B_i\, e^{-i2\phi_m}\,|-2i\rangle\right], \tag{76}$$

where $s = \pm 1$ (+ corresponding to the level splitting to higher energy and - to the one splitting to lower energy), and A_i and B_i are defined below.

$$A_i = \frac{-\left|\sum_j \frac{n_{1i}\, n_{0j}\, (a_{ji})^2}{\epsilon_{1i} - \epsilon_{0j}}\right|}{\sum_j \frac{n_{1i}\, n_{0j}\, (a_{ji})^2}{\epsilon_{1i} - \epsilon_{0j}}}, \tag{77}$$

and

$$B_i = \frac{-\left|\sum_j \frac{n_{2i}\, n_{3j}\, (c_{ji})^2}{\epsilon_{2i} - \epsilon_{3j}}\right|}{\sum_j \frac{n_{2i}\, n_{3j}\, (c_{ji})^2}{\epsilon_{2i} - \epsilon_{3j}}} \tag{78}$$

The higher order terms in the wave functions coming about because H' connects states differing by $\Delta\mu = \pm 1$ have been neglected.

When these higher order terms are included for the wave function representing the $\mu = 0$ ground state, the wave function becomes in first order,

$$|(0)\ i\rangle = |0i\rangle + \sum_j \left\{ \frac{a_{ij}^{+}\, e^{-i\phi_m} H |1j\rangle}{\epsilon_{0i} - \epsilon_{1j}} - \frac{n_{1j} n_{0i}\, a_{ji}\, e^{i\phi_m} H |-1j\rangle}{\epsilon_{0i} - \epsilon_{1j}} \right\}. \tag{79}$$

Using the electric dipole operator described by Equations 31, the matrix elements used in the transition probability (Equation 32) for the even numbered electron case are given

below (43).

$$\langle (0)i | P_\perp | (\pm 2) i' s' \rangle \tag{80}$$
$$= \frac{1}{\sqrt{2}} e^{-i\phi} \left[\langle 0i | P_x | 2i' \rangle - B_{i'} \eta_{0i} \eta_{2i'} s' \langle 0i | P_x | 2i' \rangle^* e^{i2(\phi - \phi_m)} \right].$$

$$\langle (\pm 1) i s | P_\perp | (3) i' \rangle \tag{81}$$
$$= \frac{1}{\sqrt{2}} e^{-i\phi} \left[\langle 1i | P_x | 3i' \rangle - A_i \eta_{1i} \eta_{3i'} s \langle 1i | P_x | 3i' \rangle^* e^{i2(\phi - \phi_m)} \right].$$

$$\langle (\pm 1) i s | P_\perp | (\pm 1) i' s' \rangle \tag{82}$$
$$= \frac{1}{2} e^{i(2\phi_m + \phi)} \left[s' A_{i'} \langle 1i | P_x | -1i' \rangle - A_i \eta_{1i} \eta_{1i'} s \langle 1i | P_x | -1i' \rangle^* e^{-i(4\phi_m + 2\phi)} \right].$$

$$\langle (\pm 1) i s | P_{11} | (\pm 2) i' s' \rangle \tag{83}$$
$$= \frac{1}{2} e^{-i2\phi_m} \left[s' B_{i'} \langle 1i | P_z | -2i' \rangle - A_i \eta_{1i} \eta_{2i'} \langle 1i | P_z | -2i' \rangle^* \right].$$

$$\langle (0)i | P_{11} | (\pm 2) i' s' \rangle \tag{84}$$
$$= e^{-i\phi_m} H \left\{ \sum_j \frac{a_{ij} s' B_{i'} \langle 1j | P_z | -2i' \rangle}{\epsilon_{0i} - \epsilon_{1j}} + \sum_j \frac{\eta_{1j} \eta_{0i} a_{ji} \eta_{1j} \eta_{2i'} \langle 1j | P_z | -2i' \rangle^*}{\epsilon_{0i} - \epsilon_{1j}} \right\}.$$

$$\langle (0)i | P_\perp | (\pm 1) j' s' \rangle$$

$$= \frac{H}{\sqrt{2}} \sum_j \left\{ \frac{a_{ij} e^{i(3\phi_m + \phi)}}{\epsilon_{oi} - \epsilon_{1j}} \langle 1j | P_x | -1 j' \rangle \right.$$

$$\left. + \frac{\eta_{1j'} \eta_{oi} a^*_{ij} e^{-i(\phi_m + \phi)}}{\epsilon_{oi} - \epsilon_{1j}} \langle 1j | P_x | -1 j' \rangle^* \right\}. \quad (85)$$

According to Murao et al. (43) if β_{33} and β_{53} are zero or sufficiently small the matrix elements of the dipole operator become,

$$\begin{aligned} \langle \mu i | P_x | \mu' i' \rangle &= \text{real} \\ \langle \mu i | P_y | \mu' i' \rangle &= \text{imaginary} \\ \langle \mu i | P_z | \mu' i' \rangle &= \text{real} . \end{aligned} \quad (86)$$

If α_{33} and α_{53} are zero or sufficiently small "real" and "imaginary" are interchanged. In the foregoing work the matrix elements of P listed below have been used (43).

$$\begin{aligned} \langle 0_i | P_\perp | 2_j \rangle &= \langle 0_i | P_x | 2_j \rangle e^{-i\phi} \\ \langle 1_i | P_\perp | 3_j \rangle &= \langle 1_i | P_x | 3_j \rangle e^{-i\phi} \\ \langle 1_i | P_\perp | -1_j \rangle &= \langle 1_i | P_x | -1_j \rangle e^{i\phi} \\ \langle 2_i | P_\perp | -2_j \rangle &= \langle 2_i | P_x | -2_j \rangle e^{-i\phi} , \end{aligned} \quad (87)$$

and other matrix elements are obtained with the help of,

$$\langle \hat{\mu} i | P_r | \hat{\mu}' i' \rangle = -\eta_{\mu i} \eta_{\mu' i'} \langle \mu i | P_r | \mu' i' \rangle^* . \quad (88)$$

For the experimental investigations carried out in this work, the angles ϕ and ϕ_m were equal, which means the vectors

$\underline{e}_{\perp}$ and $\underline{H}$ (defined in Figure 3) are parallel. $\underline{e}_{\perp}$ is the direction of polarization of the incident light and $\underline{H}$ is the applied magnetic field.

In order to interpret the data in a consistent manner, it was found that one had to take the α's to be nearly zero so that the matrix elements, as given by Equations 86, of P_x are imaginary such that $\langle P_x \rangle^* = -\langle P_x \rangle$. The matrix elements of the electric dipole operator for transitions of interest are given below.

$$\langle (0)\lambda | P_{\perp} | (\pm 2)\lambda' s' \rangle = \frac{1}{\sqrt{2}} e^{-i\phi_m} \langle 0\lambda | P_x | 2\lambda' \rangle [1 + B_{\lambda'} \eta_{0\lambda} \eta_{2\lambda'} s'] . \tag{89}$$

$$\langle (\pm 1)\lambda s | P_{\perp} | (3)\lambda' \rangle = \frac{1}{\sqrt{2}} e^{-i\phi_m} \langle 1\lambda | P_x | 3\lambda' \rangle [1 + A_{\lambda} \eta_{1\lambda} \eta_{3\lambda'} s] . \tag{90}$$

$$\langle (\pm 1)\lambda s | P_{\perp} | (\pm 1)\lambda' s' \rangle = \frac{1}{2} \langle 1\lambda | P_x | -1\lambda' \rangle [s' A_{\lambda'} e^{3i\phi_m} + A_{\lambda} s \eta_{1\lambda} \eta_{1\lambda'} e^{-3i\phi_m}] . \tag{91}$$

$$\langle (\pm 1)\lambda s | P_{\parallel} | (\pm 2)\lambda' s' \rangle = e^{-2i\phi_m} \langle 1\lambda | P_z | -2\lambda' \rangle [s' B_{\lambda'} + A_{\lambda} \eta_{1\lambda} \eta_{2\lambda'} s] . \tag{92}$$

$$\langle (0)i | P_{\parallel} | (\pm 2)\lambda' s' \rangle = \sum_j \frac{a_{ij} e^{-i\phi_m} H}{\epsilon_{0i} - \epsilon_{1j}} \langle 1j | P_{\pm} | -2\lambda' \rangle [s' B_{\lambda'} - \eta_{0i} \eta_{2\lambda'}]. \tag{93}$$

$$\langle (0)i | P_{\perp} | (\pm 1)\lambda' s' \rangle = \frac{1}{\sqrt{2}} \sum_j \frac{a_{ij} e^{i\phi_m} H}{\epsilon_{0i} - \epsilon_{1j}} \langle 1j | P_x | -1\lambda' \rangle [s' A_{\lambda'} e^{i3\phi_m} - \eta_{1\lambda'} \eta_{0i} e^{-i3\phi_m}]. \tag{94}$$

Since the matrix elements of M_x are real (43), the a_{ij}'s are real and this property has been used in the above work.

In order to analyse the observed spectra in light of the theory, the A's, B's and η's must be determined for each level. These terms for the $\mu = 0$ and $\mu = \pm 1$ levels of the ground multiplet can be determined in the following way. To do this, the wave functions representing these states are expanded in terms of the eigenfunctions of the free ion as in Equation 10, but here the terms arising from intermultiplet interactions will be neglected. The ground multiplet level structure will be assumed to be the theoretical one given by Wong and Richman (39). If the wave function representing the lowest energy $\mu = 0$ state is $|0i\rangle = a\phi_{60} + (b/\sqrt{2})(\phi_{66}+\phi_{6-6})$, then $\eta_{0i} = 1$, and if the wave function representing the

lowest energy $\mu = \pm 1$ state is $|1i\rangle = a'\phi_{61} + b'\phi_{6-5}$ and $|-1i\rangle = a'\phi_{6-1} + b'\phi_{65}$, then $\eta_{1i} = -1$, where use of the time reversal property of Equations 40 and 41 was made. When one considers the only significant contribution to A_i arises from the matrix element between the lowest energy $\mu = 0$ level and $\mu = \pm 1$ level (the other $\mu = 0$ levels are quite energetically far from the $\mu \pm 1$ level) A_i becomes equal to 1 since $\eta_{0i} = 1$, $\eta_{1i} = -1$, and $\epsilon_{1i} > \epsilon_{0i}$. Using these assignments of A_i and the η's for the lowest energy $\mu = 0$ and $\mu = \pm 1$ levels of the $^3H_6$ multiplet, Tables 5 through 10 give the results of the matrix elements of Equations 89 through 94 for various types of levels to which transitions are made.

Table 5. $\langle(0)\ i|P_\perp|(\pm 2)\ i's'\rangle$

s'	$\eta_{2i'}$	$B_{i'}$	I^a
1	1	1	1
1	1	-1	0
1	-1	1	0
1	-1	-1	1
-1	-1	-1	0
-1	-1	1	1
-1	1	-1	1
-1	1	1	0

[a]Where $I = \left|(2/\sqrt{2})\ e^{-i\phi_m}\langle 0i|P_x|2i'\rangle\right|^2$.

Table 6. $\langle(0)\ i \mid P_{\parallel} \mid (\pm 2)\ i's' \rangle$

s'	$\eta_{2i'}$	$B_{i'}$	I^a
1	1	1	0
1	1	-1	1
1	-1	1	1
1	-1	-1	0
-1	-1	-1	1
-1	-1	1	0
-1	1	-1	0
-1	1	1	1

[a] Where $I = \left| 2 \sum_j \frac{a_{ij}\, e^{-i\phi_m} H}{\epsilon_{0i} - \epsilon_{1j}} \langle 1j | P_z | -2i' \rangle \right|^2$.

Table 7. $\langle(\pm 1)\ is \mid P_{\parallel} \mid (\pm 2)\ i's' \rangle$

s	s'	$B_{i'}$	$\eta_{2i'}$	I^a
1	1	1	1	0
1	1	1	-1	1
1	1	-1	1	1
1	1	-1	-1	0
1	-1	1	1	1
1	-1	1	-1	0
1	-1	-1	1	0
1	-1	-1	-1	1
-1	1	1	1	1
-1	1	1	-1	0
-1	1	-1	1	0
-1	1	-1	-1	1
-1	-1	1	1	0
-1	-1	1	-1	1
-1	-1	-1	1	1
-1	-1	-1	-1	0

[a] Where $I = \left| e^{-2i\phi_m} \langle 1i | P_z | -2i' \rangle \right|^2$

Table 8. $\langle(\pm 1)\ is\ |\ P_\perp\ |\ (3)\ i'\rangle$

s	$\eta_{3i'}$	I^a
1	1	o
1	-1	1
-1	-1	0
-1	1	1

[a]Where $I = \left| (2/\sqrt{2})\ e^{-i\phi_m} \langle 1i|P_x|3i'\rangle \right|^2$.

Table 9. $\langle(\pm 1)\ is\ |\ P_\perp\ |\ (\pm 1)\ i's'\rangle$

s	s'	$A_{i'}$	$\eta_{1i'}$	I^a	I'^b
1	1	1	1	0	1
1	1	1	-1	1	0
1	1	-1	1	1	0
1	1	-1	-1	0	1
1	-1	1	1	1	0
1	-1	1	-1	0	1
1	-1	-1	1	0	1
1	-1	-1	-1	1	0
-1	1	1	1	1	0
-1	1	1	-1	0	1
-1	1	-1	1	0	1
-1	1	-1	-1	1	0
-1	-1	1	1	0	1
-1	-1	1	-1	1	0
-1	-1	-1	1	1	0
-1	-1	-1	-1	0	1

[a]Where $I = |\langle 1i|P_x|-1i'\rangle \cos 3\phi_m|^2$.

[b]Where $I' = |\langle 1i|P_x|-1i'\rangle \sin 3\phi_m|^2$.

Table 10. $\langle (0)i | P_{\perp} | (\pm 1) i's' \rangle$

s'	$\eta_{1i'}$	$A_{i'}$	I^a	I'^b
1	1	1	0	1
1	1	-1	1	0
1	-1	1	1	0
1	-1	-1	0	1
-1	1	1	1	0
-1	1	-1	0	1
-1	-1	1	0	1
-1	-1	-1	1	0

[a] Where $I = \frac{1}{2} \left| \sum_j \frac{H\, e^{i\phi_m}\, a_{ij} \langle 1j | P_x | -1i' \rangle}{\varepsilon_{0i} - \varepsilon_{1j}} \cos 3\phi_m \right|^2$.

[b] Where $I' = \frac{1}{2} \left| \sum_j \frac{H\, e^{i\phi_m}\, a_{ij} \langle 1j | P_x | -i' \rangle}{\varepsilon_{0i} - \varepsilon_{1j}} \sin 3\phi_m \right|^2$.

The intensities of the absorbed radiation are proportional to the I and the I'. The 0 means that the intensity is zero, and 1 means that the intensity is proportional to I or I'. It should be recalled that the above tables are for the odd parity α's equal to zero (or at least sufficiently small), $\eta_{0i} = 1$, $\eta_{1i} = -1$, and $A_i = 1$. As shall be pointed out in the discussion of the data, the odd parity α's are smaller than the odd parity β's but are not actually equal to zero. However to explain the majority of the spectra, the α's can be considered to be zero. Any exceptions will be noted.

In the following paragraphs several different types of transitions will be discussed. These discussions will follow very closely those given for the parallel magnetic field case. From the measurement of the line splittings, the splitting of the individual levels will be inferred. In the following discussions, explicit use of the data in Tables 5 through 10 has been made.

Case 1 In this case, transitions from the non degenerate $\mu = 0$ ground state to the $\mu = \pm 2$ levels, split by the magnetic field perpendicular to the c-axis, will be considered. The transitions considered are shown in Figures 5a and 5b. The energies of the components of the $\mu = \pm 2$ levels are

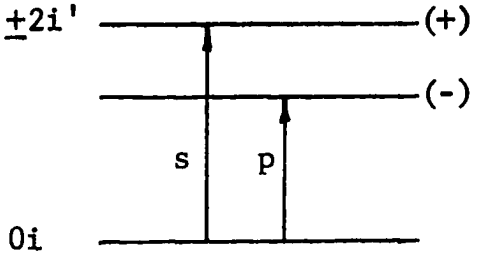

Figure 5a. Transitions for $\eta_{2i'} = \pm 1$, $B_{2i'} = \pm 1$

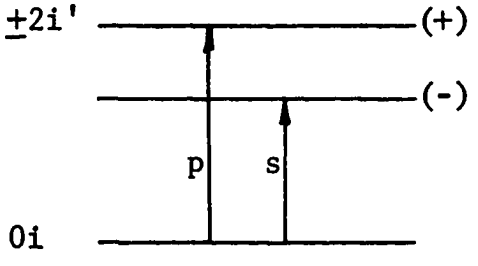

Figure 5b. Transitions for $\eta_{2i'} = \mp 1$, $B_{2i'} = \pm 1$

given by Equation 70. Here as for the parallel field case, the second order shifting of the levels cancels out when line splittings are measured. Thus the splitting of the (0-2) line

(as it appears in both polarizations) is,

$$\Delta_{line} = \Delta_{\perp}(\pm 2i') , \tag{95}$$

where the λ subscript has been suppressed.

Case 2 The transitions from the $\mu = \pm 1$ level of the ground multiplet to $\mu = 3$ levels will be considered. The transitions are shown in Figures 5c and 5d. The dotted line

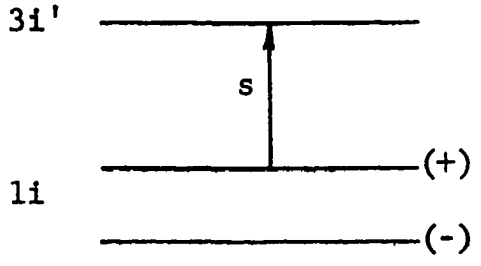

Figure 5c. Transition for $\eta_{3i'} = -1$

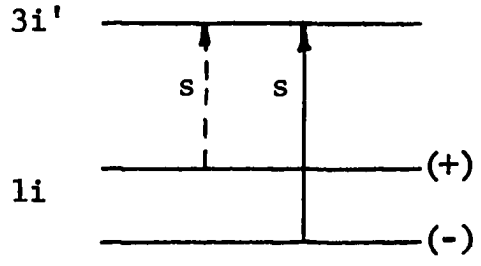

Figure 5d. Transition for $\eta_{3i'} = 1$

in Figure 5d is for the transition that is observed in the $^3F_4$ multiplet, which means that the α's are not actually zero but have some finite value. Therefore, for the $^3F_4$ multiplet, the splitting of the $\mu = \pm 1$ level of the ground multiplet is obtained from the splitting of the (1-3) line when observed as given by the equation below,

$$\Delta_{line} = \Delta_{\perp}(\pm 1i) \tag{96}$$

Case 3 In this case, the transitions from the $\mu = \pm 1$ level of the ground multiplet to the $\mu = \pm 2$ levels of excited multiplets will be considered. The transitions are shown in

in Figures 5e and 5f. The level splittings are obtained in

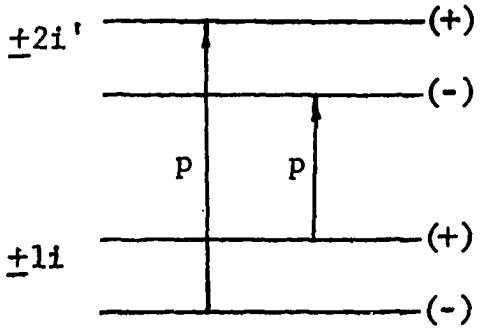

Figure 5e. Transitions for $\eta_{2i'} = \pm 1$, $B_{i'} = \pm 1$

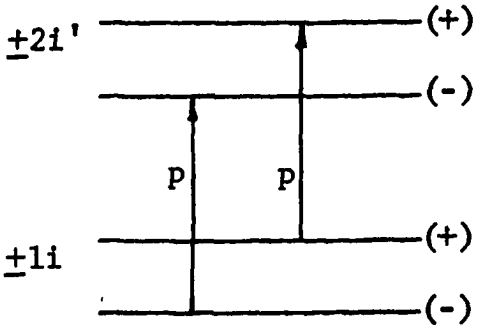

Figure 5f. Transitions for $\eta_{2i'} = \pm 1$, $B_{i'} = \mp 1$

the following manner. For the Figure 5e case the line splitting is,

$$\begin{aligned} \Delta_{line} &= E_+(2i') - E_-(1i) - \left[E_-(2i') - E_+(1i)\right] \\ &= \Delta_\perp(\pm 2i') + \Delta_\perp(\pm 1i). \end{aligned} \tag{97}$$

So,

$$\Delta(\pm 1i) = \Delta_{line} - \Delta_\perp(\pm 2i'). \tag{98}$$

For the Figure 5f case,

$$\begin{aligned} \Delta_{line} &= \left|E_-(2i') - E_-(1i) - \left[E_+(2i') - E_+(1i)\right]\right| \\ &= \left|\Delta_\perp(\pm 1i) - \Delta_\perp(\pm 2i')\right| \end{aligned} \tag{99}$$

So,

$$\Delta(\pm 1i) = \Delta_{line} + \Delta_\perp(\pm 2i') \tag{100}$$

for $\Delta_\perp(\pm 2i') < \Delta_\perp(\pm 1i)$, as it is for all the cases measured.

Case 4 Another case to consider are transitions from the $\mu = \pm 1$ level of the ground multiplet to $\mu = \pm 1$ levels of excited multiplets. These transitions are pictured in Figures 5g and 5h. In Figure 5g the splitting of the (1-1) line for

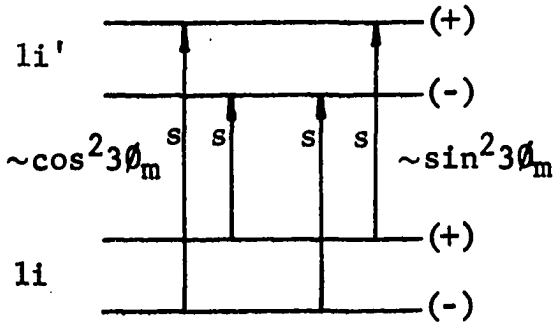

Figure 5g. Transitions for $\eta_{1i'} = \pm 1$, $A_{i'} = \pm 1$

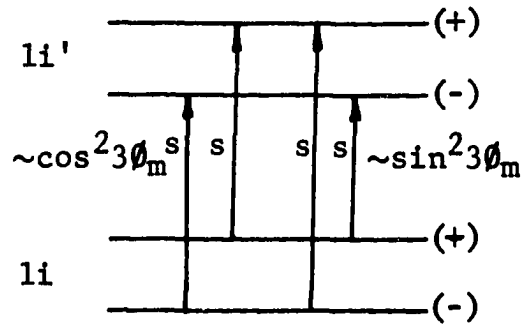

Figure 5h. Transitions for $\eta_{1i'} = \pm 1$, $A_{i'} = \mp 1$

$\phi_m = 0$ is,

$$\begin{aligned} \Delta_{line} &= E_+(1i) - E_-(1i) - \left[E_-(1i) - E_+(1i) \right] \\ &= \Delta_\perp(\pm 1i') + \Delta_\perp(\pm 1i). \end{aligned} \tag{101}$$

So,

$$\Delta_\perp(\pm 1i') = \Delta_{line} - \Delta_\perp(\pm 1i) \tag{102}$$

In Figure 5h the splitting of the (1-1) line for $\phi_m = 0$ is,

$$\begin{aligned} \Delta_{line} &= \left| E(1i') - E(1i) - \left[E_-(1i') - E_-(1i) \right] \right| \\ &= \left| \Delta_\perp(\pm 1i') - \Delta_\perp(\pm 1i) \right|. \end{aligned} \tag{103}$$

So for $\Delta_\perp(\pm 1i') < \Delta_\perp(\pm 1i)$,

$$\Delta_\perp(\pm 1i') = \Delta_{line} + \Delta_\perp(\pm 1i) \tag{104}$$

and for $\Delta_\perp(\pm 1i') < \Delta_\perp(\pm 1i)$,

$$\Delta_\perp(\pm 1i') = \Delta_\perp(\pm 1i) - \Delta_{line}. \qquad (105)$$

Case 5 The last case to consider is that pictured in Figures 5i and 5j which are for transitions from the $\mu = 0$ ground state to $\mu = \pm 1$ levels of excited multiplets. Any line splitting would have to be measured at two different angles.

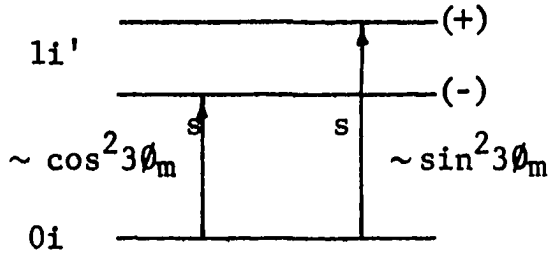

Figure 5i. Transitions for $\eta_{1i'} = \pm 1$, $A_{i'} = \pm 1$

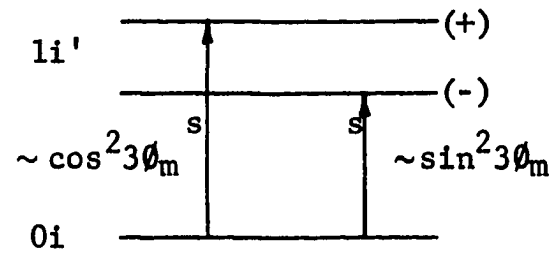

Figure 5j. Transitions for $\eta_{1i'} = \pm 1$, $A_{i'} = \mp 1$

An additional selection rule over and above the electric dipole and/or magnetic dipole selection rules is one involving the η's (43). Transitions between two non degenerate states are (43),

$$\langle \lambda \mu i | P_r | \lambda' \mu' i' \rangle = - \eta_{\lambda \mu i} \eta_{\lambda' \mu' i'} \langle \lambda \mu i | P_r | \lambda' \mu' i' \rangle^*, \qquad (106)$$

since $|\lambda \mu i\rangle = |\lambda \tilde{\mu} i\rangle$ for a non degenerate state. Thus if the matrix elements of P_r are real, it must be that $\eta_{\lambda \mu i} \cdot \eta_{\lambda' \mu' i'} = -1$ or else the matrix element is zero; or if the matrix elements of P_r are imaginary it must be that

$\eta_{\lambda\mu i}\,\eta_{\lambda'\mu'i'} = 1$ or else the matrix element is zero. It will be shown that it is the latter case which seems to fit the experiment for r = z, i.e., the matrix elements of P_z are imaginary which implies that the α_{33} and α_{53} are sufficiently small so as to be neglected for the most part. The choice of the odd parity α's = 0 and β's $\neq$ 0 involves choosing the η's properly and then fitting the experimental data.

It can be shown that the wave function representing the lowest $\mu = 3$ level of the $^3F_4$ multiplet is

$$\phi_{3i} = (1/\sqrt{2})[\phi_{43} - \phi_{4-3}] \qquad (107)$$

where the intermultiplet interactions have been neglected. Therefore,

$$T\phi_{3i} = \eta_{3i}\phi_{3i} = \phi_{3i} \qquad (108)$$

and hence, $\eta_{3i} = 1$. It was shown previously that $\eta_{0i} = 1$ for the $\mu = 0$ ground state of the ground $^3H_6$ multiplet. Hence in order to observe this (0-3) transition it must be that the matrix elements of P_z are imaginary. A similar type of argument can be used for the lowest $\mu = 3$ level of the $^1G_4$ multiplet.

The assignment of $\eta_{3i} = 1$ for the lowest $\mu = 3$ level of the $^3F_4$ multiplet is in agreement with the data obtained for the magnetic field perpendicular to the c-axis. This is

shown in the experimental section.

If the low lying $\mu = 3$ levels of the $^3F_4$ and $^1G_4$ multiplets are represented by wave functions of the type given by Equation 107, then the high $\mu = 3$ levels are represented by,

$$\phi_{3i} = (1/\sqrt{2})[\phi_{43} + \phi_{4-3}] \qquad (109)$$

and $\eta_{3i} = -1$. Hence for the matrix elements of P_z imaginary, there should be no transitions to these high lying $\mu = 3$ levels. Experimentally this more or less is what is observed. For these two multiplets there is only one strong (0-3) line in each multiplet which is identified as the transition from the $\mu = 0$ level of the ground multiplet to the $\mu = 3$ levels of these two multiplets. There are other (0-3) lines but they are absorbed quite weakly. Both lines will probably be observed to some extent because the odd parity α's are not strictly zero as indicated in previous remarks when discussing the perpendicular field case. The additional selection rule on the η's is similar to the one found by Grohmann, Hellwege, and Kahle (64) for D_{3h} symmetry.

If for the two $\mu = 3$ levels of the $^3F_3$ multiplet, the upper (-) and lower (+) levels are represented by the wave function,

$$\phi_{3i} = (1/\sqrt{2})[\phi_{33} \mp \phi_{3-3}] \qquad (110)$$

then $\eta_{3i'} = -1$ for the upper $\mu = 3$ level and $\eta_{3i'} = 1$ for the lower $\mu = 3$ level of this multiplet. This assignment of the η's agrees with the data obtained for the magnetic field perpendicular to the c-axis as will be pointed out later.

EXPERIMENTAL INVESTIGATION

Experimental Apparatus and Procedure

The spectrograph

A Jarrell-Ash 3.4 meter Ebert mounting (65, 66, 67) spectrograph was used to analyse the absorption spectra of the single crystals of thulium ethylsulphate. In order to separate the various orders one above the other on the photographic plate, a Jarrell-Ash order sorter was used (68). A schematic drawing of the spectrograph, order sorter, and optical bench is shown in Figure 6. In order to obtain the high dispersions, it was necessary to work in the high orders. A 7,500 grooves per inch ruled grating was selected because it gave maximum intensity to the high orders for the spectral lines. The grating angle at which maximum intensity occurred was when the light made an angle of 60^{o} with the normal to the grating face. The grating was ruled by Harrison and Associates at Massachusetts Institute of Technology, Boston, Massachusetts. The dispersions in the spectral regions of interest are listed in Table 11.

The procedure in obtaining spectra was to place the sample in the position indicated in Figure 6. The sample absorbs certain wave lengths from the continuous spectrum emitted by the

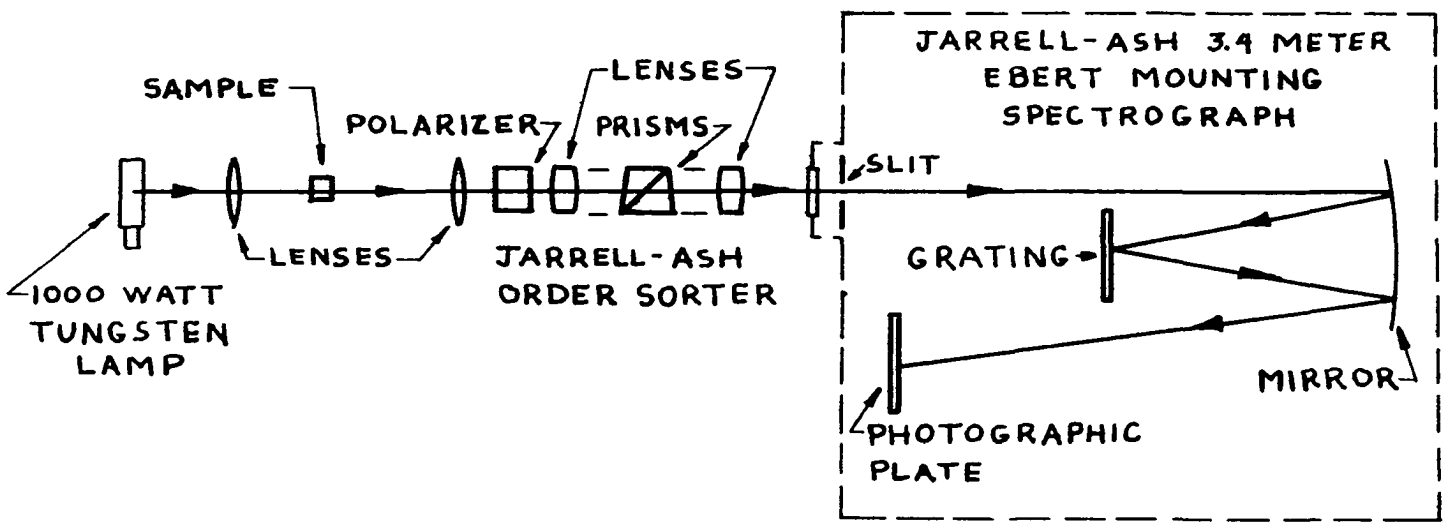

Figure 6. Schematic drawing of the spectrograph with the order sorter and optical bench

tungsten bulb. This absorbed radiation appears as unexposed portions on the photographic plate. Typical slit widths ranged from 90 to 150 microns and in some cases up to 370 microns were used, while the exposure times ranged from two minutes to ten minutes. To calibrate the photographic plates, the sample was replaced with an iron arc burning in air. The wave lengths of the spectral lines of iron are well known (69, 70).

Table 11. Dispersions obtained with the 7,500 grooves per inch grating

Multiplet	Order	Wavelength in Å	Wavenumber in cm^{-1}	Grating Angle	dispersions Å/mm	cm^{-1}/mm
$^3F_4$	7	7863-7940	12590-12713	54.70	0.77	1.226
"	"	"	"	55.14	0.78	1.242
$^3F_3$	8	6880-6948	14389-14530	54.70	0.67	1.402
"	"	"	"	55.14	0.68	1.420
$^3F_2$	8	6607-6664	15003-15131	54.70	0.78	1.788
$^1G_4$	12	4671-4735	21114-21400	56.80	0.43	1.937
$^1D_2$	16	3565-3589	27854-28039	57.80	0.31	2.389

In order to determine the polarization of the absorbed light, a Glan polarizing prism (71) with a 12 mm aperature was placed in front of the order sorter. The polarizing prism

determines the direction of the electric vector associated with the electromagnetic radiation. The polarizer was lined up such that the electric vector of the incident light was either parallel or perpendicular to the c-axis of the sample. For simplicity, the polarizations parallel and perpendicular to the c-axis of the crystal are designated as Epc and Esc respectively.

The magnet

For the Zeeman studies, the magnetic field was supplied by an Arthur D. Little rotating and height-adjustable model electromagnet. The d.c. current for the magnet was supplied by a d.c. generator driven by an a.c. electric motor. The field windings of the d.c. generator were controlled by a current regulating device.

For a working gap of 1-9/16 inches and pole faces tapered from 11 inches to 5-3/4 inches, the maximum field was 28,200 gauss. The field was measured by a nuclear magnetic resonance gaussmeter using the resonances of protons and deuterons. Table 12 shows the field for various currents used.

Table 12. Magnetic field versus current

Nominal field	Field in gauss	Applied current in amps
1/4	7,150	35
1/2	14,400	70
3/4	21,500	110
1	28,200	399

Sample preparation

The single crystal samples used in the spectral analysis were grown by Mr. H. O. Weber of Dr. Spedding's chemistry group. The method given below is that used by Mr. Weber.

The thulium ethylsulphate (chemical formula $Tm(C_2H_5SO_4)_3 \cdot 9H_2O$) was obtained by reacting thulium chloride with sodium ethylsulphate. The thulium chloride was prepared from thulium oxide of 99.95% purity which was prepared by the rare earth separation group of the Ames Laboratory of the U. S. Atomic Energy Commission. The sodium ethylsulphate was purchased from the Amend Drug and Chemical Company, New York.

The thulium oxide was reacted with an equivalent amount of C. P. hydrochloric acid. This mixture was heated just below the boiling point until most of the oxide had dissolved in the acid. Water with a conductivity of 5×10^{-7} mhos was added to this to adjust the concentration of the thulium chloride to about two molar. A one per cent excess of the

thulium oxide was then added to the solution, and it was heated for two more hours. The excess oxide was filtered off, and the pH of the resulting solution was adjusted to 3.0 by carefully adding dilute hydrochloric acid to it and checking the pH with a pH meter. The solution was then heated for one hour to destroy any thulium oxychloride and then was cooled. The pH of the solution was checked, and the above process was repeated until the pH remained unchanged after heating. This solution was evaporated to the point where crystals formed. The solution was cooled slightly, and about 500 ml of absolute alcohol were added to it. This thulium chloride solution was added slowly with stirring to a one per cent excess of sodium ethylsulphate dissolved in alcohol. The precipitated sodium chloride was allowed to digest overnight. The supernatant alcoholic solution containing the thulium ethylsulphate was decanted into a sidearm suction flask. The alcohol was distilled from the solution under reduced pressure with a vacuum pump and collected in a cold trap. The remaining salt was dissolved in a minimum amount of conductance water and filtered. It was then purified by fractional crystallization to remove any sodium chloride or sodium ethylsulphate that may have been present. Some of the purified thulium ethylsulphate

hydrate was then dissolved in absolute alcohol in a sidearm flask. The alcohol was distilled off under a reduced pressure until the solution was at the saturation point; this was then set aside in a glove box where the temperature was controlled at 25.0°C. Crystals formed and grew as the alcohol slowly evaporated.

The crystals grown in alcohol were found to be clearer, to have less of a tendency to have occlussions, and to have a sharper spectra than crystals grown in water. The alcohol grown crystals had less of a tendency to hydrolyze and form rare earth hydroxides resulting in clear crystals. The sharper spectra probably resulted from the light scattering, by occlussions and the hydroxides, being less in the alcohol grown crystals than in the water grown crystals. Other workers (36, 39) grew their crystals in water. The crystals grown by the process outlined above were checked to see if they were hydrated thulium ethylsulphate, i.e., if the thulium ion had the nine water molecules of hydration or if the water molecules had been replaced by alcohol molecules. The check has been performed by Mr. W. J. Haas. He compared the density of the crystals, space group, lattice constants, and the absorption spectra of crystals grown in alcohol to those

grown in water and found them to be the same. He also calculated the number of molecules per unit cell assuming that alcohol had replaced the waters of hydration and found under this assumption that there was not an integer number of molecules in the unit cell. The same calculation assuming nine water molecules of hydration gave two (Rare Earth)$(C_2H_5SO_4)_3 \cdot 9H_2O$ "molecules" per unit cell. An Iodoform test for alcohol content in the crystals was performed and no detectable amounts of alcohol were found. It is therefore concluded that the crystals grown in alcohol are indeed hydrated thulium ethylsulphate.

Grinding procedure and mounting

In order to obtain crystals of the proper thickness that would bring out certain features of the spectra, it was necessary to grind the single crystals to a desired thickness. Typical thicknesses of crystals to observe the Zeeman splittings were .2 mm, .5 mm, and .9 mm in the 100 per cent Tm ES crystals.

The crystals normally grew to a size of about 2 mm thick by 5 mm long by 3 mm wide. A crystal of this thickness was checked on a polarizing microscope to determine if the crystal was a single crystal. When the light passes through the single

crystal perpendicular to the c-axis and through the crossed nicol prisms of the microscope, a null in the intensity of the light is observed every 90^{o} as the crystal is rotated. The direction of the null corresponds to a direction either parallel or perpendicular to the c-axis.

The crystal orientation having been determined in the above manner, the crystal was ground down to the desired thickness using fine emery paper. An alcohol lubricant was used to grind the last .1 mm to smooth the scratches left by the emery paper. The crystals were slightly soluble in alcohol.

The crystals were then mounted on a slotted copper strip (by means of masking tape) with the c-axis in such a manner so as to be either parallel or perpendicular to the applied magnetic field. The crystals were carefully aligned on the copper strips by aligning the direction of the null intensity (using the polarizing microscope) with the edge of the strip. The copper strip was suspended in the dewar from a stainless steel rod.

For the spectra that were taken where the angle ϕ_m was varied, cylindrically shaped single crystals were used. The axis of the cylinder was parallel to the c-axis of the crystal. Experimentally, crystals of a diameter smaller than 3 mm could

not be used. The spectra from 100 per cent Tm ES crystals of this diameter were quite broad and could not be quantitatively analysed; therefore a crystal of 10 per cent concentration of Tm in Y ethylsulphate was used. The spectra from these diluted crystals were relatively sharp. To obtain the cylindrical crystals, the crystals were mounted on a rotating shaft and ground down to approximately 3 mm by using emery paper and finished off using an alcohol lubricant. The cylindrical crystals were mounted in a quartz tube and suspended from a stainless steel rod in the dewar.

Dewar

The dewar used in obtaining low temperatures was of the type pictured in Figure 7. The transparent tip and windows were made of quartz so as to allow the transmission of ultraviolet light.

The liquid coolants used in the inside chamber were liquid helium ($4^{o}K$) and liquid hydrogen ($20^{o}K$). The outside radiation shield was filled with liquid nitrogen. The samples were immersed directly in the liquid bath.

Photographic plates

All the plates used in taking the spectra were prepared by the Eastman Kodak Company. The emulsion types used were,

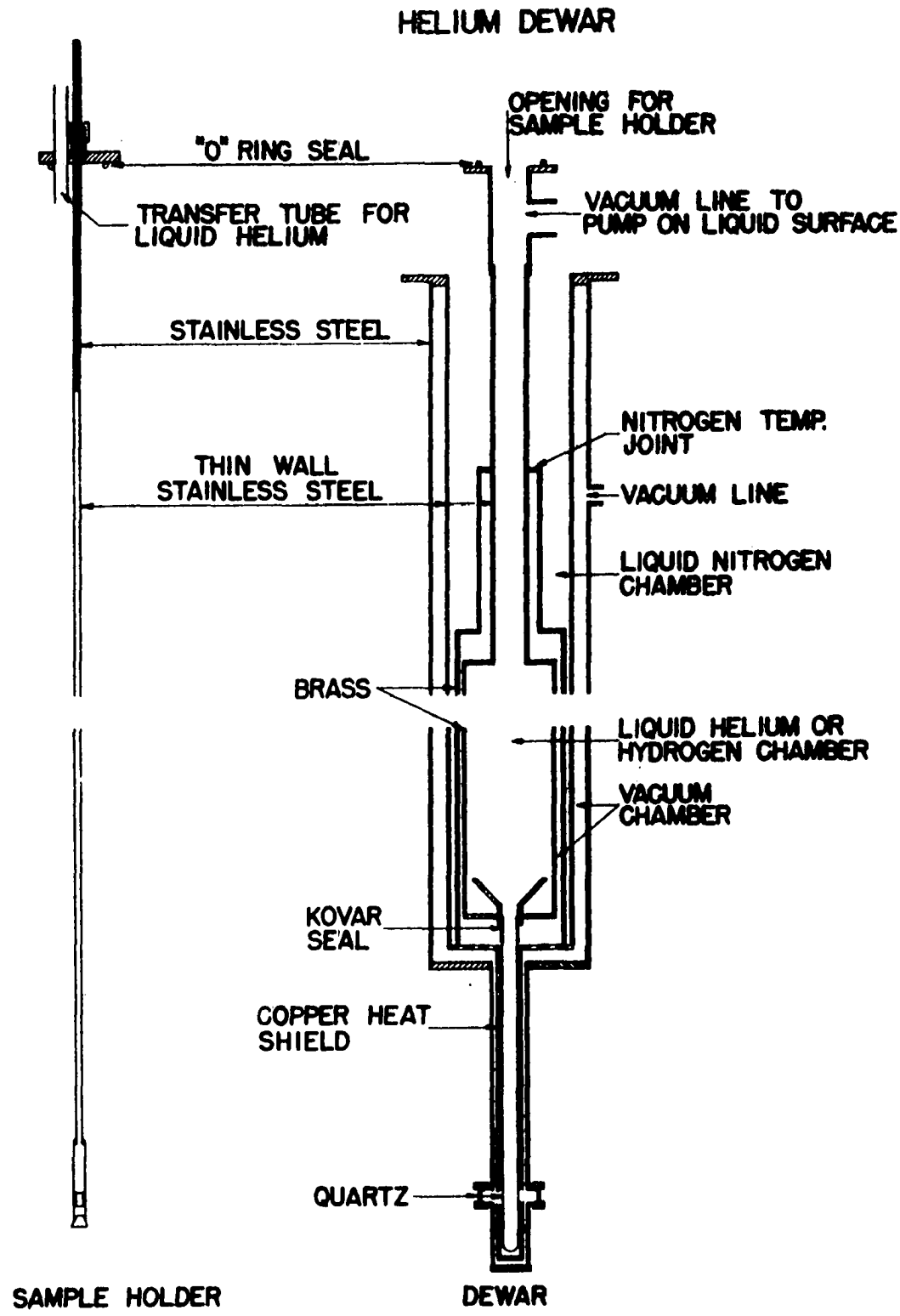

Figure 7. Dewar and sample holder

1-N, 103a-0, 103-0, 103a-F, and III-0. The regions of sensitivity and extra sensitivity of the various emulsion types are given in Table 13.

Table 13. Regions of sensitivity of photographic emulsions

Emulsion type	Wave lengths are given in thousands of Å	
	Sensitive	Extra sensitive
N	2.5 - 9	6.9 - 9
F	2.5 - 7	4.5 - 6.9
0		2.5 - 5

The plates were developed in Kodak D-19 developer and fixed in Kodak general purpose fixer. A stop bath of a dilute solution of acetic acid was used. The plates were dried by passage of heated air over the plates.

Measurement of the plates

The spectrographic plates were measured on a Sinclair Smith and a Jarrell-Ash recording microphotometers. The Sinclair Smith machine had a precision screw of .5 mm per turn and the Jarrell-Ash machine had 1 mm per turn. The plates were carefully aligned on the table so that the slit in front of the phototube tracked precisely a particular order that was to be measured.

In all but one multiplet there were not enough iron lines in the order of interest to calibrate the plate. For those cases where there were an insufficient number of iron lines, iron lines from adjacent orders were used. The wave lengths of these lines in the adjacent orders were converted to wave lengths in the order of interest by means of the relation[1] (68),

$$n\lambda = n'\lambda', \qquad (111)$$

where n and n' are the order numbers, λ is the wave length of the iron line, and λ' is the wave length projected into the n' order. The projected wave lengths were then converted into wave numbers by means of the Bureau of Standards tables (72).

In order to calibrate a particular order at a particular grating angle, an order with a sufficient number of iron lines in it was selected for measurement. The arc was traced by means of the recording microphotometer and the separations of the iron lines from a starting iron line were measured from the chart. Having correctly identified the iron lines their wave lengths were looked up in tables (69). These wave lengths were

---

[1]From the grating formula $n\lambda = d(\sin i \pm \sin r)$ (71) where angles i and r are the angles of incidence and reflection respectively and d is the grating spacing in Å, it is apparent that for fixed angles i and r that $n\lambda$ is a constant such that Equation 111 results.

mathematically projected into the order to be calibrated by means of Equation 111, and then converted to wave numbers from the tables given in reference (72). Two iron lines were selected as end iron lines and a linear dispersion was calculated.

$$\text{Disp.} = D = (\bar{\nu}_2 - \bar{\nu}_1) \text{ /Distance in mm.} \qquad (112)$$

Measuring the distance the other iron lines were from $\bar{\nu}_1$ on the chart; their wave numbers were calculated by means of,

$$\bar{\nu}_n = x_n D + \bar{\nu}_1 , \qquad (113)$$

where x_n is the distance $\bar{\nu}_n$ is from $\bar{\nu}_1$. The difference between the calculated wave number $\bar{\nu}_n$ and the MIT value $\bar{\nu}$ ($\Delta\bar{\nu}_n$) was used to determine a correction curve. The equation for the correction curve was,

$$\Delta\bar{\nu}_n = A(\bar{\nu}_n - \bar{\nu}_1)^2 + B(\bar{\nu}_n - \bar{\nu}_1) + C. \qquad (114)$$

A computer program was developed by Mr. W. J. Haas to determine the calibration constants A, B, and C.

The distance the absorption spectral lines were from the end iron line $\bar{\nu}_1$ was measured from the charts and their uncorrected wave numbers were calculated from Equation 113. Then the correction curve determined from the calibrating iron lines was used to make the necessary corrections to the wave numbers of the various spectral lines. A computer program was also

developed by Mr. Haas to accomplish this purpose.

Table 14. Calibration errors for transitions from $^3H_6$ to various multiplets

Multiplet	Standard deviation cm^{-1}	Number of lines used in calibration
$^3F_4$	± 0.008	8
$^3F_3$	± 0.009	8
$^3F_2$	± 0.005	6
$^1G_4$	± 0.007	11
$^1D_2$	± 0.005	6

Experimental Data

The assignments of the electronic levels and multiplet designations used in this work are the same as other authors (35, 37, 39) except where specifically noted in the following discussions. The energy level diagrams with energies rounded off to the nearest cm^{-1} and transitions are shown in Figures 8, 9, 10, 11, and 12. The observed transitions are shown for the two light polarizations and the two field directions as well as for the zero field case. In the figures are lines which appear for the magnetic field perpendicular to the

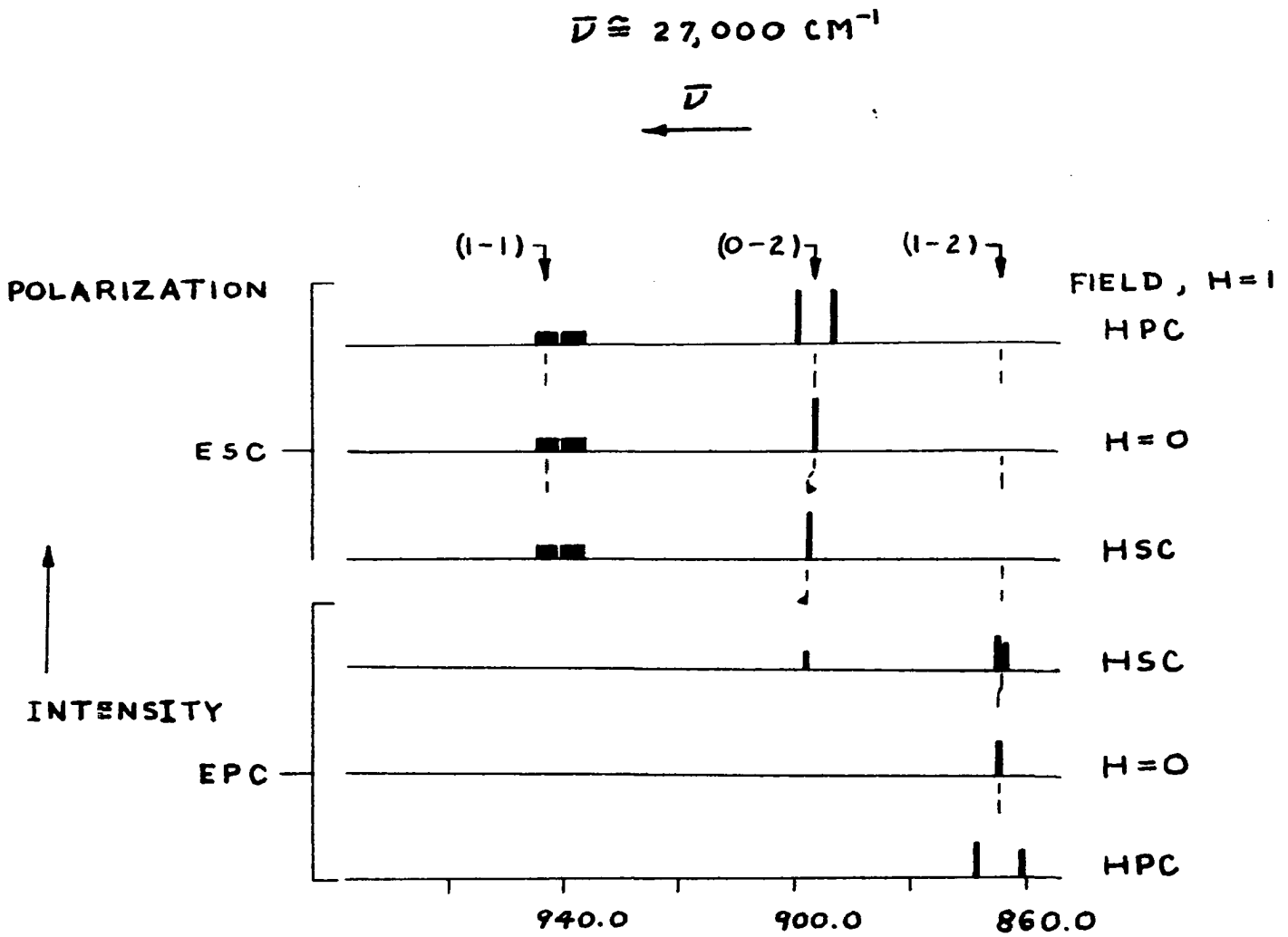

Figure 8a. Transitions to the $^1D_2$ multiplet at 20 K°

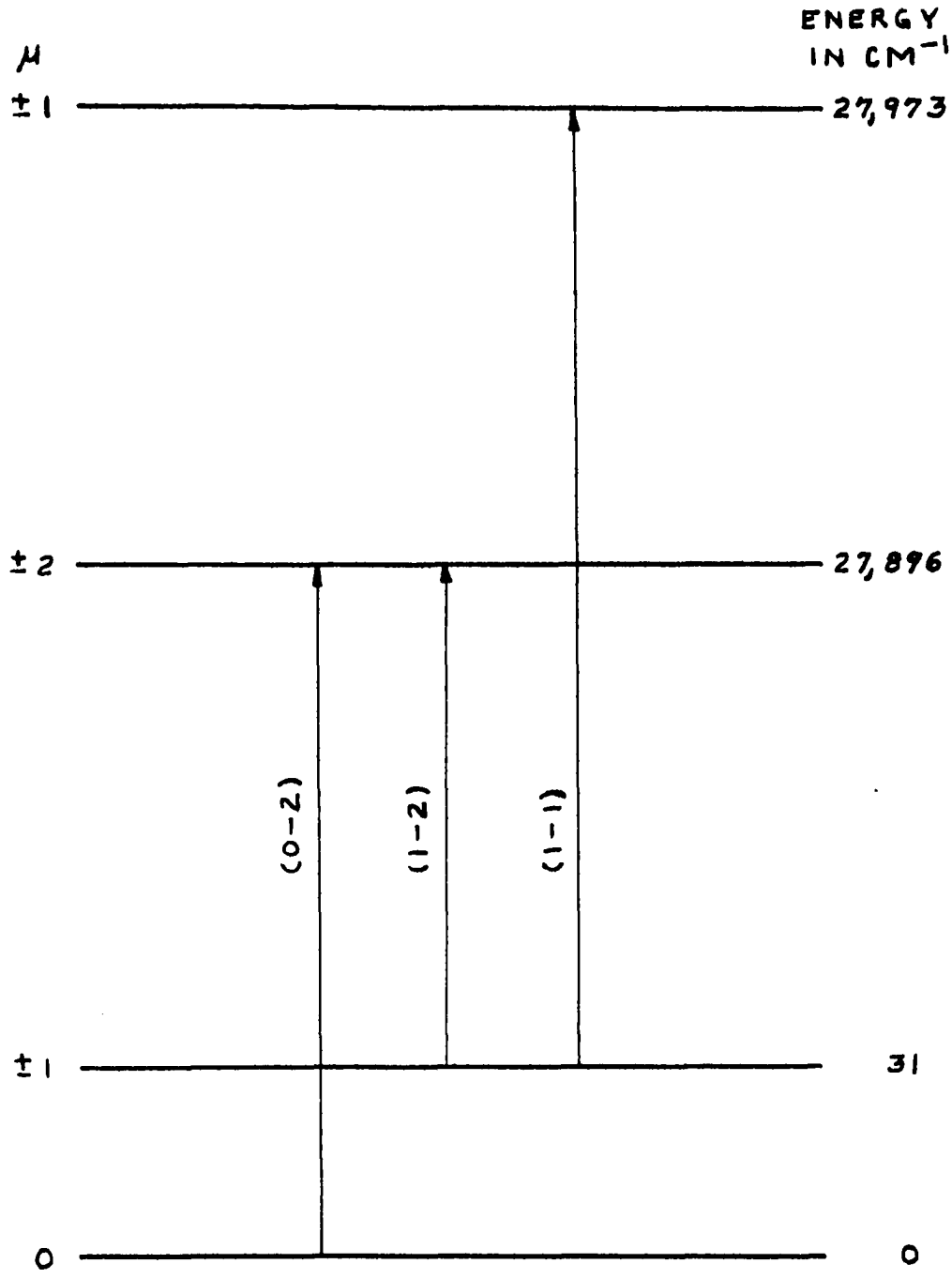

Figure 8b. Energy level diagram of the $^1D_2$ multiplet with the observed transitions

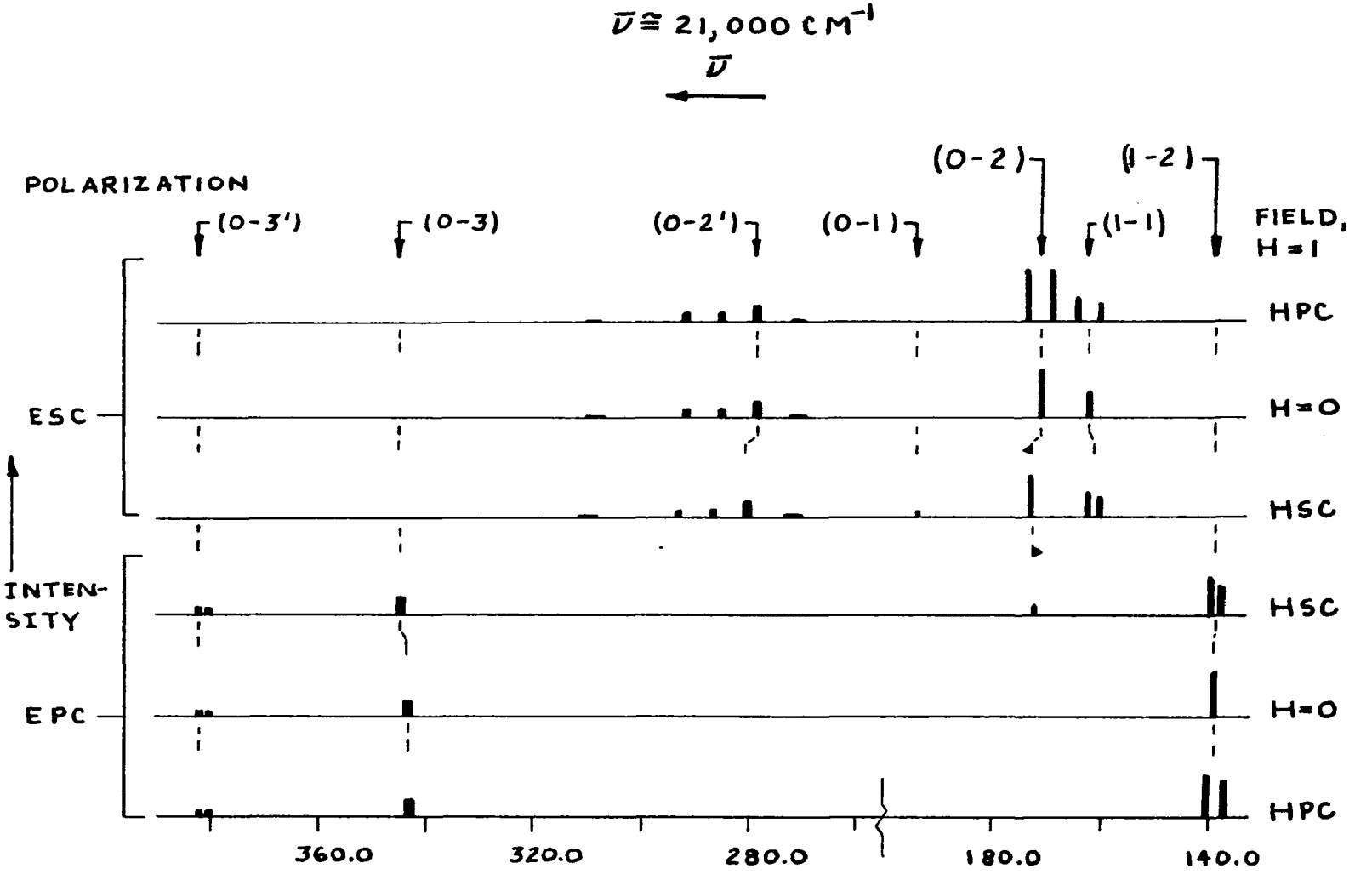

Figure 9a. Transitions to the $^1G_4$ multiplet at 20°K

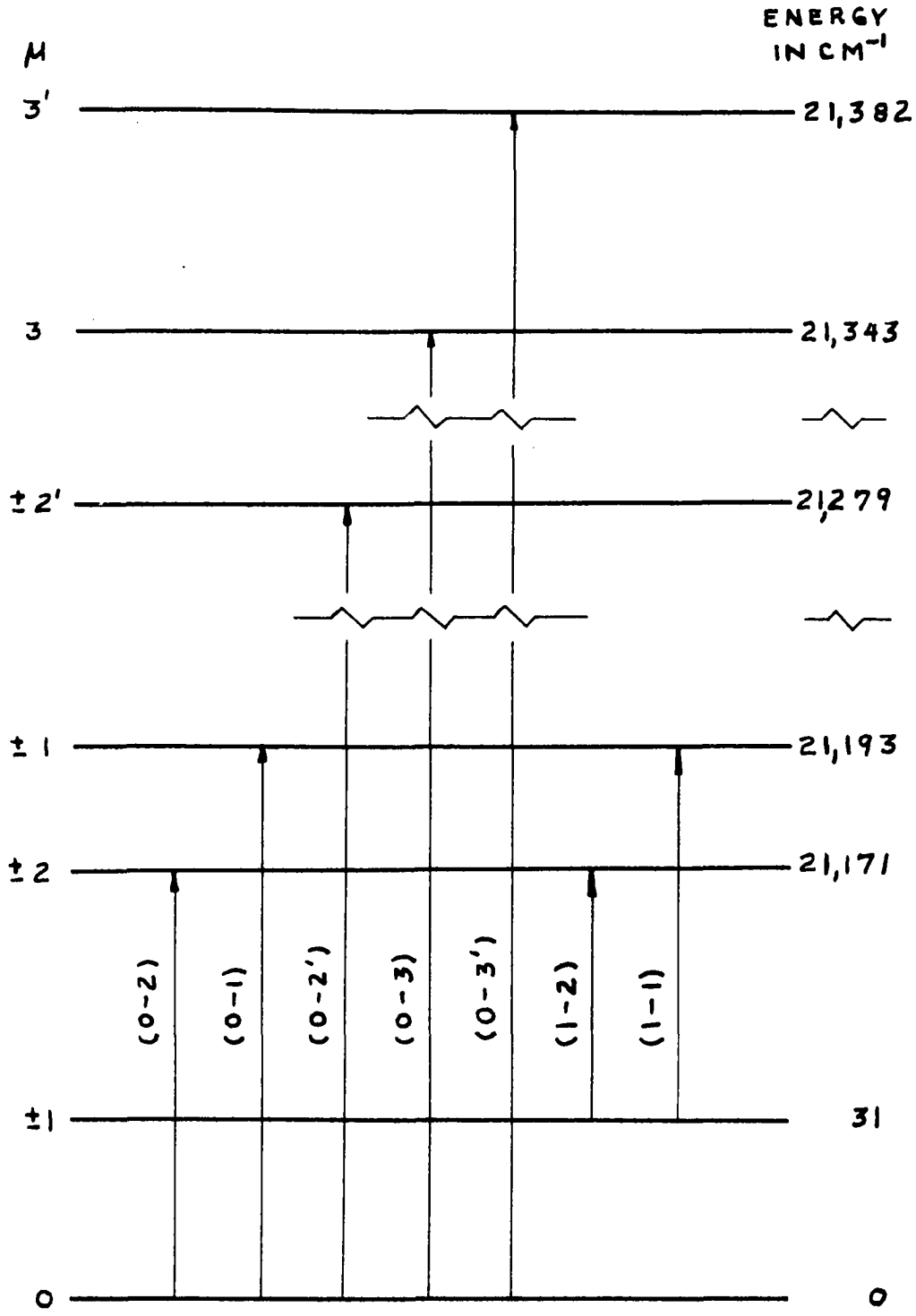

Figure 9b. Energy level diagram of the $^1G_4$ multiplet with the observed transitions

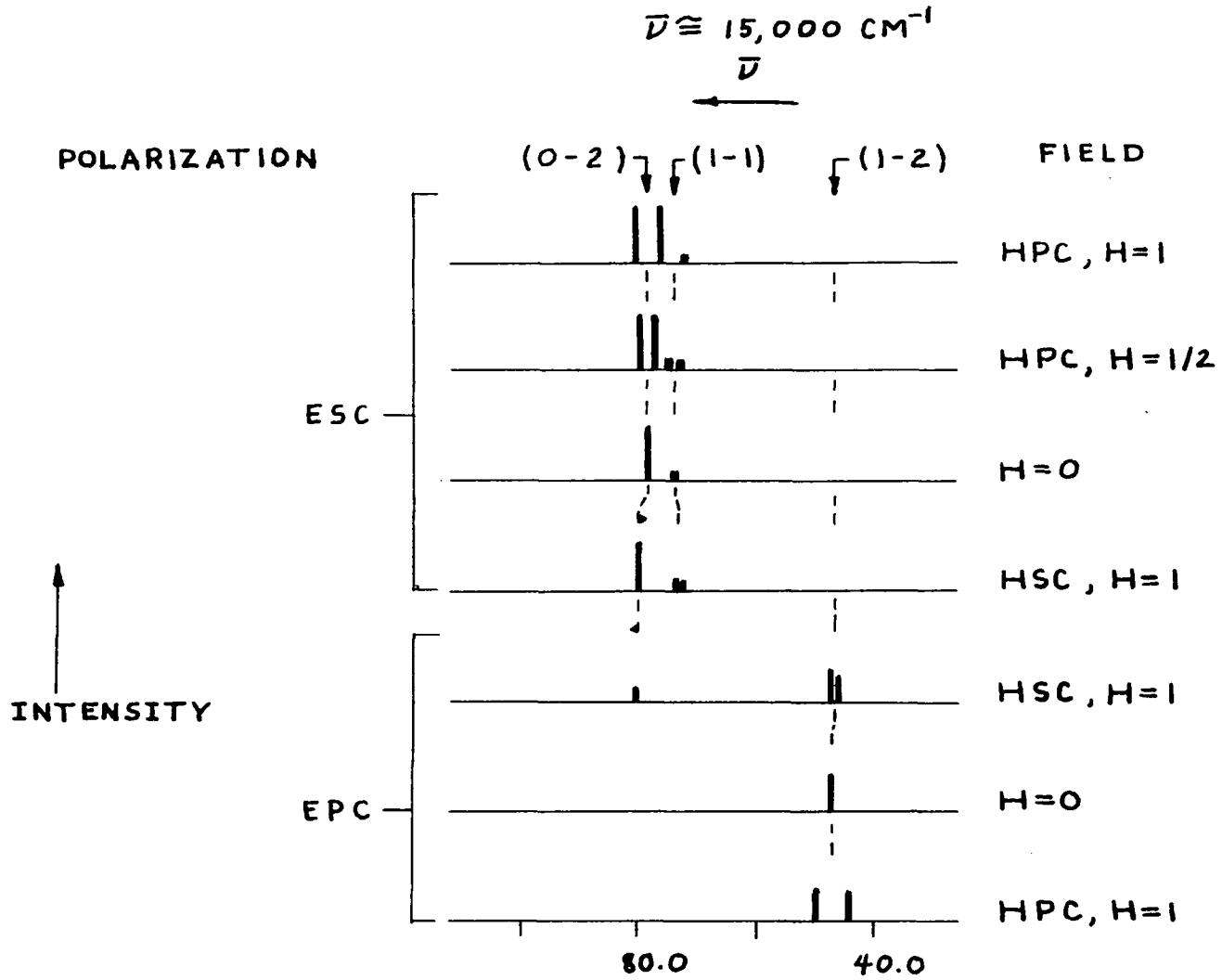

Figure 10a. Transitions to the $^3F_2$ multiplet at 20°K

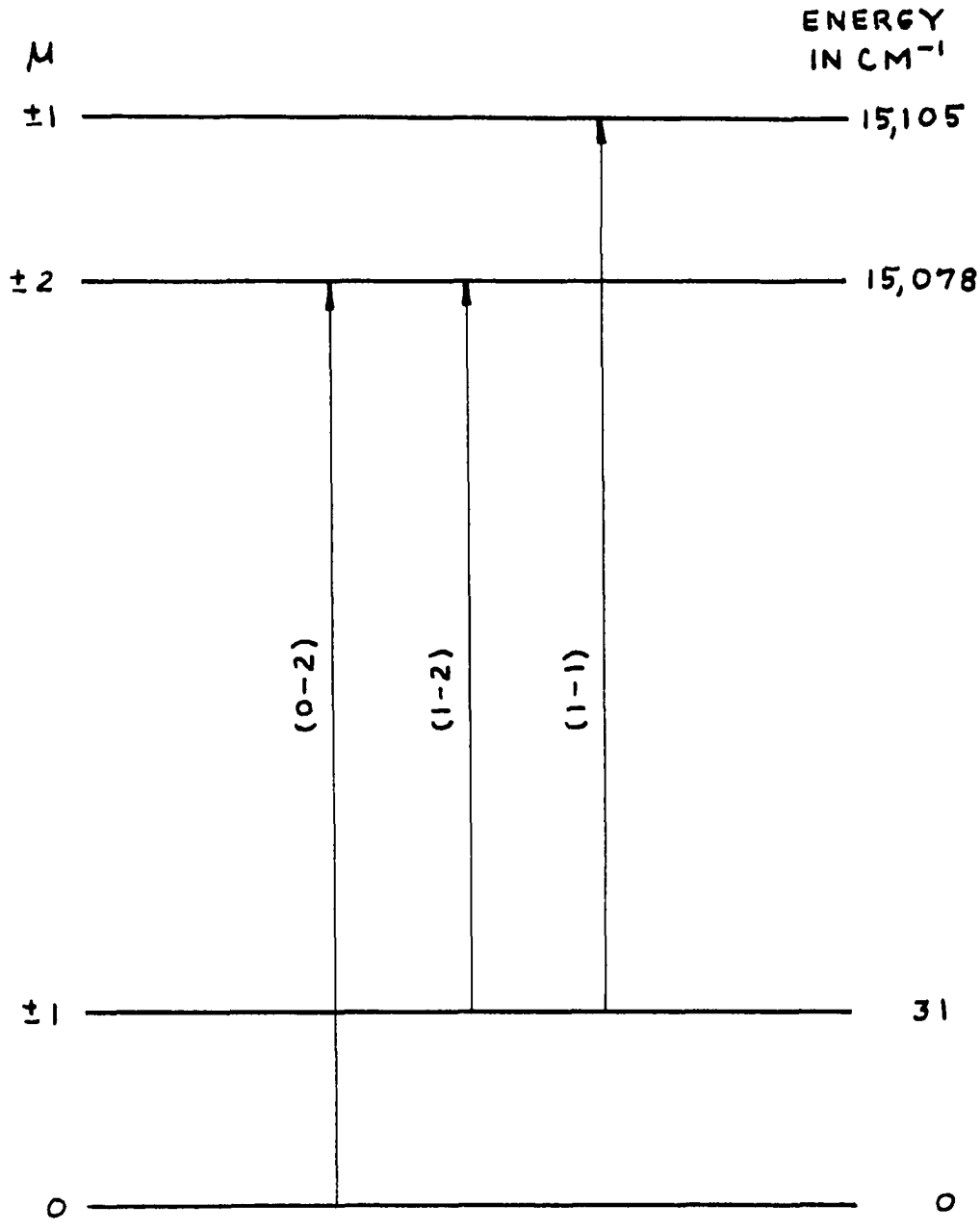

Figure 10b. Energy level diagram of the $^3F_2$ multiplet with the observed transitions

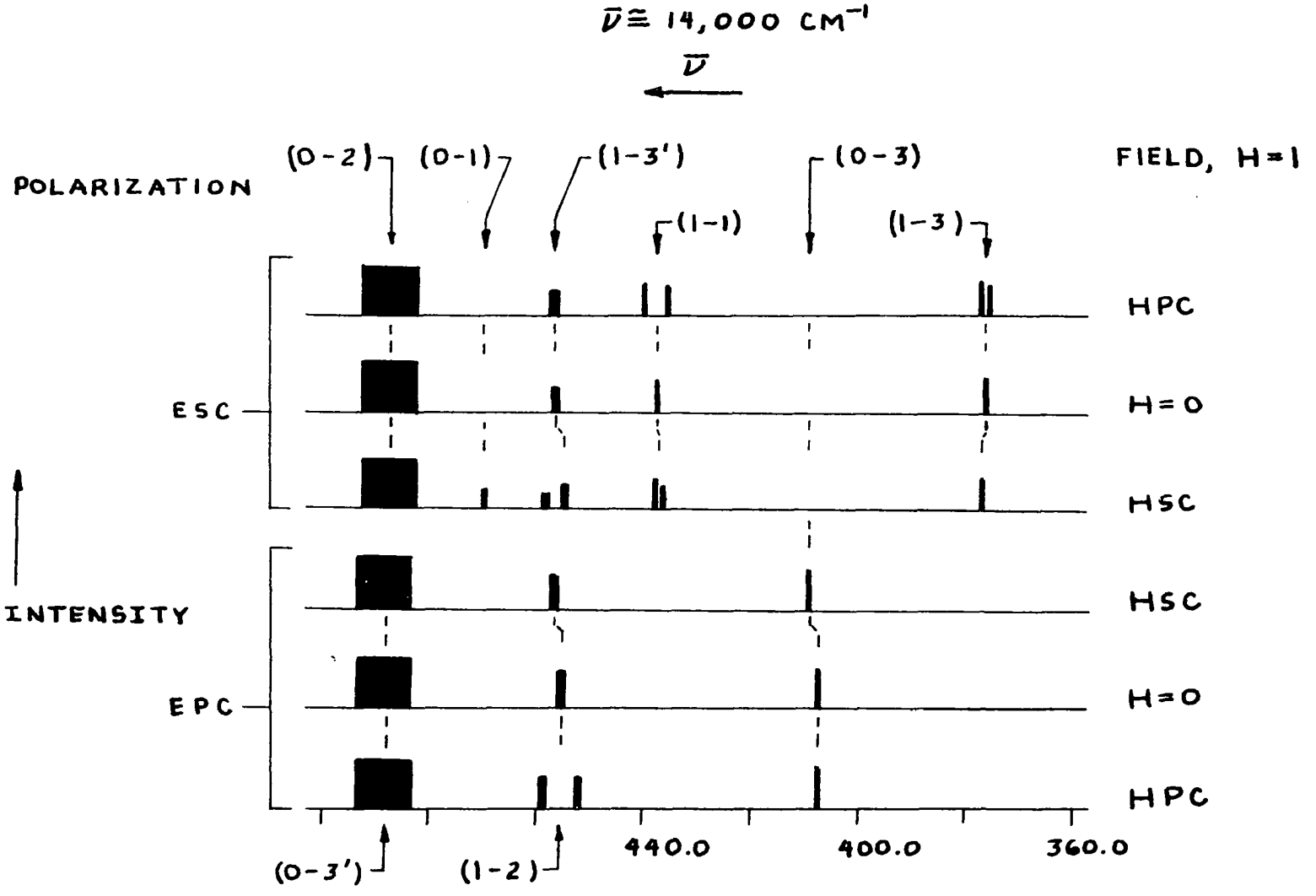

Figure 11a. Transitions to the $^3F_3$ multiplet at 20°K

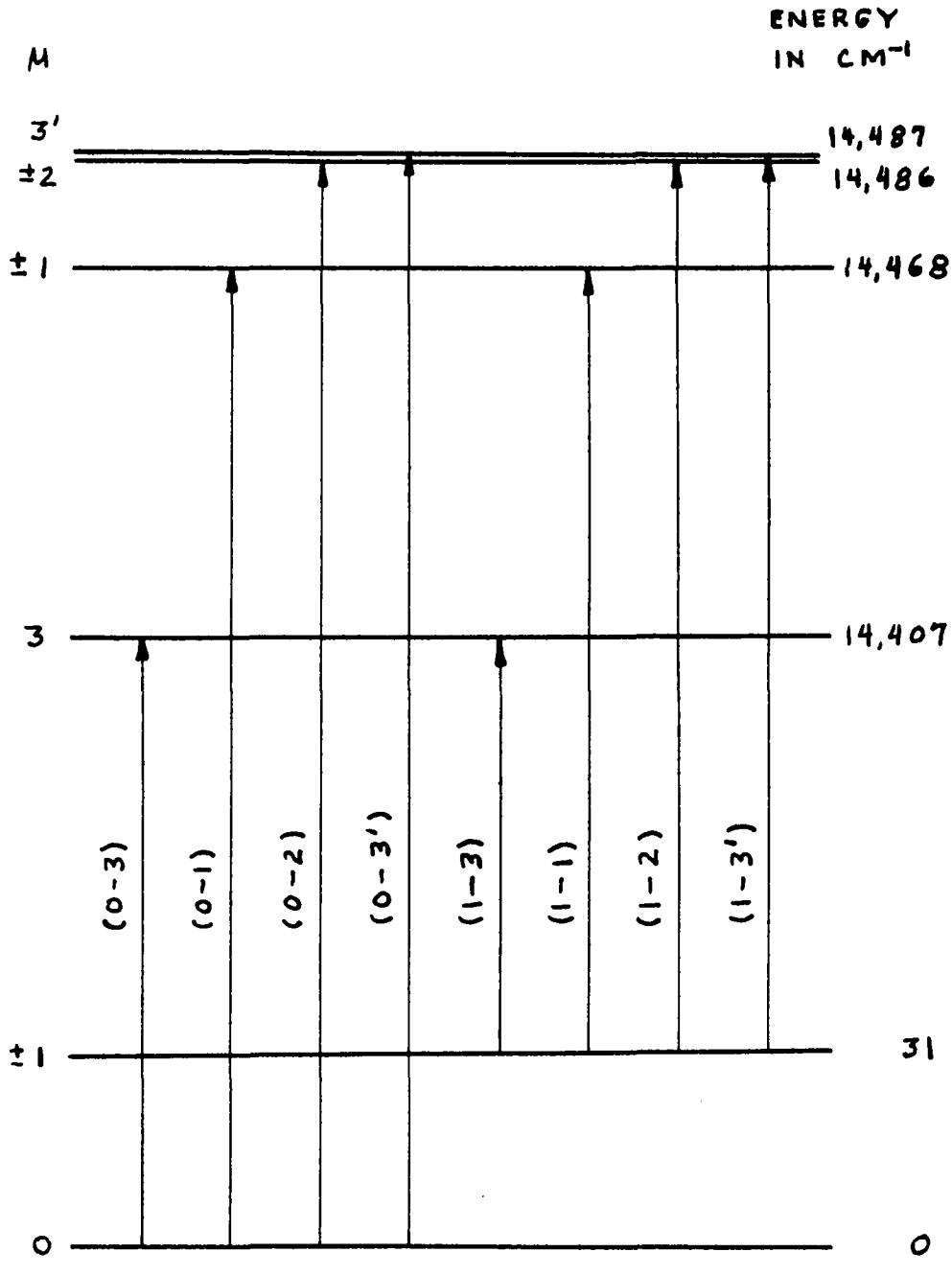

Figure 11b. Energy level diagram of the $^3F_3$ multiplet with the observed transitions

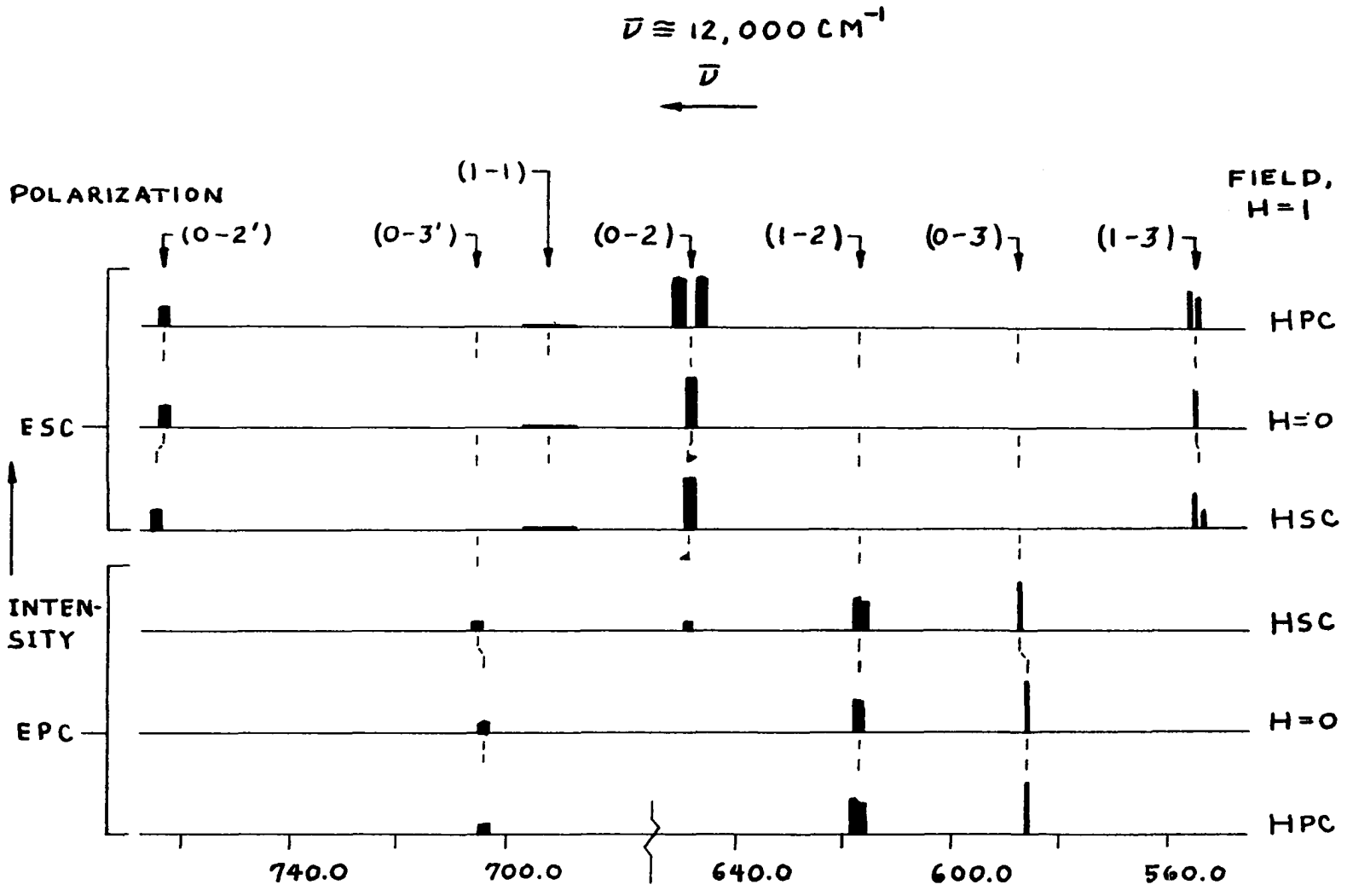

Figure 12a. Transitions to the $^2F_4$ multiplet at 20°K

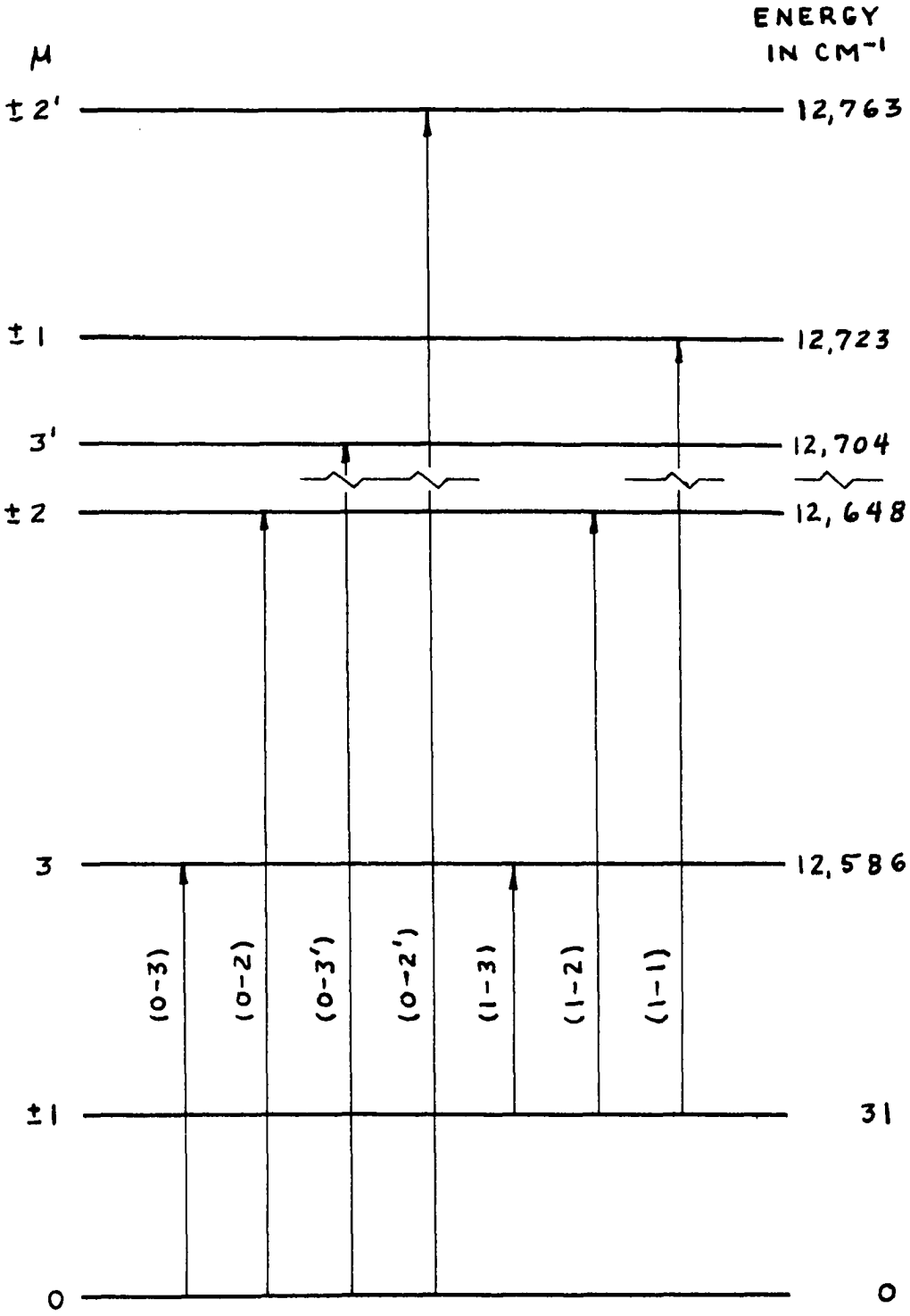

Figure 12b. Energy level diagram of the $^3F_4$ multiplet with the observed transitions

c-axis but are not present at zero field or for the field parallel to the c-axis. Spectra taken when $\emptyset_m$ was varied are shown in Figures 13 and 14. Table 15 gives the transitions which obey the electric dipole selection rules of Equation 30.

Table 15. Transitions obeying the electric dipole selection rules

Transitions From μ	To μ	Name of transition	Polarization observed in
0	2	(0-2)	s
0	-2	(0-2)	s
0	3	(0-3)	p
1	-1	(1-1)	s
-1	1	(1-1)	s
1	-2	(1-2)	p
-1	2	(1-2)	p
1	3	(1-3)	s
-1	3	(1-3)	s

The measurements of the spectral lines are given in Tables 16 and 17 for the magnetic field parallel and perpendicular to the c-axis of the crystal as well as for zero magnetic field. The spectra were taken for crystal temperatures of 4 and 20°K and the measurements are divided into these two temperature classes. The parallel and perpendicular light polarizations are denoted by p and s respectively, and the parallel and perpendicular magnetic field directions are given by Hpc and Hsc respectively. All transitions were considered to be electric

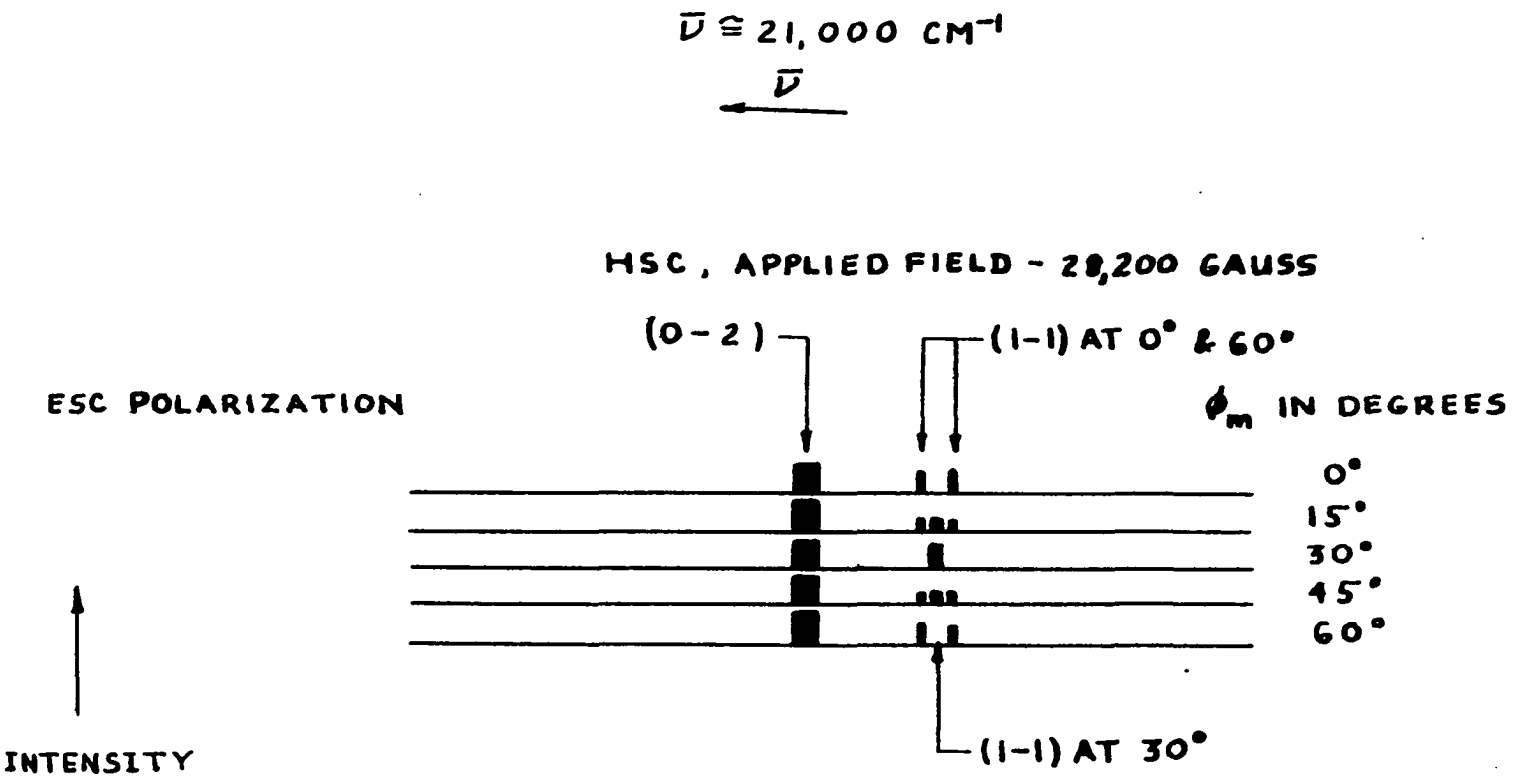

Figure 13. The (1-1) transition for the $^1G_4$ multiplet for various ϕ_m angles agreeing with Figure 5g

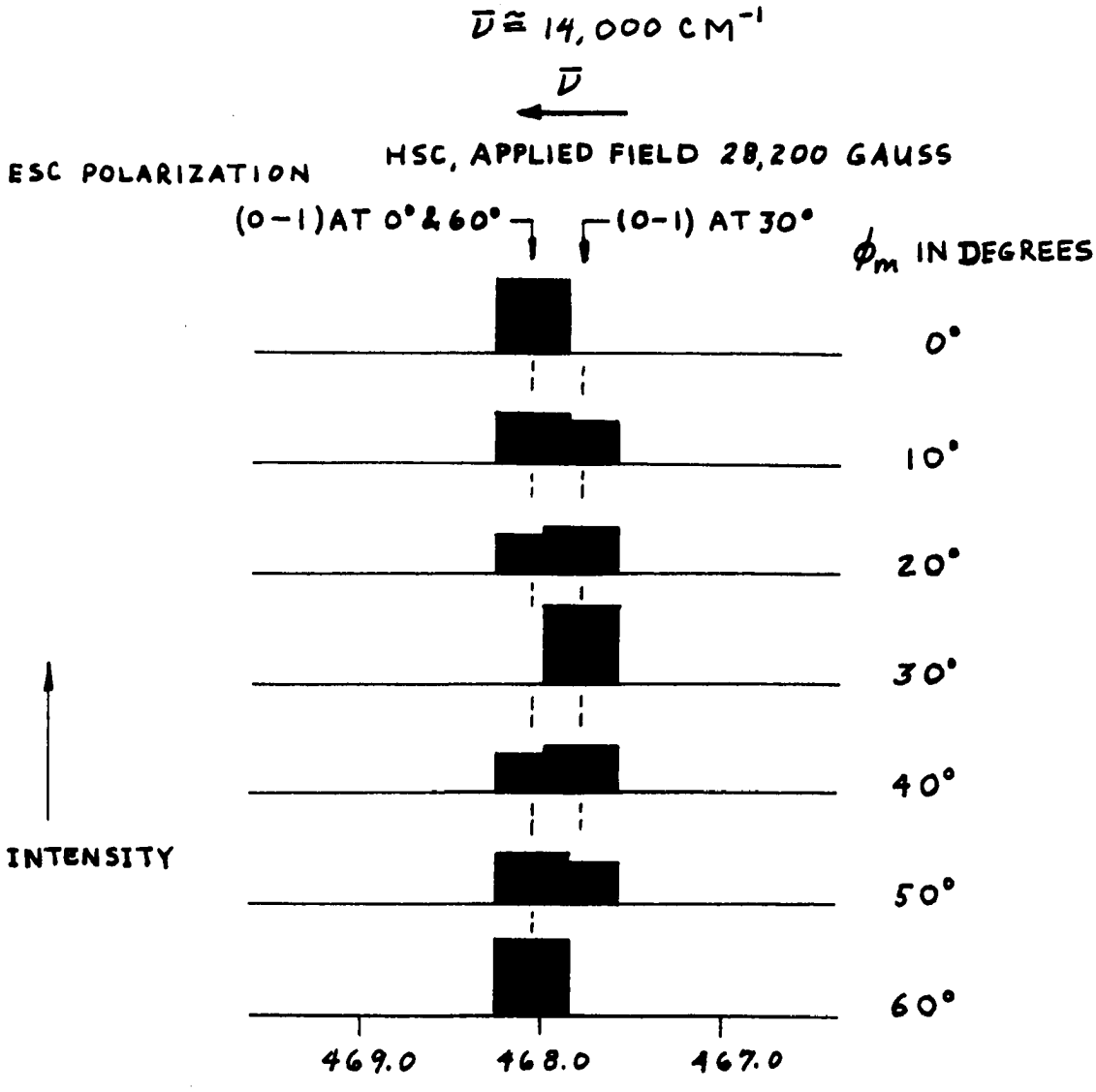

Figure 14. The (0-1) transition for the $^3F_3$ multiplet for various ϕ_m angles agreeing with Figure 5j

dipole in nature. As a matter of convenience, levels in a multiplet with the same μ quantum number will be distinguished by calling the one at lower energy μ and the one at higher energy μ' when the i subscripts are not used.

The line splittings with magnetic fields were taken from the data of Tables 16 and 17 and are given in Tables 18 and 19. For the Hsc case, the line splittings for the (0-2) transitions were obtained by taking the difference in energies between the (0-2) transitions as they appeared in the two light polarizations in accordance with the theory as discussed in a previous section. While the actual line positions varied between crystal temperatures of 4^{o} and $20^{o}K$, the Zeeman splittings of the lines did not vary outside the experimental error. Therefore to calculate level splittings and splitting factors, the Zeeman data obtained at these two temperatures were averaged together.

The level structure of thulium ethylsulphate was determined by observing transitions from the ground state ($\mu = 0$) and the first excited state ($\mu = \pm 1$) of the $^{3}H_{6}$ multiplet. For electric dipole transitions, transitions from the $\mu = 0$ level of the $^{3}H_{6}$ multiplet to a $\mu = \pm 2$ level of another multiplet, denoted by (0-2), appear in the perpendicular polariza-

tion, and transitions to a $\mu = 3$ level, (0-3), appear in the parallel polarization in accordance with Table 15. Also from the table, the (1-1) and (1-3) transitions would appear in the perpendicular polarization and the (1-2) transitions would appear in the parallel polarization. The energies of the $\mu = \pm 2$ and $\mu = 3$ levels were obtained directly from the energies of the (0-2) and (0-3) transitions, where the $\mu = 0$ level of the $^3H_6$ multiplet was always taken as the zero of energy. The energies of the $\mu = \pm 1$ levels of excited multiplets were obtained by adding the energy of the $\mu = \pm 1$ level of the $^3H_6$ multiplet to the energy of the (1-1) transitions.

In multiplets where there are two $\mu = 3$ levels there should be a (0-3) transition to only one of them for the odd parity α's equal to zero and the odd parity β's unequal to zero. This behavior is due to the η selection rule for transitions between non-degenerate states as discussed in a previous section. (A similar result happens when the α's are non-zero and the β's are zero.) However in the multiplets where there are two $\mu = 3$ levels, there were at least two (0-3) transitions observed. As has been stated, the odd parity α's are not actually zero; therefore both transitions could be observed where one of them will in general be much

weaker than the other. Transitions of the type (0-3) will also be observed for $n_{gs} \neq 0$ for the final state (like those of Equation 24); therefore it is possible that some of the weak (0-3) transitions are transitions to final $\mu = 3$ levels for $n_{gs} \neq 0$. In the tables n_{gs} is not specified. The transitions are tentatively identified as transitions between "pure electronic" states ($n_{gs} = 0$) except where specifically noted in the following discussions.

When the crystal temperature is $4^{o}K$, only the ground state (a $\mu = 0$ level of the $^{3}H_{6}$ multiplet) is appreciably populated; therefore, all the lines observed in the spectra are transitions from this $\mu = 0$ level. At a crystal temperature of $20^{o}K$ one of the $\mu = \pm 1$ levels of the $^{3}H_{6}$ multiplets becomes appreciably populated; then transitions from this $\mu = \pm 1$ level can also be observed in the spectra. Table 4 shows that for $J = 6$ there are three $\mu = 0$ levels and two $\mu = \pm 1$ levels. However in this investigation, transitions from only the low lying $\mu = 0$ level and the low lying $\mu = \pm 1$ level were observed. In the following discussions the low lying $\mu = 0$ and $\mu = \pm 1$ levels will be referred to as the $\mu = 0$ level and the $\mu = \pm 1$ level and no further reference will be made to the other two $\mu = 0$ levels and the other $\mu = \pm 1$ level.

Since in spectra only differences in energy are measured, the $\mu = 0$ ground state was taken as the zero of energy for both crystal temperatures and both magnetic field directions. All energy shifts of the levels due to the temperature and magnetic field show up in the reported positions of the other levels.

The splittings of the $\mu = \pm 2$ levels were observed directly from the splittings of the (0-2) transitions for Hpc in accordance with Equation 57 and Figure 4a. Johnsen (35) observed that some of the $\mu = \pm 2$ levels did not split with magnetic field as was also observed in this work. The degeneracies of these levels are removed by the magnetic field as pointed out by previous arguments. The apparent lack of splitting of some of the levels, however, is probably due to small splitting factors for these levels; therefore the two components cannot be resolved. According to the theoretical values given in Table 28, this seems to be the case.

For Hpc the splittings of the $\mu = \pm 1$ levels of the excited multiplets were obtained from the splittings of the (1-1) transitions and knowing the splitting of the $\mu = \pm 1$ level of the $^3H_6$ multiplet; the interpretations Equations 60 and 61 and Figures 4b and 4c were used. The splitting of the

$\mu = \pm 1$ level of the $^3H_6$ multiplet was measured directly by measuring the splittings of the (1-3) transitions (Figure 4f) and indirectly by measuring the (1-2) line splittings with the interpretations of Equations 63 and 64 and Figures 4d and 4e.

In analysing the spectra for the case where the magnetic field is perpendicular to the c-axis, it is extremely important that the theory as given in a previous chapter is applied. There are transitions observed which violate the electric dipole selection rules. This violation comes about because the initial and final states are no longer "pure" μ quantum states for the magnetic field perpendicular to the c-axis. All μ quantum states are "mixed" together in some order of perturbation and therefore the μ quantum number loses its significance. Although for Hsc μ is no longer a good quantum number, the names of the transitions for the zero field case will still be used but now the polarization of the observed line must be specified.

For Hsc the splittings of the $\mu = \pm 2$ levels were obtained from measuring the difference in energy between the (0-2) transitions appearing in the parallel and perpendicular polarizations. This is in accordance with Equation 95 and Figures 5a and 5b. The splittings of the $\mu = \pm 1$ levels were obtained

from the splittings of the (1-1) transitions and knowing the splitting of the $\mu = \pm 1$ level of the $^3H_6$ multiplet. The spectra were analysed using Equations 102, 104, and 105 and Figures 5g and 5h. Splittings of the (1-2) lines were analysed using Equations 98 and 100 along with the Figures 5e and 5f, and the (1-3) transitions were analysed using Figures 5c and 5d.

The level positions for temperatures 4^oK and 20^oK are listed in Table 25. The splittings of the levels for the magnetic field parallel to the c-axis are listed in Table 26, and for the magnetic field perpendicular to the c-axis the splittings are listed in Table 27. The associated splitting factors as defined by Equations 51 and 72 are given in Tables 28 and 29 respectively. In determining the parallel field splitting factors, only the level splittings obtained for fields of 21,500 and 28,200 gauss were used. For fields of 14,400 gauss the line splittings, from which the level splittings were obtained, were not completely resolved for most of the lines measured. The error limits for the level positions listed in Table 25 are estimated from using the data for the various lines obtained for Hsc and Hpc and fitting the energy of the lines to a polynomial of the form $E = AH^2 + BH + C$. A

computer program developed by Mr. Haas was used to accomplish this purpose. The error limit estimates were made from the standard deviations of the polynomial fitting and how much the constant C deviated from the measured zero field value. The error limits for the line and level splittings and splitting factors are a result of averaging the data and obtaining an average deviation. It should be noted that for the error limits of the $\mu = \pm 1$ level splittings of the excited multiplets, the error limit of the $\mu = \pm 1$ level splitting of the $^3H_6$ multiplet was added to the error limits of the splittings of the (1-1) lines.

In order to check the angular dependence of the intensities of the transitions for the Hsc case implied by Equations 91 and 94, spectra were taken for various angles ϕ and ϕ_m (experimentally, $\phi = \phi_m$). For the multiplets $^1G_4$ and $^3F_3$ the so-called rotation spectra (spectra taken for various angles ϕ_m) are pictured in Figures 13 and 14. The crystal used for the rotation spectra was a cylindrically shaped crystal of 10 per cent Tm in Y ethylsulphate.

A multiplet by multiplet interpretation of the data is given below for the zero field case and the two magnetic field cases.

Table 16. Measurement of the lines of 100 per cent Tm ES for Hpc values are in cm^{-1}

Line	Mult.	Magnetic field H=0	H=1/4	H=1/2	H=3/4	H=1	Temp. °K	Thickness mm	Polarization
0-2	$^1D_2$	27895.60	27894.92 27896.36	27894.16 27897.10	27893.42 27897.80	27892.72 27898.48	4	.2	s
0-2	"	27895.85	27895.71	27894.18 27897.11	27893.47 27897.84	27892.81 27898.66	20	.8	s
1-2	"	27864.51	27863.41 27865.28	27862.45 27866.31	27861.58 27867.26	27860.69 27868.17	20	.8	p
0-2	$^1G_4$	21170.58	21169.92 21171.18	21169.36 21171.76	21168.75 21172.25	21168.16 21172.76	4	.2	s
0-2'	"	21278.69	21278.68	21278.43	21278.50	21278.46	4	.2	s
0-3	"	21343.11	21342.97	21342.90	21342.87	21342.93	4	.2	p
1-2	"	21139.39	21139.04 21139.69	21138.49 21140.09	21138.24 21140.52	21137.83 21140.84	20	.2	p
1-1	"	21161.50	21161.62	21160.48 21162.66	21160.08 21163.14	21159.65 21163.64	20	.2	s
0-2	"	21170.66	21170.16 21171.38	21169.54 21171.93	21168.87 21172.44	21168.33 21172.98	20	.2	s
0-2'	"	21278.88	21278.66	21278.78	21278.79	21278.50	20	.2	s
0-3	"	21343.10	21343.31	21343.16	21343.28	21343.46	20	.2	p

Table 16. (Continued)

Line	Mult.	Magnetic field H=0	H=1/4	H=1/2	H=3/4	H=1	Temp. °K	Thickness mm	Polarization
0-2	$^1G_4$	21170.57	21169.82 21171.16	21169.27 21171.69	21168.67 21172.22	21168.06 21172.72	4	.5	s
0-2'	"	21277.98	21278.52	21278.50	21278.48	21278.42	4	.5	s
0-3	"	21343.12		21343.05		21343.06	4	.5	p
0-3'	"	21379.52		21378.95		21377.79	4	.5	p
0-3'	"	21382.10		21382.09		21382.05	4	.5	p
1-1	"	21161.60	21161.59	21160.54 21162.56	21160.11 21163.12	21159.67 21163.66	20	.5	s
0-2	$^3F_2$	15078.38	15077.94 15078.80	15077.40 15079.36	15076.92 15079.82	15076.46 15080.31	4	.2	s
1-2	"	15047.17	15047.16	15045.77 15048.62	15045.17 15049.24	15044.46 15049.98	20	.2	p
0-2	"	15078.45	15078.47	15077.53 15079.46	15077.02 15079.93	15076.55 15080.40	20	.2	s
1-2	"	15047.19	15046.56 15047.86	15045.81 15048.60	15045.12 15049.27	15044.48 15049.98	20	.5	p
1-1	"	15073.95	15074.06	15073.09 15074.94	15072.66	15072.34	20	.5	s

Table 16. (Continued)

Line	Mult.	Magnetic field H=0	H=1/4	H=1/2	H=3/4	H=1	Temp. °K	Thickness mm	Polarization
1-1	$^3F_2$			15073.12 15074.93		15072.31	20	.5	s
0-2	"	15078.49	15078.44	15077.49 15079.46	15077.00 15079.90	15076.50 15080.38	20	.5	s
0-3	$^3F_3$	14407.17	14407.16	14407.11	14407.06	14406.98	4	.2	p
0-2	"	14486.40	14485.96	14485.50	14485.48	14486.04	4	.2	s
0-3'	"	14487.41	14487.26	14487.80	14487.91	14488.72	4	.2	p
1-3	"	14375.90	14375.92	14375.91	14375.18 14376.42	14374.94 14376.57	20	.2	s
1-3	"		14375.99	14375.94	14375.29 14376.51	14375.00 14376.61	20	.2	s
0-3	"	14407.16	14407.24	14407.20	14407.14	14407.08	20	.2	p
1-1	"	14436.96	14437.04	14435.94 14438.20	14435.32 14438.78	14434.79 14439.30	20	.2	s
1-1	"		14437.06	14435.91 14438.17	14435.38 14438.75	14434.84 14439.32	20	.2	s
1-2	"	14455.16	14455.26	14453.67 14457.01	14452.84 14457.87	14452.10 14458.71	20	.2	p

Table 16. (Continued)

Line	Mult.	Magnetic field H=0	H=1/4	H=1/2	H=3/4	H=1	Temp. °K	Thickness mm	Polarization
1-3'	$^3F_3$	14456.12	14456.03	14456.40	14456.44	14456.58	20	.2	s
0-2	"	14486.45	14486.10	14486.03	14486.49	14485.81	20	.2	s
0-3'	"	14487.39	14487.47	14487.58	14487.58	14487.71	20	.2	p
1-2	"		14455.33	14453.61 14456.98	14452.87 14457.86	14452.04 14458.73	20	.5	p
0-3	$^3F_4$	12585.78	12585.78	12585.78	12585.74	12585.71	4	.2	p
0-2	"	12648.29	12648.30	12647.41 12648.98	12646.83 12650.04	12646.37 12650.57	4	.2	s
0-3'	"	12703.90	12703.90	12703.97	12703.89	12703.84	4	.2	p
0-2'	"	12762.92	12762.92	12762.90	12762.91	12762.94	4	.2	s
1-3	"	12554.64	12554.71	12554.30 12555.11	12554.06 12555.29	12553.81 12555.43	20	.2	s
0-3	"	12585.96	12586.03	12586.01	12585.94	12585.92	20	.2	p
1-2	"	12617.05	12617.18	12617.19	12616.94	12617.16	20	.2	p
0-2	"	12648.42	12648.46	12647.59 12649.39	12647.00 12649.89	12646.48 12650.48	20	.2	s

Table 16. (Continued)

Line	Mult.	Magnetic field H=0	H=1/4	H=1/2	H=3/4	H=1	Temp. °K	Thickness mm	Polarization
0-2	$^3F_4$		12648.44	12647.65 12648.97	12646.98 12649.84	12646.51 12650.59	20	.2	s
1-1	"	12691.8	12692.1	12691.7	12690.0	12691.5	20	.2	s
0-3'	"	12703.94	12704.18	12703.90	12704.41	12704.08	20	.2	p
0-2'	"	12762.98	12763.02	12763.07	12763.10	12762.96	20	.2	s

Table 17a. Measurement of the lines of 100 per cent Tm ES for Hsc values are in cm^{-1}

Line	Mult.	Magnetic field H=0	H=1/4	H=1/2	H=3/4	H=1	Temp. ^{o}K	Thick-ness mm	Polari-zation
0-2	$^{1}D_{2}$	27895.60	27895.70	27895.91	27896.46	27896.96	4	.2	s
0-2	"					27896.72	4	.5	s
0-2	"					27896.89	4	.5	p
0-2	"	27895.60				27896.94	20	.2	s
0-2	"					27897.11	20	.2	p
1-2	"	27864.34				27863.43 27864.85	20	.2	p
0-2	"	27895.85	27895.98	27896.07	27896.43	27897.08	20	.8	s
1-2	"	27864.51	27864.49	27864.47	27864.28	27864.15	20	.8	p
0-2	"			27896.08	27896.46	27897.09	20	.8	p
0-2	$^{1}G_{4}$	21170.58		21170.94	21171.32	21171.91	4	.2	s
0-2	"				21171.24	21171.76	4	.2	p
0-1	"			21193.10	21193.06	21193.24	4	.2	s
0-2'	"	21278.69		21279.12	21279.85	21281.08	4	.2	s

Table 17a. (Continued)

Line	Mult.	Magnetic field H=0	H=1/4	H=1/2	H=3/4	H=1	Temp. °K	Thick-ness mm	Polari-zation
0-3	$^1G_4$	21343.11	21343.09	21343.17	21343.68	21344.06	4	.2	p
1-2	"	21139.39	21139.34	21139.30	21138.75 21139.58	21138.16 21139.81	20	.2	p
1-1	"	21161.50	21161.40	21161.03	21160.35 21161.83	21159.44 21162.00	20	.2	s
0-2	"	21170.66	21170.72	21171.01	21171.40	21171.94	20	.2	s
0-2	"				21171.36	21171.82	20	.2	p
0-2'	"	21278.88	21278.92	21279.35	21279.79	21281.11	20	.2	s
0-3	"	21343.10	21343.52	21343.53	21343.70	21344.46	20	.2	p
1-2	"					21138.31 21139.90	20	.9	p
1-1	"					21159.62 21162.13	20	.9	s
0-2	$^3F_2$	15078.38	15078.46	15078.74	15079.14	15079.67	4	.2	s
0-2	"				15079.18	15079.74	4	.2	p
1-2	"	15047.17	15047.18	15047.08	15046.72 15047.30	15046.07 15047.46	20	.2	p

Table 17a. (Continued)

Line	Mult.	Magnetic Field H=0	H=1/4	H=1/2	H=3/4	H=1	Temp. °K	Thickness mm	Polarization
1-1	$^3F_2$	15073.94	15073.90	15073.93	15074.04	15073.64	20	.2	s
0-2	"	15078.45	15078.58	15078.82	15079.26	15079.77	20	.2	s
0-2	"				15079.26	15079.86	20	.2	p
1-1	"	15073.87	15073.91	15073.86	15073.92	15073.48	20	.8	s
0-2	"	15078.38	15078.48	15078.76	15079.18	15079.72	20	.8	s
0-2	"				15079.26	15079.78	20	.8	p
0-3	$^3F_3$	14407.17	14407.30	14407.52	14407.95	14408.53	4	.2	p
0-1	"		14468.27	14468.50	14468.83	14469.21	4	.2	s
0-2	"	14486.40	14486.36	14486.94	14487.35	14488.12	4	.2	s
0-3'	"	14487.41	14487.26	14487.80	14487.91	14488.72	4	.2	p
1-3	"	14375.90	14375.96	14376.01	14376.14	14376.34	20	.2	s
0-3	"	14407.16	14407.29	14407.58	14407.97	14408.50	20	.2	p
1-1	"	14436.96	14436.97	14436.82	14436.62	14435.64 14437.04	20	.2	s

Table 17a. (Continued)

Line	Mult.	Magnetic Field H=0	H=1/4	H=1/2	H=3/4	H=1	Temp. °K	Thickness mm	Polarization
1-2	$^3F_3$	14455.16	14455.26	14455.44	14455.75	14456.16	20	.2	p
1-3'	"	14456.12	14456.38	14455.05	14454.80	14454.56	20	.2	s
1-μ	"			14456.78	14457.36	14458.03	20	.2	s
0-1	"		14468.45	14468.60	14468.94	14469.38	20	.2	s
0-2	"	14486.45	14486.53	14486.70	14487.73	14488.07	20	.2	s
0-3'	"	14487.39	14487.57	14487.78	14488.09	14488.55	20	.2	p
0-3	$^3F_4$	12585.78	12585.89	12586.11	12586.51	12587.04	4	.2	p
0-2	"	12648.29	12648.44	12648.66	12649.03	12649.60	4	.2	s
0-2	"				12649.10	12649.75	4	.2	p
0-3'	"	12703.90	12703.98	12704.17	12704.45	12704.92	4	.2	p
0-2'	"	12762.92	12763.01	12763.27	12763.66	12764.18	4	.2	s
1-3	"	12554.64	12554.64	12554.62	12554.01 12554.81	12553.51 12554.97	20	.2	s
0-3	"	12585.96	12586.06	12586.32	12586.68	12587.18	20	.2	p
1-2	"	12617.05	12617.10	12617.10	12617.07	12617.06	20	.2	p

Table 17a. (Continued)

Line	Mult.	Magnetic Field H=0	H=1/4	H=1/2	H=3/4	H=1	Temp. °K	Thickness mm	Polarization
0-2	$^3F_4$	12648.42	12648.47	12648.76	12649.18	12649.74	20	.2	s
0-2	"				12649.24	12649.80	20	.2	p
0-3'	"	12703.94	12704.10	12704.41	12704.49	12705.11	20	.2	p
0-2'	"	12762.98	12763.05	12763.29	12763.73	12764.31	20	.2	s
1-3					12554.10 12554.94	12553.58 12555.07	20	.9	s

Table 17b. Rotation spectral data for the (1-1) line of the $^1G_4$ multiplet for a 10 per cent Tm in Y ES crystal with Hsc and H = 1

ϕ'^a in degrees	Line position in cm^{-1}	Relative intensity	ϕ'^a in degrees	Line position in cm^{-1}	Relative intensity
30	21158.70	15	65		2
		2		21159.89	23
	61.10	18			2
35	58.61	17	70		5
		1		59.89	17
	61.14	20			4
40	58.60	15	75		6
		4		59.86	17
	61.11	17			8
45	58.63	13	80		8
	59.88	7		59.87	11
	61.13	15			13
50		6	85	58.63	14
	59.88	16		59.88	7
		9		61.14	16
55		2	90	58.63	14
	59.85	20			4
		4		61.16	18
60		2	95	58.60	15
	59.84	22			2
		3		61.16	17

[a]Where $\phi' = \phi_m + \phi_o$.

Table 17c. Rotation spectral data for the (0-1) line of the $^3F_3$ multiplet for a 10 per cent Tm in Y ES crystal with Hsc and H = 1

ϕ'[a] in degrees	Line position in cm^{-1}	Level splitting Angles	Splitting in cm^{-1}
30	14468.06	30-60	0.18
40	68.03	60-90	0.12
50	67.88		
60	67.87		
70	67.89		
80	67.94		
90	67.99		
100	68.01		

[a]Where $\phi' = \phi_m + \phi_o$.

Table 18. Line splittings for Hpc

Transition	Multiplet	H=1/2	H=3/4	H=1	Number of observations
(0-2)	$^1D_2$	2.94±0.01	4.38±0.00	5.81±0.05	2
(1-2)	"	3.86	5.68	7.47	1
(0-2)	$^1G_4$	2.40±0.01	3.54±0.02	4.64±0.02	3
(1-2)	"	1.60	2.29	3.01	1
(1-1)	"	2.09±0.08	3.04±0.03	3.99±0.00	2
(0-2')	"	No line splitting observed			
(0-2)	$^3F_2$	1.96±0.04	2.90±0.01	3.86±0.01	3
(1-2)	"	2.82±0.03	4.11±0.04	5.50±0.01	2
(1-1)	"	1.83±0.02			2
(1-3)	$^3F_3$		1.23±0.00	1.62±0.01	2
(1-1)	"	2.26±0.00	3.41±0.04	4.50±0.02	2
(1-2)	"	3.36±0.02	5.00±0.02	6.65±0.04	2
(1-3)	$^3F_4$	0.81	1.24	1.62	1
(0-2)	"		2.98±0.15	4.09±0.07	3
(0-2')	"	No line splitting observed			

Table 19. Line splittings for Hsc

Line	Multiplet	Splittings in cm^{-1} H=3/4	Splittings in cm^{-1} H=1	Number of observations
(0-2)	$^1D_2$		0.17±0.00	2
(1-2)	"		1.42	1
(1-1)	$^1G_4$		2.54±0.03	2[a]
(1-1)	"		2.52±0.01	7[b]
(1-1)	"		2.53±0.02	9[c]
(0-2)	"	0.06±0.02	0.13±0.01	2
(1-2)	"		1.62±0.02	2
(0-2)	$^3F_2$	0.04±0.03	0.07±0.01	3
(1-2)	"		1.39	1
(1-1)	$^3F_3$		1.40	1
(0-2)	$^3F_4$	0.07±0.00	0.11±0.04	2
(1-3)	"		1.48±0.02	2

[a]Measured from 100 per cent Tm ES.

[b]Measured from 10 per cent Tm in Y ES.

[c]This is the average of the above data given in a and b.

$^3H_6$ multiplet

The first of the multiplets that will be discussed in some detail is the $^3H_6$ multiplet which has been identified as the ground multiplet (35, 36, 37, 38, 39). Transitions from the $\mu = 0$ level (taken as the zero of energy) and the $\mu = \pm 1$ level are shown in Figures 8 through 14.

The zero field energy of the $\mu = \pm 1$ level was determined by measuring the energy of transitions from it and from the $\mu = 0$ level to the same level in various multiplets. To assure accuracy, only sharp lines in regions of good dispersion were used to calculate the energy of the $\mu = \pm 1$ level. Lines appearing in the spectra for the $^3F_4$, $^3F_3$, $^3F_2$, and $^1G_4$ multiplets were used. The lines in the $^3F_4$ selected for use were the (0-3) line at 12586 cm^{-1} (at 20°K) and the (1-3) line at 12555 cm^{-1}. For simplicity, the line energies will be rounded off to the nearest wave number for the purposes of discussion on this multiplet as well as in the discussions for the other multiplets to follow. The line energies used in the actual calculations are given in Tables 16, 17a, 17b, and 17c. The difference in energy between the (0-3) line at 20°K and the (1-3) line was 31.31 cm^{-1}. Table 20 gives the energy differences between the (0-3) and (1-3) or the (0-2) and (1-2) lines

used for the determination of the energy of the $\mu = \pm 1$ level. The (0-3) or the (0-2) line energies used, as well as the (1-3) or the (1-2) line energies, were those energies obtained for a crystal temperature of 20°K.

Table 20. Determination of the energy of the $\mu = \pm 1$ level at 20°K

Multiplet[a]	Transitions at 20°K[b]	Energy in cm^{-1}	Crystal thickness mm
$^3F_4$	(0-3)-(1-3)	31.31	.2
$^3F_3$	(0-3)-(1-3)	31.26	.2
$^3F_2$	(0-2)-(1-2)	31.28	.2
$^3F_2$	(0-2)-(1-2)	31.30	.5
$^1G_4$	(0-2)-(1-2)	31.28	.2
Average of the above energies and the average deviation		31.29 ± 0.02	

[a]Multiplet in which the transitions were observed.

[b]The difference between the indicated transitions gave the energy in the energy column.

The splitting of the $\mu = \pm 1$ level for the magnetic field parallel to the c-axis was determined from the splitting of the (1-3) line in the $^3F_4$ and $^3F_3$ multiplets and the splitting of the (1-2) line in the $^3F_2$ and $^1G_4$ multiplets. For Hpc the (1-3) line split at a full field of 28,200 gauss by amounts

1.62 cm^{-1} for the $^3F_4$ multiplet and 1.62 cm^{-1} for the $^3F_3$ multiplet. The line splittings for Hpc are given in Table 18. The (1-2) line split 5.50 cm^{-1} in the $^3F_2$ multiplet and 3.01 cm^{-1} in the $^1G_4$ multiplet for Hpc at full field. The $\mu = \pm 2$ level splittings for the $^3F_2$ and $^1G_4$ multiplets from Table 26 for Hpc are 3.86 cm^{-1} and 4.64 cm^{-1} respectively at the full field of 28,200 gauss. To obtain the parallel field splittings for the $\mu = \pm 1$ level, Equations 63 and 64, and Figures 4d and 4e were used for the $^3F_2$ and $^1G_4$ (1-2) line splittings respectively. The $\mu = \pm 1$ level splitting for Hpc as measured in the $^3F_2$ multiplet was found to be 1.64 cm^{-1}, and the splitting as measured in the $^1G_4$ multiplet was found to be 1.63 cm^{-1}. Averaging the results obtained from the various multiplets, the result for the parallel field splitting for the $\mu = \pm 1$ level was 1.63 ± 0.01 cm^{-1} at full field. In a similar manner the three-quarter field (21,500 gauss) splitting was found to be 1.23 ± 0.01 cm^{-1} and the half field (14,400 gauss) splitting was 0.82 ± 0.02 cm^{-1}. The parallel splitting factor $g_{||}$ defined by Equation 51 ($\Delta_{||} = g_{||} \beta H$) was determined from the splittings at full (H = 1) and three-quarter (H = 3/4) fields. The result is $g_{||} = 1.23 \pm 0.01$ as given in Table 28. The splitting factor reported here is

considerably more accurate than the 1.0 ± 0.2 reported by Johnsen (35). It should be noted that while Johnsen (35) defined his splitting factors as one half of the ones defined in this work, the splitting factor he reported for the $\mu = \pm 1$ level was of the type used here. This discrepancy between Johnsen's definition and the splitting factor he reported was brought out by Wong and Richman (39). Throughout the rest of the discussions for the various multiplets, the level splittings were obtained for various field strengths but usually only the full field value will be discussed in detail.

The $\mu = \pm 1$ level splitting for the Hsc case was determined from the (1-3) line splitting appearing in the $^3F_4$ multiplet and the (1-2) line splittings appearing in the $^3F_2$ and $^1G_4$ multiplets. From Table 19 these line splittings are 1.48 cm^{-1}, 1.39 cm^{-1}, and 1.62 cm^{-1} at full field for the lines given above. The (1-2) line splittings were analysed using Equations 100 and 98, and Figures 5f and 5e for the $^3F_2$ and $^1G_4$ multiplets respectively. Table 27 gives the level splittings of the $\mu = \pm 2$ levels at H = 1 for the $^3F_2$ and $^1G_4$ multiplets as 0.07 cm^{-1} and 0.13 cm^{-1} respectively. As will be shown in later discussions, the assignments of $\eta_{2i'} = \pm 1$ and $B_{i'} = \pm 1$ (order of signs is important) were made for the

$\mu = \pm 2$ level of the $^1G_4$ multiplet and $\eta_{2i'} = \pm 1$ and $B_{i'} = \mp 1$ for the $\mu = \pm 2$ level of the $^3F_2$ multiplet. The splittings of the $\mu = \pm 1$ level as measured in the $^3F_2$ and $^1G_4$ multiplets were found to be 1.46 cm^{-1} and 1.49 cm^{-1} respectively. Averaging the above determinations for the $\mu = \pm 1$ level splitting, the result was that the splitting is 1.48 ± 0.02 cm^{-1} at a full field of 28,200 gauss. The level splitting could not be determined for the lower fields because the lines from which the measurements would have been made were not resolved sufficiently for good measurements. The splitting factor defined by Equation 72 ($\Delta_\perp = g_\perp \beta^2 H^2$) was found to be for the $\mu = \pm 1$ level $g_\perp = 0.85 \pm 0.01$. This result, as well as the perpendicular splitting factors for all the levels where a determination of the factor was made, is listed in Table 29.

The ground state ($\mu = 0$) is a non-degenerate level and therefore does not split when a magnetic field is applied. By Equation 55 and the work of Murao et al. (43), it is clear that the energy of this non-degenerate level is affected by the magnetic field. The $\mu = 0$ level shifts to lower energies quadratic in the applied magnetic field for magnetic fields both parallel and perpendicular to the c-axis. The level center for the $\mu = \pm 1$ level is also shifted quadratic in the applied

magnetic field for both field directions (Equations 44, 48, and 69). The energy dependence of the level center of the $\mu = \pm 1$ level (referred to the $\mu = 0$ level as the zero of the energy) was calculated using many of the same lines that were used to determine the level splitting. The two components of the (1-3) line splitting were averaged to give the energy difference between the $\mu = \pm 1$ level center and the $\mu = 3$ level of the excited multiplet. In a similar manner the (1-2) line components were averaged together as well as the (0-2) line components. Taking the difference between the energies of the line centers, (0-3)-(1-3) and (0-2)-(1-2), for a full field of 28,200 gauss parallel to the c-axis, the energy difference between the level center of the $\mu = \pm 1$ level and the $\mu = 0$ level became 31.30 cm^{-1} as measured in the $^3F_4$ multiplet, 31.30 cm^{-1} as measured in the $^3F_3$ multiplet, 31.26 cm^{-1} as measured in the $^3F_2$ multiplet, and 31.31 cm^{-1} as measured in the $^1G_4$ multiplet. The energy difference between the center of the $\mu = \pm 1$ level and the $\mu = 0$ level is then 31.29 ± 0.02 cm^{-1} for Hpc. For Hsc a similar type calculation was made and the result was that the difference in energy between the center of the $\mu = \pm 1$ level and the $\mu = 0$ level at full field was 32.94 cm^{-1} as measured in the $^3F_4$ multiplet, 33.04 cm^{-1} as measured

in the $^3F_2$ multiplet, and 32.90 cm^{-1} as measured in the $^1G_4$ multiplet. This then gives this energy difference to be 32.96 ± 0.05 cm^{-1}.

$^1D_2$ multiplet

The line at 27896 cm^{-1} was identified as the transition from the $\mu = 0$ level of the ground multiplet to the $\mu = \pm 2$ level of this multiplet (Figures 8a and 8b). For the full magnetic field of 28,300 gauss, this (0-2) line split 5.81 cm^{-1} for the field parallel to the c-axis and split 0.13 cm^{-1} for the field perpendicular to the c-axis. The (0-2) line splitting is the $\mu = \pm 2$ level splitting for both field directions. For Hsc the (0-2) line appearing in the p polarization occurred at a higher energy than the line appearing in the s polarization. From Figure 5b, this means $\eta_{2i'} = \pm 1$ and $B_{i'} = \mp 1$. The (1-2) line appearing at 27864 cm^{-1} split 7.47 cm^{-1} for Hpc and 0.17 cm^{-1} for Hsc at full field. Since the splitting of the $\mu = \pm 1$ level of the $^3H_6$ multiplet was known, the splitting of the $\mu = \pm 2$ level was determined using Equation 63 and Figure 4d for Hpc and Equation 99 and Figure 5f for Hsc. The results from the (0-2) line splitting and the (1-2) line splitting were averaged together to give the splitting listed in Tables 26 and 27. The splitting factors,

$g_{\parallel}$ and $g_{\perp}$, were determined from the level splittings and were found to be for the $\mu = \pm 2$ level, $g_{\parallel} = 4.40 \pm 0.02$ and $g_{\perp} = 0.08 \pm 0.03$. $g_{\parallel}$ was calculated using the level splitting obtained at the H = 3/4 and H = 1 fields.

At 27937 and 27942 cm^{-1} were two lines identified as (1-1) transitions. From Table 4 for J = 2, there should be only one $\mu = \pm 1$ electronic level; therefore one of the (1-1) lines may be a transition to a $\mu = \pm 1$ quantum level for $n_{gs} = 1$ like that of Equation 24. The energies of these (1-1) lines are listed in Table 21 along with the relative intensities of the lines. The energies of the levels, obtained by adding the 31.29 cm^{-1} energy of the $\mu = \pm 1$ level of the $^3H_6$ multiplet to the energies of the (1-1) lines, are listed in Table 22. The level chosen as the $\mu = \pm 1$ electronic level was arbitrarily chosen as the level at 27973 cm^{-1} because it had the more intense transition to it. Due to the broadness and overlap of the two (1-1) lines, no line splitting for either field direction could be determined.

Table 21. (1-1) transitions for the $^1D_2$ multiplet at 20°K

Wave number	Intensity[a]
27937.4 ± 0.2	22
27942.13 ± 0.06	28

[a]These intensities are relative intensities.

Table 22. Energy of the $\mu = \pm 1$ levels[a] for the $^1D_2$ multiplet at 20°K

Energy in cm^{-1}
27968.7 ± 0.2
27973.42 ± 0.08

[a]These levels have a μ quantum number of ± 1.

$^1G_4$ multiplet

The line at 21171 cm^{-1}, a (0-2) line, at (H = 1) split by amounts 4.64 cm^{-1} for Hpc and 0.13 cm^{-1} for Hsc. Since for Hsc the line appearing in the s polarization occurred at a higher energy than the one in the p polarization, from Figure 5a, $\eta_{2i'} = \pm 1$ and $B_{i'} = \pm 1$ for this $\mu = \pm 2$ level. The line splittings are the level splittings. The spectra are shown in Figure 9a and the energy level diagram is shown in Figure 9b.

From the level splittings the splitting factors were calculated to be, $g_{||} = 3.52 \pm 0.02$ and $g_{\perp} = 0.07 \pm 0.01$. The (1-2) line at 21139 cm^{-1} split 3.01 cm^{-1} for Hpc and 1.62 cm^{-1} for Hsc. Equation 64 and Figure 4e were used to analyse the splitting for Hpc, and Equation 98 and Figure 5e were used to analyse the splitting for Hsc. Using the ± 2 level splitting from above, the splitting of the $\mu = \pm 1$ level of the ground multiplet was determined as already mentioned. The assignments of $\eta_{2i'} = \pm 1$ and $B_{i'} = \pm 1$ are consistent for discussing the (0-2) line and the (1-2) line.

Table 4 shows that there should be two $\mu = \pm 2$ electronic levels for J = 4. In this multiplet one of the $\mu = \pm 2$ electronic levels was taken as the level at 21171 cm^{-1}. The other one was chosen to be the one at 21278 cm^{-1} ($\mu = \pm 2'$). There were additional (0-2') lines as shown in Figure 9a. The energies of these levels with μ quantum number ± 2 are listed in Table 23 along with the relative intensities of the transitions to these levels. The $\mu = \pm 2'$ electronic energy level is also listed in Table 23 along with the intensity of the (0-2') transition. The (0-2') transitions other than the 21278 cm^{-1} one are believed to be transitions to electron-phonon coupled states of the type given by Equation 24. The $\mu = \pm 2'$

electronic level showed no splitting for either field direction. From Table 28 the theoretical splitting factor for the $\mu = \pm 2'$ level for Hpc is 0.72 which means at full field the splitting would be 0.94 cm^{-1}. Because of the broadness of the (0-2') line, a splitting of this size would probably not be observed. None of the other (0-2') lines in the band showed a splitting either. The assignment of the ± 2 level at 21278 cm^{-1} as an electronic level was made because it had the most intense transition to it of all the other lines in the small band near 21278 cm^{-1}; also this assignment agrees with other workers (35, 37). This assignment disagrees with Wong and Richman who chose the level at 21308 cm^{-1} as an electronic level.

Table 23. Lines observed at approximately 21278 cm^{-1} at 4°K

μ[a]	Energy in cm^{-1}	Intensity[b]
2	21270.0 ± 0.2	11
2	21278.69 ± 0.08	40
2	21283.85 ± 0.09	25
2	21290.67 ± 0.07	23
2	21308.3 ± 0.1	12

[a]This is the μ quantum number of the level.

[b]These are relative intensities.

For J = 4 there should be two $\mu = 3$ electronic levels. The lines at 21343 cm^{-1} and 21382 cm^{-1} were identified at the (0-3) and (0-3') transitions to the $\mu = 3$ and $\mu = 3'$ electronic levels. Near the line at 21382 cm^{-1} was a line obeying the selection rules of a $\mu = 3$ level. This line appeared at 21380 cm^{-1} and was believed to be a transition to an electron-phonon coupled state because its intensity was weaker than that of the line at 21382 cm^{-1}. For the thicknesses of crystals used, no other (0-3) transitions were observed. The assignment of the $\mu = 3'$ electronic level disagrees with the energy given for this level by Wong and Richman (39). They assigned a level at 21512 cm^{-1} to be the $\mu = 3'$ electronic level.

The line at 21161 cm^{-1} was identified at a (1-1) transition. The energy of the $\mu = \pm 1$ level of this multiplet would then be 21192.79 cm^{-1}. The (1-1) line split 3.99 cm^{-1} for Hpc and 2.53 cm^{-1} for Hsc at the full field of 28,200 gauss. The $\mu = \pm 1$ level splitting of this multiplet was found using Equation 60 and Figure 4b for Hpc and Equation 102 and Figure 5g for Hsc.

The transitions from the $s = \pm 1$ components of the ground multiplet μ levels to the $s' = \mp 1$ components of the μ levels of

an excited multiplet are known as the outer components. The transitions from the $s = \pm 1$ components to the $s' = \pm 1$ components are known as the inner components. From Figure 5g the intensities of the outer components are a maximum at $\phi_m = 0^o$ while the intensities of the inner components are zero for the assignment of $\eta_{1i'} = \pm 1$ and $A_{i'} = \pm 1$. The spectra shown in Figure 13 are of the type given in Figure 5g; the intensities of the outer components are a maximum at $\phi_m = 0^o$ and $\phi_m = 60^o$ while the intensities of the inner components are a maximum at $\phi_m = 30^o$. Both the inner and outer components are observed at 15^o and 45^o but are less intense than at their maximum values. The data of Table 17b for the two components of the (1-1) line show the splitting of the outer components at $\phi_m = 0^o$ to be 2.53 cm^{-1} while at $\phi_m = 30^o$ the splitting of the inner components can not be resolved. ($\phi' = 30^o$ means $\phi_m \cong 0^o$). Discussion of the intensities of the inner and outer components of the (1-1) line will be taken up in more detail when the angle between the crystallographic a and x-axes is calculated. The splitting factors for this $\mu = \pm 1$ level were found to be $g_{\parallel} = 1.80 \pm 0.02$ and $g_{\perp} = 0.60 \pm 0.02$.

$^3F_2$ multiplet

The energies of the $\mu = \pm 2$ level and the $\mu = \pm 1$ level of this multiplet were obtained from lines identified as the (0-2) and (1-1) transitions. The (0-2) line occurred at 15078 cm^{-1} and the (1-1) line occurred at 15074 cm^{-1}. The intensity of the (1-1) line was very weak. The line was observed in .2 mm thick crystals, but it was extremely weak. Figure 10a shows the observed spectra and Figure 10b shows the energy level diagram with the transitions.

The (0-2) line at 15078 cm^{-1} split 3.86 cm^{-1} for Hpc and 0.07 cm^{-1} for Hsc at the full magnetic field. Since the line in the p polarization was at a higher energy than the line in the s polarization, from Figure 5b $\eta_{2i}' = \pm 1$ and $B_i' = \mp 1$. The (1-2) line at 15047 cm^{-1} split 5.05 cm^{-1} for Hpc and 1.39 cm^{-1} for Hsc. From the splittings of the (1-2) line and the (0-2) line, the splitting of the $\mu = \pm 1$ level of the $^3H_6$ multiplet was calculated as mentioned previously. Equation 63 and Figure 4d were used to interpret the Hpc data of the (1-2) line splitting and Equation 100 and Figure 5f were used to interpret the Hsc data of the (1-2) line splitting to get the $^3H_6$ multiplet's $\mu = \pm 1$ level splitting. The assignments of $\eta_{2i}' = \pm 1$ and $B_i' = \mp 1$ are consistent in interpreting the (0-2) and

(1-2) lines of this multiplet.

The (1-1) line at 15074 cm^{-1} was a weak transition as mentioned above. The $\mu = \pm 1$ level zero field energy was obtained by adding the energy of the $^3H_6$ multiplet's $\mu = \pm 1$ level energy to the energy of the (1-1) line. The zero field level energy is given in Table 25. The line splitting could only be observed at the half field value for Hpc because of the overlapping of the higher energy component of the (1-1) line and the low energy component of the (0-2) line for H = 3/4 and H = 1. The splitting of the (1-1) line was found to be 1.83 for Hpc at a field of 14,400 gauss. The $\mu = \pm 1$ level splitting for Hpc was determined from Equation 60 and Figure 4b and was found to be 1.01 ± 0.04 cm^{-1} which means $g_{||} = 1.56 \pm 0.07$. The (1-1) line splitting for Hsc could not be resolved sufficiently for an accurate determination of the splitting. The line did show a tendency to split for Hsc, however.

$^3F_3$ multiplet

The two lines (Figure 11a) observed in the parallel polarization at 14407 cm^{-1} and 14487 cm^{-1} were identified as transitions to the two $\mu = 3$ electronic levels of this multiplet from the $\mu = 0$ level of the ground multiplet. Figure 11b shows the energy level diagram with the observed transitions.

From Table 4 for J = 3 there should be two μ = 3 electronic levels. The level at 14407 cm^{-1} was designated as μ = 3 with the (0-3) and (1-3) transitions to it, and the level at 14487 cm^{-1} was designated as μ = 3' with the (0-3') and (1-3') transitions to it. The (0-3) line was relatively sharp; whereas the (0-3') line was very broad and, hence, no accurate measurement of it could be made. The lines at 14376 cm^{-1} and 14456 cm^{-1} were identified as the (1-3) and (1-3') transitions respectively. From the energy of the (1-3') line, the energy of the μ = 3' level was determined by adding the 31 cm^{-1} of the ground $\mu = \pm 1$ level energy to the (1-3') line energy to get 14487.41 cm^{-1}. The (1-3') line was fairly sharp so that the measurement of the level energy is fairly accurate.

At full field the (1-3) line at 14376 cm^{-1} split 1.62 cm^{-1} for Hpc. (This is the splitting of the $^3H_6$ multiplet's $\mu = \pm 1$ level.) The (1-3) line did not show a splitting for Hsc which is in agreement with Table 8. The (1-3) line for Hsc (H = 1) shifted to a higher energy by an amount 0.44 cm^{-1} indicating that the transition came from the s = -1 component of the $\mu = \pm 1$ level. According to Table 8, this means $\eta_{3i'} = 1$. The (1-3') line at 14456 cm^{-1} showed a tendency to split for Hpc but could not be completely resolved. This line did

not show a splitting for Hsc. For Hsc the (1-3') line shifted to a lower energy by an amount 1.56 cm^{-1} indicating the transition came from the s = 1 component of the $^3H_6$ multiplet's $\mu = \pm 1$ level. According to Table 8, this means $\eta_{3'i'} = -1$.

The line at 14486 cm^{-1} appearing in the perpendicular polarization was identified as the (0-2) line. This (0-2) line was extremely broad and showed no splitting for Hpc. For Hsc any (0-2) line appearing in the parallel polarization would be at an energy of approximately the same as the (0-3) line. Therefore, the (0-2) line in the parallel polarization could not be observed. The (1-2) line at 14455 cm^{-1} split for Hpc (H = 1) by an amount 6.65 cm^{-1}. Using Equation 63, Figure 4d, and the splitting of the $^3H_6$ multiplet's $\mu = \pm 1$ level splitting, the $\mu = \pm 2$ level splitting was calculated to be 5.02 cm^{-1}. The $g_{||}$ splitting factor was found to be $g_{||} = 3.78 \pm 0.03$. Any line splitting of the (1-2) line for Hsc could not be determined because of the braodness of the line. Therefore, no $\mu = \pm 2$ level splitting for Hsc could be determined. The zero field energy of the $\mu = \pm 2$ level was determined from the energy of the (1-2) line in a manner similar to determination of the energy of the $\mu = 3'$ level from the

(1-3') line.

The $\mu = \pm 1$ level position and splitting was determined from the line at 14437 cm^{-1} identified as a (1-1) transition. This (1-1) line split at full field 4.50 cm^{-1} for Hpc and by an amount 1.40 cm^{-1} for Hsc. The line splittings are given in Tables 18 and 19. The parallel field splitting of the $\mu = \pm 1$ level was determined from Equation 60 and Figure 4b. Subtracting the splitting of the $^3H_6$ multiplet's $\mu = \pm 1$ level from the (1-1) line splitting gave a parallel field splitting of 2.87 cm^{-1}. The splitting factor was calculated to be $g_{||} = 2.18 \pm 0.04$. The perpendicular field splittings of the $\mu = \pm 1$ level was determined from Equation 105 and Figure 5h with $\phi_m = 0^o$. The assignments of $\eta_{1i'} = \pm 1$ and $A_{i'} = \mp 1$ were made. The intensities of the inner and outer components of the (1-1) line obeyed those of Figure 5h for spectra taken when the angle ϕ_m was varied. The line splittings of the inner and outer components of the (1-1) line could not be resolved very well at the angles $\phi_m = 0^o$ and $\phi_m = 30^o$. In addition to determining the $\mu = \pm 1$ level splitting for Hsc from the splitting of the (1-1) line, the level splitting was determined from the (0-1) line as will be discussed.

The line which appeared at 14469 cm^{-1} for a field of

28,200 gauss perpendicular to the c-axis was identified as the (0-1) transition. This line vanished at zero magnetic field. The dependency of the intensity on ϕ_m was checked for this line. It was found to obey the type of behavior given in Figure 5j. Data for this line are listed in Table 17c and the spectra for various angles ϕ_m are shown in Figure 14. Table 17c shows an angular dependence of the energy, but this is only an illusion as will be pointed out in more detail in the section where the angle $\bar{\phi}$ is determined. From Figure 5j, the $\mu = \pm 1$ level splitting of this multiplet could be obtained by taking the difference in the energies of the (0-1) line as it appears at $\phi_m = 0^o$ and $\phi_m = 30^o$. The energy of the (0-1) line at $\phi' = 30^o$ ($\phi' = 30^o$ means $\phi_m \cong 0^o$) was more than that for the (0-1) line at $\phi' = 60^o$ ($\phi_m \cong 30^o$) indicating the (0-1) line follows the behavior given in Figure 5j with the assignments $\eta_{1i'} = \pm 1$ and $A_{i'} = \mp 1$. The data of Table 17a for the (0-1) line are then for transitions to the s = 1 component of the $\mu = \pm 1$ level. The $\mu = \pm 1$ level splitting obtained from the (1-1) line and from the difference in energy of the (0-1) line at $\phi_m = 0^o$ and $\phi_m = 30^o$ were used to determine a perpendicular splitting factor, $g_\perp = 0.07 \pm 0.02$.

Near the line identified as the (1-3') transition was a

line at 14458 cm^{-1} at full field for Hsc which obeyed the same selection rules as the (1-3') line. This line does not appear at a crystal temperature of $4^{o}K$, but does appear at a temperature of $20^{o}K$. Therefore, this line was a transition from the $\mu = \pm 1$ level of the $^{3}H_{6}$ multiplet. The energy difference between this 14458 cm^{-1} line and the (1-3') line was too large to be a splitting of the (1-3') line. This energy difference was found to be 3.50 cm^{-1} while a splitting of the (1-3') line would have to be 1.48 cm^{-1}. The angular dependence of the intensity of this line at 14458 cm^{-1} as ϕ_m was varied did not fit that of a (1-0) line. It is felt that this line was a transition to an electron-phonon coupled state.

$^{3}F_{4}$ multiplet

The two lines appearing in the perpendicular polarization (Figure 12a) at 12648 cm^{-1} and 12763 cm^{-1} were identified as transitions to the two $\mu = \pm 2$ levels of this multiplet from the ground $\mu = 0$ level. The energy level diagram for this multiplet is shown in Figure 12b. The (0-2) line at 12648 cm^{-1} was found to split 4.09 cm^{-1} for Hpc and 0.11 cm^{-1} for Hsc at full field. For Hsc the (0-2) line in the p polarization occurred at a higher energy than the one which appeared in the s polarization; this means $\eta_{2i'} = \pm 1$ and $B_{i'} = \mp 1$ in

accordance with Figure 5b. The splitting factors of the $\mu = \pm 2$ level at 12648 cm^{-1} were found to be $g_{\parallel} = 3.0 \pm 0.1$ and $g_{\perp} = 0.06 \pm 0.02$. The components of the (0-2) line from which the measurements of the splitting were made were quite broad resulting in a relatively large error limit for Hpc. The splitting of the (1-2) line at 12617 cm^{-1} could not be resolved sufficiently for either magnetic field direction. The (0-2') line at 12763 cm^{-1} did not show a splitting for either field direction. The theoretical parallel splitting factor for the $\mu = \pm 2'$ level from Table 28 is $g_{\parallel} = 0.23$ which means at full field the theoretical splitting would be 0.30 cm^{-1}. A splitting of this magnitude would not have been detected for the (0-2') line. Neither a (0-2') line appeared in the p polarization for Hsc nor a (1-2') line appeared in the spectra taken; therefore no perpendicular splitting factor was obtained for the $\mu = \pm 2'$ level.

The two lines (0-3) and (0-3') appearing in the parallel polarization at 12586 cm^{-1} and 12704 cm^{-1} were identified as transitions to the two $\mu = 3$ levels for this $J = 4$ multiplet. The (0-3) line at 12586 cm^{-1} was strong and sharp, whereas the (0-3') line at 12704 cm^{-1} was broad and weak.

The line at 12556 cm^{-1} was identified as a (1-3) transi-

tion. This (1-3) line showed a splitting at full field of 1.62 cm^{-1} for Hpc and 1.48 cm^{-1} for Hsc. This splitting would be the splitting of the $^3H_6$ multiplet's $\mu = \pm 1$ level as pointed out in a previous discussion. When the magnetic field is applied perpendicular to the c-axis, Table 8 shows that only one component of the (1-3) line should be observed. In this case, however, both components were observed. The intensity of the transition from the s = -1 component of the $^3H_6$ multiplet's $\mu = \pm 1$ level was stronger than the intensity of the transition from the s = 1 component. The line from the s = 1 component to the $\mu = 3$ level was weaker than one would expect because of the population difference of the s = 1 and s = -1 components. The difference in the intensities of the two (1-3) line components for Hsc was more than the difference for Hpc (Figure 12a). From Table 8 for $\eta_{3i'} = 1$ the (1-3) transition that should be observed is the transition from the s = -1 component. The assignment of $\eta_{3i'} = 1$ is in agreement with the results for the η selection rule for a (0-3) type transition; for the odd parity α's = 0 and the odd parity β's $\neq$ 0, the η selection rule for the (0-3) transition from previous results was $\eta_{0i}\,\eta_{3i'} = 1$. $\eta_{0i} = 1$, therefore, $\eta_{3i'} = 1$ also.

If in Tables 5 through 10 the odd parity β's are zero and the odd parity α's are non-zero, the zero (0) and the (1) in the I columns would be interchanged. Therefore for $\eta_{3i'} = 1$, transitions from the s = 1 component could then be observed if the odd parity α's are non-zero. However, the magnitude of the odd parity α's must be much smaller than the magnitude of the odd parity β's. This conclusion is reached because of two reasons. The first reason is the good description of the spectral lines in this multiplet as well as lines in the other multiplets by the theory was very good. The second reason is that the transition from the s = 1 component is quite a bit weaker than the transition from the s = -1 component in the (1-3) transition of this multiplet.

The line at 12692 cm^{-1} was identified as a (1-1) transition. This line was very broad and quite weak for spectra from a thin crystal. However, when the crystal was made thicker, the line intensity became stronger but the line also became very much broader. Therefore, the accuracy of the reported position of the $\mu = \pm 1$ level for this multiplet is probably as accurate as one can expect. No splitting of this (1-1) line was detected for either direction of the magnetic field due to the broadness of the line. The assignment of

the energy of the $\mu = \pm 1$ electronic level from the energy of the (1-1) line disagrees with the assignment by Wong and Richman (39). No (1-1) line for the thicknesses of crystals used was observed to a $\mu = \pm 1$ energy level corresponding to that of Wong and Richman, indicating that it would be a very weak transition. It is therefore believed, the $\mu = \pm 1$ level of Wong and Richman could very likely be an electron-phonon coupled state of the type given by Equation 24.

With the discussion of the $^3F_4$ multiplet, the discussions of the various multiplets are concluded. It is apparent that the spectra taken for the magnetic field perpendicular to the c-axis can be explained with a consistent choice of the η's, B's, and A's. To describe the line splittings of the (0-2), (1-2), (1-1), and (0-1) lines, a proper choice of the above quantities was needed. The line intensities that showed a dependence on the angle ϕ_m were the (1-1) and (0-1) lines. The other line intensities did not show an angular dependence.

Theoretical splitting factors and tabulation of results

It has been shown that there are 91 separate energy levels for a f^{12} configuration of electrons or a f^2 configuration of positive holes (1, 4, 52). This means that there are 91

different products of the single 4f electron wave functions which obey the Pauli exclusion principle. Therefore when the product wave function representation is used, the secular determinant is 91 by 91.

The 91 by 91 matrix has been diagonalized getting a best fit for the crystal field constants, F integrals, and ζ as mentioned previously. Here, however, it is of interest to add the additional perturbation of that given by Equation 43 for the parallel Zeeman effect where H is the magnitude of the magnetic field. The appropriate matrix elements (only diagonal ones result) were added to those of Spedding and Haas and the resulting matrix was diagonalized for various magnetic fields using Wong and Richman's (39) crystal field constants and Margolis' (38) F's and ζ as given in Table 24. The magnetic fields used were 5, 15, and 30 kilogauss. From the resulting splittings, the splitting factors defined by Equation 51 ($\Delta_{\parallel} = g_{\parallel} \beta H$) were calculated and found to be essentially independent of magnetic field. The results are listed in Table 28 along with the theoretical values of Wong and Richman (39) and the experimental values determined in this work. The difference between the splitting factors found from the 91 by 91 matrix diagonalization and those of Wong and

Richman (39) is due to the fact the 91 by 91 matrix takes into account the interaction of all multiplets via the crystal field, whereas the operator equivalent method used by Wong and Richman does not.

Since the theoretical energies of the multiplet centers, crystal field splittings, and magnetic field splittings do not agree exactly with experiment, the Hamiltonian used (Equation 4 plus Equation 43) is obviously not the complete Hamiltonian. This point will be discussed in some detail in a later chapter. Although the agreement between experiment and theory is not exact, there is good qualitative agreement indicating the Hamiltonian used was a fairly good approximation to the correct Hamiltonian.

The 91 by 91 matrix including the perpendicular magnetic field perturbation (Equation 66) instead of the parallel field perturbation could not be diagonalized. Smaller matrices to diagonalize were required. The choice made was to use the intermediate coupling free ion wave functions (Equation 2) as basis functions. The largest matrix to diagonalize would then be 13 by 13 in the case for J=6. (J_z ranges from 6 to -6 in integer steps). The form of the perpendicular magnetic field interaction given by Equation 68 was used. To determine the

effective Lande' g_L factor $g(\gamma J)$, the $\phi_{\gamma JM}$'s were expressed as a linear combination of Russell Saunders wave functions $\phi_{LSM_LM_S}$ where L is the total orbital angular momentum with z projection M_L and S is the total spin angular momentum with z projection M_S. The expansion coefficients were found from the secular equations where the F integrals and ξ of Margolis (38) were used. Using the $\phi_{\gamma JM}$'s, the effective Lande' g_L factors $g(\gamma J)$ were calculated for the various multiplets. The $\phi_{\gamma JM}$'s were then used as basis functions to diagonalize the Hamiltonian when the crystal field interaction and perpendicular magnetic field interaction (Equation 68) were included. The crystal field constants of Wong and Richman (39) were used. The matrices were diagonalized for the various multiplets and for various magnetic fields. The splittings were found to be independent of the angle the magnetic field makes with the crystallographic x-axis (ϕ_m) in agreement with the theory of Murao et al. (43). From Equation 72 ($\Delta_\perp = g_\perp \beta^2 H^2$) the perpendicular splitting factors were calculated. For some of the levels with large splittings (about one cm^{-1}), there were some slight field dependencies of the splitting factors. In most of the cases, however, the effect of the field dependence was smaller than the experimental error in

measuring the splitting factor. Since the field dependence of the experimentally determined $g_{\perp}$-factors could not be obtained for the levels where the theoretical $g_{\perp}$-factor did show a field dependence, the theoretical splitting factors were calculated at the same field (28,200 gauss) which the experimental ones were determined. The results are given in Table 29. The approximation used here for calculating $g_{\perp}$ compared to the approximation of Wong and Richman (39) for calculating $g_{\parallel}$.

The theoretical $g_{\perp}$-factors are zero for the $\mu = \pm 2$ levels when $J = 2$. This is because there are no $\mu = 3$ states for the needed off diagonal matrix elements of Equation 70 in the approximation used. The experimental splitting factors for the two $J = 2$ multiplets measured were not zero indicating there are intermultiplet interactions which are important.

From Equations 44, 48, 69, and 70, the energy of the level centers are affected by the magnetic field for both field directions. The theoretical and experimental $g_{\parallel}$ and $g_{\perp}$ splitting factors of Tables 28 and 29 are given for only the level splittings and not for the shifting of the level centers with magnetic field.

Table 24. Comparison of constants for thulium ethylsulphate

Constant	Gruber and Conway (36,37)	Margolis[a] (38)	Wong and Richman (39)
F_2	450 cm^{-1}	451.1 cm^{-1}	
F_4	62.1	68.07	
F_6	6.795	7.437	
ζ_{4f}	-2700	-2656	
$A_{20}\langle r^2\rangle$	13		129.8 cm^{-1}
$A_{40}\langle r^4\rangle$	-80		-71.0
$A_{60}\langle r^6\rangle$	-32		-28.6
$A_{66}\langle r^6\rangle$	300		432.8

[a]The values given here are for no orbit-orbit interaction.

Table 25. The energy levels of Tm ethylsulphate at zero field

Level	Multiplet	Energy in cm^{-1} (H = 0) $4.2^{o}K$	$20^{o}K$
± 1	$^{1}D_{2}$		27973.42±0.08
± 2	"	27895.60±0.02	27895.60±0.03
3'	$^{1}G_{4}$	21382.1±0.1	
3	"	21343.11±0.04	21343.88±0.08
± 2'	"	21278.69±0.08	2.278.88±0.08
± 1	"		21192.79±0.07
± 2	"	21170.58±0.02	21170.66±0.02
± 1	$^{3}F_{2}$		15105.22±0.05
± 2	"	15078.38±0.01	15078.45±0.02
3'	$^{3}F_{3}$		14487.41±0.07
± 2	"		14486.45±0.03
± 1	"		14468.24±0.04
3	"	14407.17±0.01	14407.16±0.01
± 2'	$^{3}F_{4}$	12762.92 ±0.03	12762.98±0.02
± 1	"		12722.7±0.5
3	"	12703.90±0.02	12703.94±0.09
± 2	"	12648.29±0.03	12648.41±0.03
3	"	12585.78±0.01	12585.96±0.01
± 1	$^{3}H_{6}$		31.29±0.02
0	"	0.00	0.00

Table 26. Level splittings for Hpc

Level	Multiplet	Level splittings in cm^{-1} H=1/2	H=3/4	H=1	Number of observations
±1	$^1D_2$	Not determined			
±2	"	2.97±0.05	4.40±0.02	5.82±0.03	3
±2'	$^1G_4$	No level splitting observed			
±1	"	1.27±0.10	1.81±0.04	2.36±0.01	2
±2	"	2.40±0.01	3.54±0.02	4.64±0.02	3
±1	$^3F_2$	1.01±0.04			2
±2	"	1.96±0.04	2.90±0.01	3.86±0.01	3
±2	$^3F_3$	2.54±0.04	3.77±0.03	5.02±0.05	2
±1	"	1.44±0.02	2.18±0.05	2.87±0.03	2
±2'	$^3F_4$	No level splitting observed			
±1	"	Not determined			
±2	"	1.56±0.16	2.98±0.15	4.09±0.07	
±1	$^3H_6$	0.82±0.02	1.23±0.01	1.63±0.01	6[a]

[a]Six observations except for H=1/2 where there was only four.

Table 27. Level splitting for Hsc

Level	Multiplet	Splittings in cm^{-1} H=3/4	H=1	Number of observations
±1	$^1D_2$	Not determined		
±2	"		0.13±0.05	3
±2'	$^1G_4$	Not determined		
±1	"		1.05±0.04	9
±2	"	0.06±0.02	0.13±0.01	2
±1	$^3F_2$	Not determined		
±2	"	0.04±0.03	0.07±0.01	3
±2	$^3F_3$	Not determined		
±1	"		0.13±0.04	3[a]
±2'	$^3F_4$	Not determined		
±1	"	Not determined		
±2	"	0.07±0.01	0.11±0.04	2
±1	$^3H_6$		1.48±0.02	4

[a]This includes the splitting as obtained from the (0-1) line as given in Table 17c.

Table 28. $g_{||}$ splitting factors for Tm ethylsulphate

μ quantum and multiplet		Nominal energy	Theoretical[a]	Theoretical[b]	Experimental[c]
± 1	$^1D_2$	27940	2.26	2.27	---
± 2	"	27896	4.55	4.54	4.40 ± 0.02
$\pm 2'$	$^1G_4$	21278	0.72	0.80	---
± 1	"	21193	1.91	1.92	1.80 ± 0.02
± 2	"	21171	3.11	3.04	3.52 ± 0.02
± 1	$^3F_2$	15105	1.38	1.51	1.50 ± 0.06
± 2	"	15078	3.11	3.02	2.91 ± 0.01
± 2	$^3F_3$	14486	4.18	4.33	3.78 ± 0.03
± 1	"	14468	2.30	2.17	2.18 ± 0.04
$\pm 2'$	$^3F_4$	12763	0.23	0.12	---
± 1	"	12723	1.88	1.91	---
± 2	"	12648	3.59	3.69	3.0 ± 0.1
± 1	$^3H_6$	31	1.11	1.09	1.23 ± 0.01

[a]Results of diagonalizing the 91 by 91 matrix.

[b]These are the theoretical results of Wong and Richman (39).

[c]Calculated from level splittings at H = 3/4 and H = 1.

Table 29. $g_\perp$ splitting factors for Tm ethylsulphate

μ quantum number and multiplet		Nominal energy	Theoretical	Experimental
±1	$^1D_2$	27940	1.80	---
±2	"	27896	0.00	0.08±0.03
±2'	$^1G_4$	21278	0.02	---
±1	"	21193	0.69	0.60±0.02
±2	"	21171	0.03	0.07±0.01
±1	$^3F_2$	15105	0.02	---
±2	"	15078	0.00	0.04±0.02
±2	$^3F_3$	14486	1.14	---
±1	"	14468	0.15	0.07±0.02
±2'	$^3F_4$	12763	0.21	---
±1	"	12723	0.12	---
±2	"	12648	0.08	0.06±0.02
±1	$^3H_6$	31	0.78	0.85±0.01

Determination of $\bar{\phi}$

For the rare earth ethylsulphates which have C_{3h} point group symmetry, Murao et al. (43) have shown that an x-axis in the basal plane can be chosen such that the β_{66} term in Equation 14 is zero. $\bar{\phi}$ measures the angle between the crystallographic a-axis and this x-axis. The calculations of Murao et al. (43) and those in this work for the line intensities were based on the assumption that the x-axis had been chosen such that $\beta_{66} = 0$. Theory predicts that for the line intensities of Tm ES that vary as the angle between the transverse magnetic field Hsc and the x-axis varies, the intensity maxima or minima occur when the magnetic field is parallel to the x-axis.

The intensities of the Zeeman line patterns of the (1-1) and (0-1) transitions vary as the angle ϕ_m is varied where ϕ_m is the angle the transverse field makes with the x-axis. This type of behavior is shown in Figures 5g, 5h, 5i and 5j. Spectral data were obtained when the angle ϕ_m was varied (Tables 17b and 17c). The spectra were obtained from a 10 per cent Tm concentration in Y ethylsulphate 3mm cylindrical crystal. The spectral lines from a 100 per cent Tm ES 3 mm cylindrical crystal were too broad to be analysed in any

quantitative manner. It was found that 3 mm was the minimum size of a cylinder that could be used. To determine $\bar{\phi}$, two other angles ϕ_o and ϕ_a had to be determined. The relation between these angles is shown in Figure 15. As will be shown, the angle ϕ_o was determined from the intensities of the components of the (1-1) and (0-1) lines for the $^1G_4$ and $^3F_3$ multiplets respectively. The angle ϕ_a was determined from back reflection X-ray pictures.

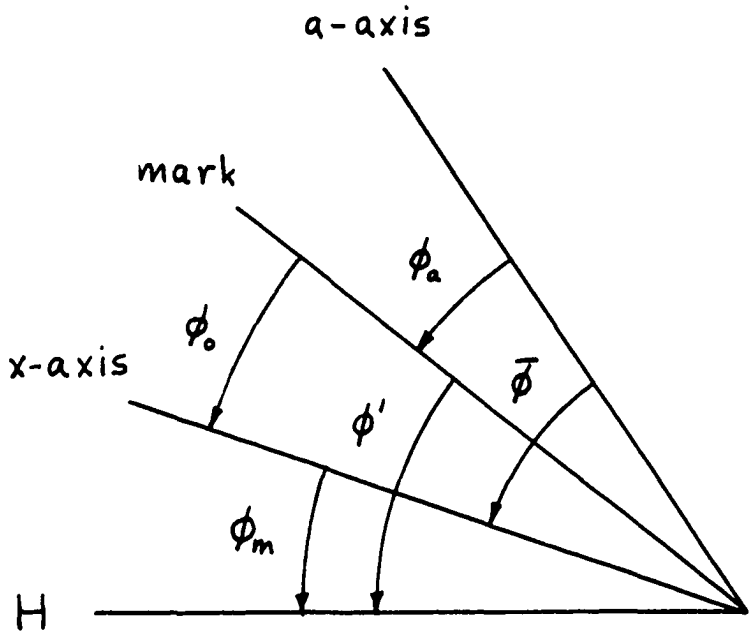

Figure 15. Angles needed to determine $\bar{\phi}$

The intensities of the inner and outer components of the Zeeman line pattern for the line at 21161 cm^{-1}, identified as the (1-1) transition for the $^1G_4$ multiplet, followed the behavior shown in Figure 5g and Table 9. Resolution between the two cases when $\phi_m = 0^o$ and when $\phi_m = 30^o$ was good. At $\phi_m = 0^o$ the outer components of the (1-1) line were resolved and these are labeled (1-1)L and (1-1)H in Table 30. At $\phi_m = 30^o$ the inner components of the (1-1) line were not resolved and this line is designated as (1-1)C. Table 17b gives the line positions and relative intensities of these lines and the spectra are shown in Figure 13. The intensities of the outer components (1-1)L and (1-1)H obey,

$$I = I_o \cos^2 3\phi_m = (I_o/2)(1 + \cos 6\phi_m), \qquad (115)$$

and the inner components (1-1)C obey,

$$I = I_o \sin^2 3\phi_m = (I_o/2)(1 - \cos 6\phi_m). \qquad (116)$$

A mark was placed on the crystal at an arbitrary point and spectra were obtained for various angles ϕ' with respect to this mark. ϕ' measures the angle between the mark and the direction of the magnetic field as shown in Figure 15. Since $\phi' = \phi_m + \phi_o$, $\phi_m = \phi' - \phi_o$. ϕ_m in Equations 115 and 116 was replaced by $\phi' - \phi_o$ and a computer program developed by Mr. W. J. Haas was used to determine the angle ϕ_o. When ϕ'

equalled ϕ_o the intensities of the outer and inner components of the (1-1) line were a maximum and a minimum respectively. The constant ϕ_o for the various components of the (1-1) transition of the $^1G_4$ multiplet is listed in Table 30.

The angle ϕ_o was also determined from the intensity of the two components of the (0-1) transition of the $^3F_3$ multiplet. The two components of the (0-1) transition are of the type shown in Figure 5j. The observed transition at $\phi_m = 0^o$ is the transition to the (+) component of the $\mu = \pm 1$ level. At $\phi_m = 30^o$ the observed transition is the one to the (-) component of the $\mu = \pm 1$ level. The transitions at 0^o and 30^o are designated as $(0\text{-}1^+)$ and $(0\text{-}1^-)$ respectively. The intensity of the $(0\text{-}1^+)$ line is that given by Equation 115 and the $(0\text{-}1^-)$ line is that given by Equation 116. At angles intermediate between 0^o and 30^o, both components would be present although not as intense as at 0^o or 30^o. At the intermediate angles the two components could not be resolved; therefore the measured energy of the line was somewhere between the energy of the $(0\text{-}1^+)$ line and the $(0\text{-}1^-)$ line depending upon the intensities of the components. The energy of the (0-1) line appeared to have a dependence upon the angle ϕ_m, however, what was really happening was the intensities of the two components

were varying with angle ϕ_m giving an apparent change in energy. The energy of the two components of the (0-1) line for the $^3F_3$ multiplet is given in Table 17c where the energy appears to change with the angle $\phi' = \phi_m + \phi_o$. The spectra of the two components of the (0-1) line are shown in Figure 14. Since the two components ($0\text{-}1^+$) and ($0\text{-}1^-$) could not be resolved, their intensities could not be used to determine the angle ϕ_o as was done for the (1-1) line of the $^1G_4$ multiplet. However, since the energy of the two components of the (0-1) line appeared to have an angular dependence, this angular dependence was used to determine ϕ_o from an equation of the form,

$$E = C + B \cos 6(\phi' - \phi_o). \qquad (117)$$

The result for the determination for ϕ_o is given in Table 30.

Having determined the angle ϕ_o, the angle that remains to be determined is the angle between the mark on the crystal and the a-axis ϕ_a. In hexagonal structures there are two sets of axes defined in the basal plane, a and b-axes. An a-axis connects nearest neighbor rare earth ions in the plane perpendicular to the c-axis, and the b-axis is defined as perpendicular to the a-axis and lying in the basal plane. Since equivalent a-axes occur every 60^o, the angle between an a-axis and a b-axis is 30^o. The a-axes are taken as passing through the

corners of a hexagonally shaped crystal and the b-axes as passing through the flat faces. It turns out that in the back-reflection X-ray pictures, the Laue pattern of the b-axes is the more intense pattern for 10 per cent Tm in Y ES. The Laue pattern of the a-axes was very faint in the X-ray pictures taken. The angle between the mark on the crystal and a b-axis is given in Table 31. Therefore, the angle between the mark on the crystal and an a-axis was $35.6^{o} \pm 0.6^{o}$.

From Figure 15, $\bar{\phi} = \phi_o + \phi_a$; therefore $\bar{\phi} = 68.6^{o}$. However, there would be an equivalent a-axis rotated 60^{o} in a counter-clockwise from the one shown; therefore $\bar{\phi} = 8.8^{o}$. ($\bar{\phi}$ would then be defined as the angle measured from an a-axis to an x-axis in a counter-clockwise direction.) Adding the error limits from the determinations of ϕ_o and ϕ_a, the error limit would be $\pm 1.0^{o}$. An additional estimated 1.0^{o} error limit will be added to account for any error in lining up the crystal in the magnetic field or for the X-ray picutres. Therefore, $\bar{\phi} = 9^{o} \pm 2^{o}$ for 10 per cent Tm in Y ethylsulphate.

Table 30. Results of the least squares fit for the angle ϕ_o

Line	Multiplet	ϕ_o in degrees
(1-1)L	$^1G_4$	32.8
(1-1)H	"	33.3
(1-1)C	"	33.9
(0-1)	$^3F_3$	32.7
Average ϕ_o in degrees		33.2 ± 0.4

Table 31. Determination of the angle between the mark on the crystal and the b-axis

X-ray picture	Angle in degrees
1	5.5
	6.0
	5.7
2	5.5
	4.0
	7.0
Average angle in degrees	5.6 ± 0.6

DISCUSSION AND CONCLUSIONS

If one were to arbitrarily make the electronic level assignments on the basis that the most intensely absorbed lines are transitions between electronic states, then the energies of the electronic levels for the multiplets measured are given in Table 25. The assignments made here on the basis of intensity agree with those of Johnsen (35) and Gruber and Conway (36, 37) who observed that for this assignment of electronic levels, the spectral lines obeyed the Ritz combination principle. It is then assumed that the weaker transitions would be transitions from electronic states to electron-phonon (vibronic) coupled states, or vice versa. Equation 23 describes the electronic states and Equation 24 describes the electron-phonon coupled states. The transitions between electronic and electron-phonon coupled states are second order transitions of the type described by Pollack and Satten (48) and Richman et al. (49). (Substantially the same results are obtained for the transitions if the first order perturbation wave functions describing the states given by Equations 23 and 24 are used.) Therefore if H_{ep} can truly be treated as a perturbation on H_L and H_o, these second order transitions will probably be less intense than the first order transitions

between electronic states. The assignment of levels because of intensities of the absorption lines is rather arbitrary and even doubtful. To be really able to tell, one needs a detailed knowledge of the matrix elements. This knowledge of the matrix elements is lacking. Not too much is known about the size of the interconfigurational interaction and details of the electron-phonon interaction have not been worked out yet.

The fact that some of the electronic level assignments given in Table 25 do not agree with Wong and Richman (39) is not too disturbing even though their crystal field constants are considered better than those of Gruber and Conway (37). The electronic level assignments in this work agree with Gruber and Conway.

As already stated, the separation of electronic transitions from the electron-phonon coupled transitions is difficult. It is therefore very likely that some of the transitions identified as transitions between electronic levels in this work as well as in the work of Wong and Richman may be transitions to electron-phonon coupled states. Taking into account level shifting due to the electron-phonon interaction (which is probably small) and the interaction with closed shells (42), the standard crystal field parameterization leaves a lot to be

desired. That is to say, this parameterization of the crystal field can give an over all qualitative agreement but in order to get exact detailed agreements, the other interactions mentioned above must be included. Therefore, the constants of Wong and Richman (39) are probably the best that can be obtained using only a free ion model (without the interaction with closed shells) perturbed by the static crystalline field.

Burns (73) has made calculations for the A_{LM} constants and Freeman and Watson (74) have made calculations for $\langle r^L \rangle$. The theoretical values of the constants $A_{LM}\langle r^L \rangle$ do not match the experimentally determined ones (37, 39) by factors from one to five. When the constants of Margolis (38) and Wong and Richman (39) were used in the diagonalization of the 91 by 91 matrix, the crystal field splittings and multiplet centers obtained were not in complete agreement with the experimental values as pointed out previously. It is felt that the electron-phonon interaction is too small to account for the differences in the multiplet centers, however, it could be large enough to account for small differences in the crystal field splittings. For the differences in the energies of the theoretical and experimental multiplet centers, crystal field splittings, and the magnetic field splittings, it is not known

if the closed shell interaction (42) and the contributions to covalent bonding by the 4f electrons (41) are of the right type and strength to account for all the differences between the theoretical and experimental values.

The zero field energy of the $\mu = \pm 1$ level of the $^3H_6$ multiplet determined in this work differs from that of other workers (35, 37, 39). This difference is probably due to the temperatures at which the determinations were made and the concentrations of Tm in the rare earth ethylsulphate crystals. In this work a temperature of 20°K was used to sufficiently populate the $\mu = \pm 1$ level in order to observe transitions from it. The other workers (35, 37, 39) used a temperature of 77°K. Part of the difference in the measured energy probably arises from a shift in the energies of the transitions due to the temperature. An energy shift of this sort was observed in this work between the temperatures of 4° and 20°K for the levels (Table 25). Another source for the energy difference would be the various concentrations of Tm used in work of Johnsen (35), Gruber and Conway (37), and Wong and Richman (39). More details of this type of energy shift are given in the following discussion.

The small differences between the data obtained in this

work and that of Johnsen (35) for the 4°K temperature could in part be due to Tm concentrations and crystal thicknesses used. In this work, measurements were made on only 100 per cent Tm ES crystals except for the rotation spectra taken. Johnsen used various concentrations of Tm in Y ES and Er ES, but did not report the shifting of the energies of the transitions for the various dilutions used. Wong and Richman (39) attributed the small differences between their data and that of Johnsen to the diluted crystals they used. Wong and Richman used 10 per cent Tm in La ES. The energies of the transitions have been reported by Spedding et al. (75) to change slightly for various concentrations of Er in Y ethylsulphate. Lines which broaden unsymmetrically as the crystal is made thicker would have a different measured energy of the absorption envelope depending on the crystal thickness. This type of behavior was found in many of the particularly broad lines. The sharp lines showed this behavior too, but to a very much less noticeable extent.

The electronic levels which are broad, probably interact strongly with lattice vibrations (phonons) as discussed previously and put into an explicit form by Equation 23. To what extent the levels are broadened by H_{ep} requires a detailed

knowledge of the interaction. Transitions of the lowest lying energy levels of each multiplet are in general the sharpest lines, indicating that the levels themselves are nearly independent of the wave vector $\underline{k}$. Transitions to the higher energy levels in each multiplet are usually broader and it is felt that the energy levels have become broadened by the electron-phonon interaction, hence, have become a function of the wave vector $\underline{k}$. This is in agreement with the perturbation calculation carried out in a previous section. The interaction term (last term of Equation 23) is large when the energy denominator becomes small, i.e., when $\epsilon_{\lambda\mu i}-\epsilon_{\lambda'\mu'i'}-\hbar\omega_{\underline{q}s} \cong 0$. When the interaction of electrons with the optical modes and the acoustic modes for large $\underline{q}$ are considered, the energy denominator becomes smaller for the higher energy levels in a particular multiplet than for the low lying levels. It is assumed that when $\underline{q}$ goes to zero for the acoustic modes H_{ep} goes to zero because for $\underline{q} = 0$ the acoustic modes correspond to a uniform translation of the unit cells (76) and hence no lattice distortions. The only part of the acoustic branch that will probably interact strongly with the electrons is the part for large $\underline{q}$.

The splitting factors of the levels for Hpc obtained in

this work have a smaller limit of error than those of Johnsen (35) because an instrument with a larger dispersion was used in this work. (The limit of error of the $\mu = \pm 2$ level of the $^3F_4$ multiplet is the same). The reader should note that Johnsen defined his splitting factor as one half that used in this work; therefore the splitting factor as well as the limit of error should be doubled for a comparison to the factors obtained in this work. The agreement of experimental values with the theoretical values (Table 28) is in qualitative agreement but is not in exact quantitative agreement. The reasons for the disagreement could be that the crystal field approximation cannot give exact agreement for reasons discussed previously. The electron-phonon interaction can affect the observed g-factors, but until details of H_{ep} are known, one cannot tell if this interaction is large enough to account for the observed disagreements between theory and experiment.

The splitting factors for Hsc were not obtained by Johnsen (35) because he failed to recognize the correct way to interpret the data and the high temperature work broadened the lines such that the (1-1) and (1-2) transitions showed no splitting. The theoretically determined splitting factors obtained in this work are only in qualitative agreement with the experi-

mentally determined ones as it was in the parallel field case.

Any Jahn-Teller splitting of the levels will also contribute to the disagreement between the experimental and theoretical g-factors for both field directions. However, any zero field splitting would give rise to an apparent field dependence of the g-factors. Experimentally there does not seem to be any field dependence of the g-factors between the fields of 21.5 and 28.2 kilogauss. This means that any Jahn-Teller splitting in Tm ES is probably very small for most of the levels.

If the wave functions representing the states of the $^3F_3$ multiplet can be thought of as being strictly eigenfunctions of J^2 and J_z ($J = 3$), then the $g_{||}$ factors of the $\mu = M = \pm 2$ and $\mu = M = \pm 1$ states would be in the ratio of 2:1. The theoretical values of Wong and Richman (39) given in Table 28 are in this ratio. However, the theoretical values obtained in this work (from diagonalization of the 91 by 91 matrix) are in the ratio of 1.819:1.000 and the experimental values of this work are in the ratio of 1.74 ± 0.05:1.00. This indicates that there is considerable intermultiplet interaction of the F multiplets via the crystal field. The theoretical and experimental ratios for the $\mu = M = \pm 2$ and $\mu = M = \pm 1$ levels of the

$^3F_2$ multiplet are 2.255:1.000 and 1.87 $\pm$0.09:1.00 respectively.

The theory of Murao, Spedding, and Good (43) as applied to thulium ethylsulphate for the magnetic field perpendicular to the c-axis has been reasonably successful in the description of the spectra in all the cases considered.

The work in this thesis by no means completes the work that could be done on Tm ES. Spectral data could be taken for the other multiplets; the $^1I_6$, ^3P's, and $^1S_0$ lie in the ultraviolet region and the $^3H_4$ and $^3H_5$ lie in the infrared region. There would be some experimental difficulties in obtaining data for these multiplets, however, some spectral data is available for these multiplets (37, 39). No real attempt was made in this work to study the intensities of the absorption lines. The intensities given in the tables and shown in the figures are at best crude estimates of the actual intensities. To compare with the theoretical calculations of Judd (34), intensity studies of absorption lines could be made. The angle between the crystallographic a and x-axes, $\bar{\emptyset}$, was determined for 10 per cent Tm in Y ES. It may be interesting to determine this angle for various host rare earth ethylsulphates, i.e., say 10 per cent Tm in various rare earth ethyl-

sulphates.

Theoretical determinations of the constants from first principles are needed. Ridley (77) has calculated the F integrals and ζ using a Hartree self-consistent method for a Tm^{3+} ion. The ratios $10F_6/F_2$ and F_4/F_2 were found to be 0.1370 and 0.1290 respectively, while the same ratios determined from the spectral data (38) are 0.1649 and 0.1509. Ridley (77) calculated the magnitude of ζ to be 2742 cm^{-1} while Margolis (38) found the magnitude of ζ to be 2656 cm^{-1} for a Tm^{3+} ion. A better method of calculating the F's and ζ would be to use the Hartree-Fock self-consistent method which takes into account the exchange interaction.

APPENDIX I

Calculation of the Characters of the C_{3h} Symmetry Group in the J Representation

Landau and Lifshitz (53) have given a brief but to the point treatment of group theory. Their notation and equations will be used in the following work. The characters for the J (total angular momentum) representation for a rotation through an angle ϕ can be found by using

$$\chi^{(J)}(\phi) = \frac{\sin(J+\frac{1}{2})\phi}{\sin\frac{1}{2}\phi} \,. \tag{A1}$$

For the C_3 operation, $\phi = 2\pi/3$ and for the C_3^2 operation, $\phi = 4\pi/3$. So for C_3 and C_3^2, the characters are given by,

$$\chi^{(J)}(C_3) = \frac{\sin(J+\frac{1}{2})2\pi/3}{\sin\frac{1}{2}2\pi/3} \,,$$

and (A2)

$$\chi^{(J)}(C_3^2) = \frac{\sin(J+\frac{1}{2})4\pi/3}{\sin\frac{1}{2}4\pi/3} \,.$$

The σ_h operator is $C_2 I$ with the character,

$$\chi^{(J)}(\sigma_h) = \chi(I)\,\chi^{(J)}(C_2) = \pm\frac{\sin(J+\frac{1}{2})\pi}{\sin\frac{1}{2}\pi}$$

$$= (\pm)(-1)^J \quad \text{for } J \text{ an integer.} \tag{A3}$$

Other intermediate results are,

$$\chi^{(J)}(\sigma_h C_3) = \chi[I\,C(\pi + 2\pi/3)]$$
$$= \chi[I\,C(5\pi/3)]$$
$$= \pm \frac{\sin(J+\frac{1}{2})\,5\pi/3}{\sin\frac{1}{2}\,5\pi/3}$$

(A4)

$$\chi^{(J)}(\sigma_h C_3^2) = \chi[I\,C(\pi + 4\pi/3)]$$
$$= \pm \frac{\sin(J+\frac{1}{2})\,\pi/3}{\sin\frac{1}{2}\,\pi/3} \quad .$$

Example

The example of J = 4 will be considered.

$$\chi^{(4)}(E) = \lim_{\Delta \to 0} \frac{\sin(9/2)\,\Delta}{\sin\frac{1}{2}\,\Delta}$$
$$= \frac{9/2}{1/2} = 9 \, .$$

$$\chi^{(4)}(C_3) = \frac{\sin(9/2)\,2\pi/3}{\sin\frac{1}{2}\,2\pi/3} = 0 \, .$$

(A5)

$$\chi^{(4)}(C_3^2) = \frac{\sin(9/2)\,4\pi/3}{\sin\frac{1}{2}\,4\pi/3} = 0 \, .$$

$$\chi^{(4)}(\sigma_h) = (\pm)(-1)^4 = (\pm) \, .$$

$$\chi^{(4)}(\sigma_h C_3) = \pm \frac{\sin(9/2)\,5\pi/3}{\sin \frac{1}{2}\,5\pi/3} = -2(\pm).$$

$$\chi^{(4)}(\sigma_h C_3^2) = \pm \frac{\sin(9/2)\,\pi/3}{\sin \frac{1}{2}\,\pi/3} = -2(\pm).$$

In the character table, Table 4, only the even parity characters (+) were used. This assignment is in agreement with experiment and the number of μ representations contained in the J representations agrees with other authors (35, 37, 39).

APPENDIX II

Calculation of the Number of μ Representations Contained in a J Representation

The number of μ irreducible representations contained in a reducible J representation is given by Equation (13) as,

$$a^{(\mu)} = \frac{1}{g} \sum_{G} \chi^{(J)}(G)\, \chi^{(\mu)}(G)^{*} . \qquad \text{(A6)}$$

The character tables for the J representation and the μ representation are given in Tables 4 and 3 respectively. The dimensionality of the group is six and the group elements, G, are E, C_3, C_3^2, σ_h, $\sigma_h C_3$, and $\sigma_h C_3^2$.

Example

The special case for J = 4 will be considered below.

For μ = 0

$$a^{(0)} = (1/6)[9\cdot 1 + 0\cdot 1 + 0\cdot 1 + 1\cdot 1 + (-2)\cdot 1 + (-2)\cdot 1]$$
$$= (1/6)\cdot 6 = 1 . \qquad \text{(A7)}$$

For μ = 1

$$a^{(+1)} = (1/6)[9\cdot 1 + 0\cdot \varepsilon + 0\cdot \varepsilon^2 + 1\cdot(-1) + (-2)\cdot(-\varepsilon) + (-2)\cdot(-\varepsilon^2)]$$
$$= (1/6)\cdot 6 = 1 \qquad \text{(A8)}$$

where $\varepsilon + \varepsilon^2 = e^{i2\pi/3} + e^{-i2\pi/3} = -1$.

A similar result exists for $\mu = -1$ as for $\mu = 1$, i.e., $a^{(-1)} = 1$.

For $\mu = 2$

$$a^{(2)} = (1/6)[9\cdot 1 + 0\cdot\varepsilon^2 + 0\cdot\varepsilon\ 1\cdot 1 + (-2)\cdot\varepsilon^2 + (-2)\cdot\varepsilon]$$
$$= (1/6)\cdot 12 = 2. \qquad \text{(A9)}$$

A similar result exists for $\mu = -2$ as for $\mu = 2$, i.e., $a^{(-2)} = 2$.

For $\mu = 3$

$$a^{(3)} = (1/6)[9\cdot 1 + 0\cdot 1 + 0\cdot 1 + 1\cdot(-1) + (-2)\cdot(-1) + (-2)\cdot(-1)]$$
$$= (1/6)\cdot 12 = 2. \qquad \text{(A10)}$$

APPENDIX III

Lattice Vibrations

The treatment of lattice vibrations given below will be somewhat of a combination of the work of Peierls (76) and Sommerfeld and Bethe (78). For additional references, the reader is referred to Born and Huang (79) and Ziman (80).

Classical treatment

The general position of a lattice point is taken as $\underline{d}_j + \underline{a}_{\bar{n}}$ where $\underline{a}_{\bar{n}}$ is a lattice vector to the $\bar{n}$-th unit cell and $\underline{d}_j$ is a vector within a unit cell to the j-th particle in the unit cell. The displacement from equilibrium of the $j\bar{n}$-th particle is given as $\underline{u}_{j\bar{n}}$.

The harmonic approximation to the actual potential that the atoms in a crystal feel due to each other is (76),

$$U - U_o = \frac{1}{2} \sum_{j,j'} \sum_{\bar{n},\bar{n}'} \sum_{k,k'} A_{j\bar{n}k;j'\bar{n}'k'} (u_{j\bar{n}})_k (u_{j'\bar{n}'})_{k'}, \tag{A11}$$

where k and k' are the Cartesian components of the vector $\underline{u}_{j\bar{n}}$. The sums of j and $\bar{n}$ run over all particles in a unit cell and over all unit cells respectively. The tensor A is symmetric with respect to interchanges of the indices $j\bar{n}k$ and $j'\bar{n}'k'$ (76). A is written by Peierls (76) as,

$$A_{j\bar{n}k;j'\bar{n}'k'} = A(\underline{a}_{\bar{n}} - \underline{a}_{\bar{n}'})_{jk;j'k'} . \tag{A12}$$

The classical equations of motion are given by,

$$M_j(\ddot{u}_{j\bar{n}})_k = -\partial[u-u_0]/\partial(u_{j\bar{n}})_k , \tag{A13}$$

so therefore,

$$M_j(\ddot{u}_{j\bar{n}})_k = -\sum_{j',\bar{n}',k'} A(\underline{a}_{\bar{n}} - \underline{a}_{\bar{n}'})\,(u_{j'\bar{n}'})_{k'} , \tag{A14}$$

where M_j is the mass of the atom at the j-th site in a unit cell. Solutions for Equation A14 of the following type [the reader is referred to (76) page 17 and (78) page 7],

$$\underline{u}_{j\bar{n}} = \underline{e}_{\underline{q}j}\left[C_{\underline{q}}\, e^{i\underline{q}\cdot\underline{a}_{\bar{n}}} + C^{*}_{\underline{q}} e^{-i\underline{q}\cdot\underline{a}_{\bar{n}}}\right], \tag{A15}$$

are used. These types of solutions satisfy the periodicity requirements. The time dependence of the normal coordinates is given by,

$$C_{\underline{q}} = C^{o}_{\underline{q}}\, e^{-i\omega_{\underline{q}}t} \text{ and } C^{*}_{\underline{q}} = C^{o*}_{\underline{q}}\, e^{i\omega_{\underline{q}}t} . \tag{A16}$$

Substitution of this solution into Equation A14 gives,

$$M_j\,\omega^2_{\underline{q}}(e_{\underline{q}j})_k = \sum_{j'k'} G(\underline{q})_{jkj'k'}\,(e_{\underline{q}j'})_{k'} , \tag{A17}$$

where

$$G(\underline{q})_{jkj'k'} = \sum_{\bar{n}''} A(\underline{a}_{\bar{n}''})_{jkj'k'} e^{i\underline{q}\cdot\underline{a}_{\bar{n}''}}.$$

There is a set of 3r linear homogeneous equations for the 3r displacements of the r atoms in a unit cell. These equations have solutions if and only if the determinant of the coefficients of $\underline{e}_{\underline{q}j}$ vanishes. In general there are 3r roots. Three of these 3r roots for $\underline{q} = 0$ will be zero corresponding to a uniform translation of the unit cell. In general there are different frequencies for different normal modes s, s = 1, 2, 3, $\cdots$, 3r. Hence the vectors $\underline{e}$ and the eigenvalues ω^2 must carry the subscript s in addition to the wave vector $\underline{q}$ subscript.

The orthogonality of the polarization vector $\underline{e}_{\underline{q}sj}$ will be taken as that given on page 19 of Peierls (76).

$$\sum_{j,\bar{n}} M_j \underline{e}_{\underline{q}sj} \cdot \underline{e}_{\underline{q}'s'j} (e^{i\underline{q}\cdot\underline{a}_{\bar{n}}})^* (e^{i\underline{q}'\cdot\underline{a}_{\bar{n}}}) = M \delta_{\underline{q},\underline{q}'} \delta_{s,s'}, \tag{A18}$$

where M is the mass of the crystal.

Then the general vector displacement from equilibrium is defined as

$$\underline{u}_{j\bar{n}} = \frac{1}{\sqrt{M}} \sum_{\underline{q},s} \underline{e}_{\underline{q}sj} [C_{\underline{q}s} e^{i\underline{q}\cdot\underline{a}_{\bar{n}}} + C^*_{\underline{q}s} e^{-i\underline{q}\cdot\underline{a}_{\bar{n}}}]. \tag{A19}$$

The kinetic plus potential energy of the system of atoms where the zero point energy is neglected is given by,

$$\begin{aligned} E &= T + U - U_o \\ &= \frac{1}{2} \sum_{j,\bar{n}} M_j \, \dot{\underline{u}}_{j\bar{n}} \cdot \dot{u}_{j\bar{n}} \\ &\quad + \frac{1}{2} \sum_{j,\bar{n},k} \sum_{j',\bar{n}',k'} A(\underline{\varrho}_{\bar{n}} - \underline{\varrho}_{\bar{n}'})_{jk;j'k'} (u_{j\bar{n}})_k (u_{j'\bar{n}'})_{k'} \, . \end{aligned} \tag{A20}$$

Making use of Equations A19, A11, and A18, the energy E becomes,

$$E = \sum_{\underline{q},s} \omega_{\underline{q}s}^2 \left[c_{\underline{q}s} c_{\underline{q}s}^* + c_{\underline{q}s}^* c_{\underline{q}s} \right] . \tag{A21}$$

Quantum treatment

To put the energy into the quantum mechanical form, it is necessary to examine the commutation properties of the normal coordinates c and c*. In terms of the displacements $\underline{u}$ and the velocities $\dot{\underline{u}}$, the c's and c*'s are,

$$\begin{aligned} c_{\underline{q}s} = \left[1/2i\omega_{\underline{q}s}\sqrt{M} \right] \sum_{j,\bar{n}} M_j e^{i\underline{q}\cdot\underline{\varrho}_{\bar{n}}} \, \underline{e}_{\underline{q}sj} \\ \cdot \left[i\omega_{\underline{q}s} \underline{u}_{j\bar{n}} - \dot{\underline{u}}_{j\bar{n}} \right] , \end{aligned} \tag{A22}$$

and $c_{\underline{q}s}^*$ is obtained by taking the complex conjugate of $c_{\underline{q}s}$. Using Equation A22 along with

$$\left[(u_{j\bar{n}})_k , M_j (\dot{u}_{j'\bar{n}'})_{k'} \right] = i\hbar \, \delta_{k,k'} \, \delta_{\bar{n},\bar{n}'} \, \delta_{j,j'} , \tag{A23}$$

the commutator relations $[c_{\underline{q}s}, c_{\underline{q}'s'}]$, $[c_{\underline{q}s}^*, c_{\underline{q}'s'}^*]$, and $[c_{\underline{q}s}, c_{\underline{q}'s'}^*]$ become,

$$[c_{\underline{\ell}s}, c_{\underline{\ell}'s'}] = [c_{\underline{\ell}s}^*, c_{\underline{\ell}'s'}^*] = 0, \tag{A24}$$

and

$$[c_{\underline{\ell}s}, c_{\underline{\ell}'s'}^*] = \frac{\hbar}{2\omega_{\underline{\ell}s}} \delta_{\underline{\ell},\underline{\ell}'} \delta_{s,s'} .$$

New operators $b_{\underline{q}s}^+$ and $b_{\underline{q}s}$, being the creation and annihilation boson operators, page 217 of (53), are defined in terms of the c's and c*'s as,

$$c_{\underline{\ell}s} = \sqrt{\frac{\hbar}{2\omega_{\underline{\ell}s}}}\ b_{\underline{\ell}s}$$

$$c_{\underline{\ell}s}^* = \sqrt{\frac{\hbar}{2\omega_{\underline{\ell}s}}}\ b_{\underline{\ell}s}^+ . \tag{A25}$$

Then the commutator relations become,

$$[b_{\underline{\ell}s}, b_{\underline{\ell}'s'}^+] = \delta_{\underline{\ell},\underline{\ell}'} \delta_{s,s'}, \tag{A26}$$

and $$[b_{\underline{\ell}s}, b_{\underline{\ell}'s'}] = [b_{\underline{\ell}s}^+, b_{\underline{\ell}'s'}^+] = 0.$$

The energy, or the Hamiltonian in terms of these new operators using Equation A26 becomes,

$$H_L = \sum_{\underline{\ell},s} \hbar\omega_{\underline{\ell}s} [b_{\underline{\ell}s}^+ b_{\underline{\ell}s} + \tfrac{1}{2}] \tag{A27}$$

which is the lattice Hamiltonian. $\frac{1}{2}\sum_{\underline{q}s}\hbar\omega_{\underline{q}s}$ is the zero point energy and is usually neglected since it is just a constant energy term.

The matrix elements of the annihilation and creation operators between occupation number states (53) are,

$$\begin{aligned}\langle n_{\underline{q}s}-1|\, b_{\underline{q}s}\,|\, n_{\underline{q}s}\rangle &= \sqrt{n_{\underline{q}s}}\\ \langle n_{\underline{q}s}\,|\, b^{+}_{\underline{q}s}\,|\, n_{\underline{q}s}-1\rangle &= \sqrt{n_{\underline{q}s}},\end{aligned} \tag{A28}$$

and all others are zero. The operators acting on the occupation number state vectors give,

$$\begin{aligned}b_{\underline{q}s}\,|\, n_{\underline{q}s}\rangle &= \sqrt{n_{\underline{q}s}}\,|\, n_{\underline{q}s}-1\rangle\\ b_{\underline{q}s}\,|\, 0\rangle &= 0,\end{aligned}$$

and (A29)

$$b^{+}_{\underline{q}s}\,|\, n_{\underline{q}s}\rangle = \sqrt{n_{\underline{q}s}+1}\,|\, n_{\underline{q}s}+1\rangle .$$

The $n_{\underline{q}s}$ quanta of vibration are known as phonons (76).

The displacement from equilibrium of an atom in terms b and b^{+} is,

$$u_{j\bar{n}} = \sum_{\underline{q}s}\sqrt{\frac{\hbar}{2\omega_{\underline{q}s}M}}\; e_{\underline{q}sj}\left[\, b_{\underline{q}s}\, e^{i\underline{q}\cdot\underline{q}_{\bar{n}}} + b^{+}_{\underline{q}s}\, e^{-i\underline{q}\cdot\underline{q}_{\bar{n}}}\,\right]. \tag{A30}$$

LITERATURE CITED

1. Condon, E. U. and Shortley, G. H. The theory of atomic spectra. 5th [edition]. London, Cambridge University Press. 1959.

2. Slater, J. C., Phys. Rev. 34, 1293 (1929).

3. Herzberg, G. Atomic spectra and atomic structure. 2nd ed. New York, N. Y., Dover Publications, Inc. 1944.

4. White, H. E. Introduction to atomic spectra. New York, N. Y., McGraw-Hill Book Co., Inc. 1934.

5. Bethe, H. A., Ann. Physik 3, 133 (1929).

6. Bethe, H. A., Z. Physik 60, 218 (1930).

7. Schlapp, R. and Penney, W. G., Phys. Rev. 41, 194 (1932).

8. Schlapp, R. and Penney, W. G., Phys. Rev. 42, 666 (1932).

9. Van Vleck, J. H. Phys. Rev. 41, 208 (1932).

10a. Van Vleck, J. H., J. Chem. Phys. 3, 803, 807 (1935).

10b. Van Vleck, J. H. The theory of electric and magnetic susceptibilities. London, Oxford University Press. 1932.

11. Van Vleck, J. H., J. Phys. Chem. 41, 67 (1937).

12. Van Vleck, J. H., J. Chem. Phys. 8, 787 (1940).

13. Finkelstein, R. and Van Vleck, J. H., J. Chem. Phys. 8, 790 (1940).

14. Freed, S., Phys. Rev. 38, 2122 (1931).

15. Spedding, F. H., Howe, J. P., and Keller, W. H., J. Chem. Phys. 5, 416 (1937).

16. Bethe, H. A. and Spedding, F. H., Phys. Rev. 52, 454 (1937).

17. Spedding, F. H., J. Chem. Phys. 5, 316 (1937).

18. Freed, S. and Merirow, R. J., J. Chem. Phys. 5, 22 (1937).

19. Spedding, F. H., Phys. Rev. 58, 255 (1940).

20. Joos, G. and Ewald, H., Naturwissenschaften 25, 636 (1937).

21. Ellis, C. B. and Hall, H., Phys. Rev. 54, 478 (1938).

22. Hellwege, K. H., Ann. Physik 4, 95, 127, 136, 143, 150 (1948).

23. Hellwege, K. H., Ann. Physik 4, 357 (1949).

24. Bleaney, B. and Stevens, K. W. H., Repts. Prog. in Phys. 16, 108 (1953).

25. Stevens, K. W. H., Proc. Phys. Soc. (London) A65, 209 (1952).

26. Elliott, R. J., Rev. Mod. Phys. 25, 167 (1952).

27. Elliott, R. J. and Stevens, K. W. H., Proc. Roy. Soc. (London) A215, 427 (1952).

28. Elliott, R. J. and Stevens, K. W. H., Proc. Roy. Soc. (London) A218, 553 (1953).

29. Elliott, R. J. and Stevens, K. W. H., Proc. Roy. Soc. (London) A219, 387 (1955).

30a. Scovil, H. E. D. and Stevens, K. W. H., Proc. Phys. Soc. (London) A65, 954 (1952).

30b. Dieke, G. H. and Heroux, L., Phys. Rev. 103, 1227 (1956).

30c. Dieke, G. H. and Hall, L. A., J. Chem. Phys. 27, 465 (1957).

30d. Dieke, G. H. and Sarup, R., J. Chem. Phys. 29, 741 (1958).

31. Ketelaar, J. A. A., Physica 4, 619 (1937).

32. Fitzwater, D. R. and Rundle, R. E., Z. Krist. 112, 362 (1959).

33. Broer, L. J. F., Gorter, C. J., and Hoogschagen, J., Physica 11, 231 (1945).

34. Judd, B. R., Phys. Rev. 127, 750 (1962).

35. Johnsen, U., Z. Physik 152, 454 (1958). Original available but not translated; translated in U. S. Atomic Energy Commission Report NP-tr-767. [Division of Technical Information Extension.] 1961.

36. Gruber, J. B. and Conway, J. G., J. Chem. Phys. 32, 1178 (1960).

37. Gruber, J. B. and Conway, J. G., J. Chem. Phys. 32, 1531 (1960).

38. Margolis, J. S. The energy levels of Pr^{3+} in $PrCl_3$. Unpublished Ph.D. thesis. Los Angeles, California, Library, University of California. 1960.

39. Wong, E. Y. and Richman, I., J. Chem. Phys. 34, 1182 (1961).

40. Gerstein, B. C., Jennings, L. D., and Spedding, F. H., J. Chem. Phys. 37, 1496 (1962).

41. Jørgensen, C. K., Pappalardo, R., and Schmidtke, H., J. Chem. Phys. 39, 1422 (1963).

42. Watson, R. E. and Freeman, A. J., Phys. Rev. 133, A1571 (1964).

43. Murao, T., Spedding, F. H., and Good, R. H. U. S. Atomic Energy Commission Report IS-871. [Iowa State Univ., Ames, Iowa.] 1964.

44. Satten, R. A., J. Chem. Phys. 27, 286 (1957).

45. Satten, R. A., J. Chem. Phys. 29, 658 (1958).

46. Satten, R. A., J. Chem. Phys. 30, 590 (1959).

47. Satten, R. A., Young, D. J., and Gruen, D. M., J. Chem. Phys. 33, 1140 (1960).

48. Pollack, S. A. and Satten, R. A., J. Chem. Phys. 36, 804 (1962).

49. Richman, I., Satten, R. A., and Wong, E. Y., J. Chem. Phys. 39, 1833 (1963).

50. Wong, E. Y. and Erath, E. H., J. Chem. Phys. 39, 1629 (1963).

51. Krishnamurthy, N. and Krishnan, R. S., Proc. Indian Acad. of Sciences A57, 352 (1963).

52. Gibbs, R. C., Wilber, D. T., and White, H. E., Phys. Rev. 29, 790 (1927).

53. Landau, L. D. and Lifshitz, E. M. Quantum mechanics non-relativistic theory. [Translated from the Russian by Sykes, J. B. and Bell, J. S.] Reading, Mass., Addison-Wesley Pub. Co. 1958.

54. Paskin, Arthur and Keller, J. M. U. S. Atomic Energy Commission Report ISC-310. [Iowa State Univ., Ames, Iowa.] 1953.

55. Barnes, R. G., Kankeleit, E., Mössbauer, R. L., and Poindexter, J. M., Phys. Rev. Letters 11, 253 (1963).

56. Dekker, A. J. Solid state physics. Englewood Cliffs, N. J., Prentice-Hall, Inc. 1957.

57. Kittel, C. Introduction to solid state physics. 2nd ed. New York, N. Y., John Wiley and Sons, Inc. 1961.

58. Mott, N. F. and Jones, H. The theory of the properties of metals and alloys. New York, N. Y., Dover Publications, Inc. 1958.

59. Cooke, A. H., Lazenby, R., and Leask, M. J. M. U. S. Air Force, AFCRL-83. [Air Force Cambridge Research Labs.] 1960.

60. Schiff, L. I. Quantum mechanics. 2nd edition. New York, N. Y., McGraw-Hill Book Co., Inc. 1955.

61. Koster, G. F. and Statz, H., Phys. Rev. 113, 445 (1959).

62. Statz, H. and Koster, G. F., Phys. Rev. 115, 1568 (1959).

63. Bethe, H. A., Z. Physik 60, 218 (1930).

64. Grohman, I., Hellwege, K. H., and Kahle, H. G., Z. Physik 164, 243 (1961).

65. Fastie, W. G., J. Optical Soc. of Am. 42, 641 (1952).

66. Fastie, W. G., J. Optical Soc. of Am. 42, 647 (1952).

67. Fastie, W. G., Crosswhite, H. M., and Gloersen, P., J. Optical Soc. of Am. 48, 106 (1958).

68. Jarrell-Ash Company. Instruction manual for 3.4 meter Ebert spectrograph Mark IV. Newtonville, Mass., author 1961.

69. Harrison, G. R. Massachusetts Institute of Technology wavelength tables. New York, N. Y., McGraw-Hill Book Co., Inc. 1957.

70. Gatterer, A. and Junkes, J. Arc spectrum of iron. 2nd ed. Cita del Vaticano, Specola Vaticana. 1947.

71. Jenkins, F. A. and White, H. E. Fundamentals of optics, 3rd ed. New York, N. Y., McGraw-Hill Book Co., Inc. 1957.

72. Coleman, C. D., Bozman, W. R., and Meggers, W. F. U. S. Dept. of Commerce, National Bureau of Standards Monograph 3, 1 (1960).

73. Burns, G., International Business Machines Research Paper RC-722, 1 (1962).

74. Freeman, A. J. and Watson, R. E., Phys. Rev. 127, 2058 (1962).

75. Spedding, F. H., Haas, W. J., and Sutherland, W. L. [To be published ca. 1964.]

76. Peierls, R. E. Quantum theory of solids. London, Oxford University Press. 1955.

77. Ridley, E. C., Proc. Cambridge Phil. Soc. 56, 41 (1960).

78. Sommerfeld, Arnold and Bethe, Hans. Electron theory of metals, part II. (Translated title) Handbuch der Physik, Bd.24, Tl.2, 2. Aufl., Julius Springer, Berlin, 1953, pages 499-579. The information cited was from the translation by the U. S. Atomic Energy Commission, AEC-tr-2055. [Division of Technical Information Extension]. 1953.

79. Born, M. and Huang, K. Dynamical theory of crystal lattices. London, Oxford University Press. 1954.

80. Ziman, J. M. Electrons and phonons. London, Oxford University Press. 1960.

ACKNOWLEDGEMENTS

The author wishes to thank: Dr. F. H. Spedding for suggesting the problem and his direction of the work as well as helpful discussions concerning the work; Dr. R. H. Good, Jr. for the many helpful discussions concerning the theory and permission to cite some of his unpublished work; the author also wishes to thank Dr. T. Murao for his helpful discussions of the theory. In addition the author wishes to thank Mr. W. J. Haas for help involving use of the computer, Mr. W. L. Sutherland for help in the operation of the spectrograph, and Mr. H. O. Weber for growing the crystals used in this work.